SOFT TEMPLATE SYNTHESIS OF AZA- AND THIAZAMETALMACROCYCLIC COMPOUNDS IN THIN GELATIN FILMS

O. V. Mikhailov[a]

Keywords: azamacrocyclic metal chelate; thiaazamacrocyclic metal chelate; thin film; molecular structure.

The problems concerned with the processes of template synthesis of 3*d*-element metal aza- and thiazamacrocyclic complexes that happen in *nano*reactors on the basis of thin films metal hexacyanoferrate(II)-gelatin-immobilized matrix implants under their contact with water solutions containing various (N,O,S)-donor atomic ligands and organic compounds having one or two carbonyl groups have been considered. It was noted that, in a series of cases, the variety of metal macrocyclic compounds obtained at template synthesis in such specific conditions considerably differs from that of metal macrocycles formed at the conditions traditional for chemical synthesis.

* Corresponding Authors
E-Mail: olegmkhlv@gmail.com
[a] Kazan National Research Technological University, K. Marx Street 68, 420015 Kazan, Russia

Introduction

The majority of chemical reactions used nowadays in the modern coordination chemistry include the processes of the so called "self-assembly" or "template synthesis", some of which have been already discussed in the literature.[1–4] In some cases an association of molecules of the initial substances gets a specific orientation under the influence of a particular "mould"; now the processes of such synthesis are widespread in the synthesis of macrocyclic compounds, and, first of all, the so-called metal macrocyclic compounds, the structure of which contains atoms of different *d*- and *f*-elements.[5] The role of a mould in the synthesis of these objects is played by the metal ion, which then enters the composition of the metal macrocyclic compound formed during self-assembly. As a rule, each of them presents a metal complex with a chelate polydentate ligand obtained not according to the scheme [metal ion + ligand → complex] classical for the metal complexes but to the scheme [metal ion + "building blocks" of the future ligand (so called ligand synthons or ligsons) → complex]. In particular, it is necessary to emphasize that the metal ion present in the reaction system (the so-called template) does not simply "conduct" the process of self-assembly; in its absence, this process does not occur at all. Rather often, the processes of self-assembly play a key role in the synthesis of such macroheterocyclic compounds which do not contain metal atoms in their structures: in this case, metal chelates formed in the beginning are subjected to demetallation. In this respect, the above reactions currently take the dominating position in the synthesis of aza-, azaoxo- and thiazamacrocycles; crown-ethers; and other systems with closed contours containing various heteroatoms in their "skeletons." The final products of these reactions (which are called template syntheses in the chemistry of macrocyclic compounds), which have a set of nontrivial physical and chemical properties, are applied widely; the list of fields where they are used includes metallurgy and medicine, industrial biotechnology and catalysis, microelectronics and agriculture, and numerous other fields of human activity.

Currently the processes of self-assembly of metal macrocyclic compounds are practically always implemented in conditions "traditional" for chemistry, namely, in the liquid (solution); solid; and, sometimes, gas phases. Traditionally, chemical synthesis is performed in macro- and, much less often, microreactors. However, so that the synthetic modes develop and improve, it is of interest and important to introduce a *nano*component not only in the chemical reaction with the purpose of obtaining metal macrocycles and performed, as was already mentioned, according to the "upwards" principle, but also in the medium where this reaction proceeds. Simply speaking, this is the idea of performing the above process of self-assembly in the nanoscale reactors. This can be done by using specific (but, in general, quite accessible to chemists) objects such as biopolymer-immobilized organizing systems on the basis of polypeptides or polysaccharides. These systems contain intermolecular cavities large enough in concepts of the "nanoworld" which can be considered original molecular *nano*reactors and in which the various chemical processes in general and those of self-assembly in particular can be implemented in principle. As a result, the *nano*-sized particles of metal macrocyclic chelates arising in the course of such processes, can be formed in the system indicated above. This paper is concerned with these systems.

Thin films gelatin-immobilized matrix as an organizing medium in the processes of self-assembly of metal macrocycles

Thin films gelatin-immobilized matrices (in further – **GIM**) with gelatin as the polymeric binding agent belong to the biopolymeric systems which, in principle, can be used to implement the processes of self-assembly of metalcomplexes. This high_molecular compound easily forms the so-called gels (solutions in the low-molecular liquids that have some solid_state properties, in particular, the absence of fluidity at low transverse strain, the ability to

keep their form, and considerable strength and elasticity). It has been well_known for a long time[6–12] that, by its chemical nature, gelatin is a polydisperse mixture of low-molecular peptides with the general formula **I** (R_1, R_i, R_j, R_k are various radicals) with the molecular mass M = 50.000–70.000

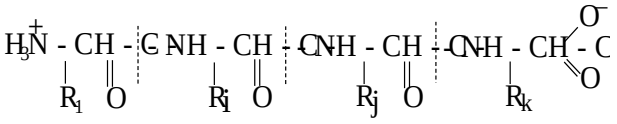

I

or their aggregates with M = 200.000–300.000 composed of 18 natural amino acids from a total of 20, except for cystine and cysteine. Gelatin is obtained from the natural fibrillary fiber of the protein collagen. Its role is to form the mesh structure keeping the strain in any connecting tissue (skin, bone, cartilage, sinews, etc.). Most of these amino acid sections (a little more than a third of the total number) is the "residue" of the elementary amino acid, glycine; the second in prevalence is the "residue" of proline; and the third, with a somewhat lower content, is alanine. Groups with labile sulfur and disulfide bridges are not characteristic for the structure of gelatin and collagen[6]. It was established by the electron-microscopic method that the diameter of the gelatin macromolecules is 14 nm, while their length is 2850 nm.[9] These numbers are in good agreement with the similar data found in ref.[10] on the measurements of the light dispersion and viscosity of gelatinous solutions. These data show that the gelatin molecule is strongly asymmetric and anisometric.[9,10] Each molecule consists of three parallel α-chains with almost identical M values of 95.000 so that the its molecular mass is approximately 280.000–290.000. However, for now, there are no exhaustive data on the distribution of gelatin macromolecules in the biopolymeric bulk.

The structure and properties of collagen and gelatin were repeatedly studied over the last several decades.[9–32] Molecules of these high-molecular compounds consist of three polypeptide chains with practically identical molecular weights, two of which are usually practically identical with respect to the set and sequence of amino acids (the so-called α1-chain), while the third (the so-called α2-chain) in this respect differs from two others[9,10,20]. The typical stoichiometric composition of collagen expressed in the number and variety of α-chains in its macromolecule is $(\alpha_1)_2\alpha_2$; less often it is $(\alpha_1)_3$.[30] The high content of proline and hydroxyproline, as well as the interesting fact that, according to the chemical analysis data on the sequence of the arrangement of the amino acid residues, each third residue is glycine, allowed authors[14,30] to make two alternative assumptions concerning the geometry of the $(\alpha_1)_2\alpha_2$, $(\alpha1)_3$ structures of the gelatin molecules, in each of which the formation of the above triple helices is postulated. However, in the structure proposed in ref.[17], one bond is needed for each amino acid residues, whereas in the structure of ref.[33], twice as many bonds are required. The unambiguous choice between these structures was impossible even after X-ray analysis, and the question about the exact gelatin structure is still under discussion. For each of the peptide fragments of the gelatin molecule, the interface of the π-electrons of the C, N, and O atoms is characteristic; therefore, all –C–C–NH–C– groups get a quasi-planar structure. The interatomic carbon-nitrogen distance in this structural fragment is 132 pm, which is much less than the length of the single C–N bond (147 pm), so its bond order is rather close to two.

At the transformation of collagen into gelatin, the poly-disperse mixture containing single (α_1 and α_2), double (β_{11} and β_{12}), and triple (γ) polypeptide chains (which, unlike collagen macromolecules, are formed as balls or clots) is formed. The structure for the gelatin molecules in which the *left*-handed spiral structure is attributed to each of such α-chains is proposed.[17,18,20] In the given structure, all polypeptide spirals are weaved with each other in a unique *right*-handed spiral; the hydrogen bonds play the largest role in its stabilization.[17] The α_2-chains are characterized by the same set of the polypeptide fragments as the α_1-chain, but in their amino acid sequence there is less proline, hydroxyproline, and lysine; however, tyrosine, valine, leucine, histidine, and hydroxylysin prevail.[12] Currently in the α_1-chain, the sequence of more than 700 amino acid residues is completely established.[11,12,25]

Having at one's disposal a polymer with such a structure, it is possible to obtain, in principle, immobilized systems with a homogeneous enough distribution of the immobilized substances in a particular part of a polymeric bulk and with good steric availability of molecules of this substance for the implementation of various chemical processes. Comparatively large intervals between the chains of the spatial mesh in the molecular structure of gelatin allow the molecules and ions of the low-molecular substances, unlike large colloid particles or macromolecules, to diffuse into the intermolecular **GIM** voids practically as easy as into the liquid phase solvents. Thus, in addition, **GIM** (both thin- and thick-layer ones) are highly transparent and plastic, which makes them very convenient to be studied by various spectroscopic methods. It is important as well that the gelatin bulk is destroyed easily enough under the influence of various proteolytic enzymes (tripsin, *Bacillus mesentericus*, *Bacillus subtilis*, etc.). Therefore, the chemical compounds immobilized in it can be easily isolated from it in the form of solid phases and analyzed by the same modern physical and chemical methods as those used to study solid substances isolated from the solid or gas phase reaction systems.

Template synthesis[34–37], which allows one, in principle, to obtain macrocyclic and supramolecular compounds of any complexity from rather simple fragments (the so-called ligand synthons or ligsons), play an important role in the synthetic methods of modern molecular nanotechnology called self-assembly. In the above version of self-assembly, a particular metal ion with a certain electron structure as a kind of a "pattern" (called sometimes a template center or simple template) provides the formation of metal complexes from the corresponding ligsons. These metal complexes have rather specific ligands (so-called chelants), the synthesis of which in the absence of the template is either complicated or cannot be performed in general. It is easy to notice from the most general considerations that the self-assembly of metal macrocyclic compounds is always accompanied by a decrease in the general entropy (ΔS) of the reaction system (sometimes it is rather large), because their composition is much more complicated when compared with the composition of the initial substances participating in its formation.

According to the classical expression for the isobaric process $\Delta G = \Delta H^0 - T\Delta S^0$ (where ΔG, ΔH^0 and ΔS^0 are the change of the free energy, standard enthalpy, and standard entropy during the reaction, respectively, and T is temperature in K), the probability of implementing any process accompanied by the decrease in the entropy decreases with the increase in the temperature. At rather low temperatures, the processes of self-assembly due to rather large activation energy values proceed with very low velocities. At rather large temperatures, when their velocities could be practically acceptable, they are thermodynamically forbidden. The situation is somewhat rescued by imposing high pressure on the reaction system at a high temperature, but even then it takes a rather long period of time (up to several hours).[34,36] One of topical problems of the modern synthetic coordination and supramolecular chemistry is to "soften" the conditions of template synthesis, and first of all, to provide its implementation in the so-called standard conditions (T = 298 K, P = 101325 Pa).

One of the possible approaches to solving this problem could be the preliminary ordering of the reaction system (i.e., the "compulsory" decrease of its entropy). It is easy to notice that this leads to a decrease in the slope of the linear dependence $\Delta G(T)$. In fact, since the entropy is an additive quantity, in the presence of such preliminary ordering, the relationship $\Delta S^0 = (\Delta S^0)' + \Delta S_{os}$, where ΔS^0 is the change of the standard entropy of the reaction in the absence of the above ordering, $(\Delta S^0)'$ is the change of the standard entropy of the reaction at the presence of the latter, and ΔS_{os} is the actual change of the entropy during the given ordering, holds. As a result, the expression (1) for $\Delta G'(T)$ in the system where the "compulsory" decrease of the entropy takes place becomes

$$\Delta G(T) = \Delta H^0 - T(\Delta S^0)' = \Delta H^0 - T(\Delta S^0 - \Delta S^0_{os}) \quad (1)$$

Since ΔS^0_{os} is negative, $\Delta S^0 < 0$, then $|\Delta S^0 - \Delta S^0_{os}| < |\Delta S^0|$. Accordingly, the range of the temperature values in which the given process of self-assembly is thermodynamically allowed (see Fig. 1) increases as well.

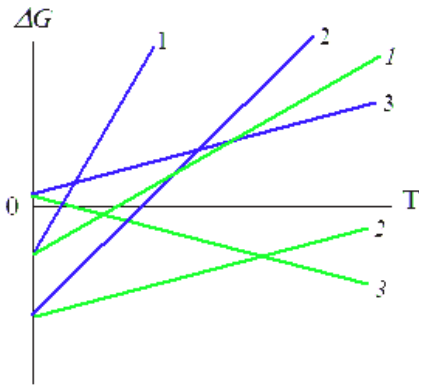

Figure 1. Schematic view of the $\Delta G(T)$ (**1, 2, 3**) and $\Delta G'(T)$ (***1, 2, 3***) dependences for three variants of the template process: **1, *1*** and **2, *2*** for the template processes with $\Delta H < 0$ which, in principle, can be implemented in the systems without a compulsory decrease in the entropy; **3, *3*** for the template processes with $\Delta H > 0$, which can be implemented only in the systems with a compulsory decrease in the entropy. The lower slope of the ***1, 2***, and ***3*** lines is clearly seen, unlike that of the **1, 2** and **3** lines.

According to[5], gelatin-immobilized matrix implants on the basis of hexacyanoferrates(II) of various *p*-, *d*-and *f*-elements (in further MHF **GIM**) with the nanoscale organization of the immobilized substance belong to systems with a preliminary decrease in entropy. As is known, the overwhelming majority of the current processes of self-assembly of the metal macrocycles refer to the so-called Schiff condensation, with the intramolecular formation of water due to the mobile hydrogen atoms of one ligson and oxygen atoms of another ligson,[34,36] therefore, the more mobile the hydrogen atoms in the corresponding ligson are, the higher the probability of the self-assembly in the given process is. In turn, this is directly connected with its proton donor ability. Since the macromolecules of gelatin as ampholyte and polyelectrolyte in the alkaline medium get a negative charge, the proton donor ability of compounds immobilized in it is much larger than that in the water solution; hence, the self-assembly according to the Schiff condensation in MHF **GIM** should proceed more effectively than in the solution or the solid phase. In as early as by the end of the previous century, in reviews[38,39], it has been noted that the character of the template synthesis in MHF **GIM** in a series of the triple metal ion– ligson A– ligson B systems considerably differs from that for the template synthesis in the so-called "traditional" conditions (i.e., in solutions and solid phase). These differences are most vividly manifested in the case of the so-called ambidentate ligsons A containing three or more donor centers and depending on the complex formation conditions, capable of being variously coordinated to a metal ion. (N,S)-donor organic compounds such as hydrazinomethanethioamide (thiosemicarbazide) $H_2N–NH–C(S)–NH_2$, hydrazinomethanethiohydrazide (thiocarbohydrazide) $H_2N–NH–C(S)–NH–NH_2$, ethanedithioamide (dithiooxamide) $H_2N–C(S)–C(S)–NH_2$, propanedithioamide-1,3 (dithiomalonamide), $H_2N–C(S)–CH_2–C(S)–NH_2$, etc., which can to be coordinated to a metal ion via N and S atoms, belong to such ligsons. One can use compounds both with one carbonyl group [in particular, methanal (formaldehyde) CH_2O, propanone-2 (acetone) $H_3C–C(O)–CH_3$] and two C=O groups [in particular, butandione-2,3 (diacetyl) $H_3C–C(O)–C(O)–CH_3$ and pentadione-2,4 (acetylacetone) $H_3C–C(O)–CH_2–C(O)–CH_3$] as accompanying ligsons B providing "stitching" of the metal cycles formed by the ligson A into a unique closed contour with formation of aza- and azathiamacrocyclic metal complexes. Further on we will discuss the processes of self-assembly in this sense.

In conclusion of this chapter, two important aspects of the terminological character should be noted.

1) As we mentioned above, the metal ion in the template synthesis plays the role of kind of an "organizing and directing force" in the formation of the metalmacrocyclic compounds which is only possible or prevails in the reaction conditions from the corresponding initial organic molecules, the synthesis of which from the given initial substances in other conditions is either complicated or cannot be performed at all. The participation of a metal ion (template) in this specific quality is obligatory. If any macrocyclic ligand can be formed from simpler organic compounds without contact with the ion of the given metal, even if it is "composed" of these compounds during the complex formation, the proceeding chemical reactions *do not refer* to the reactions of the template synthesis or self-assembly of metal macrocyclic compounds.[5,34,36]

Thus, the process of self-assembly between Ni(II), salicylaldehyde, and ammonia proceeding according to the general scheme (2)

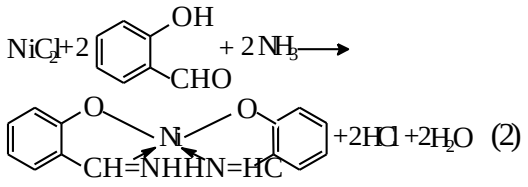

(2)

It is a template synthesis, because the ligand that is formed, salicylaldimine, does not arise at the interaction of salicylic aldehyde with NH_3, whereas the reaction between Ni(II), salicylaldehyde, and any alkylamines NH_2R according to the scheme (3)

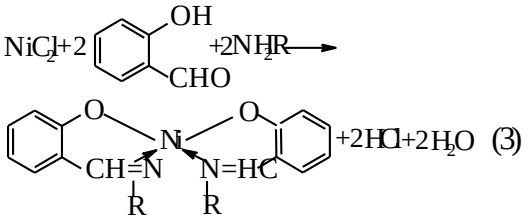

(3)

It is not a template synthesis, because the ligand that is formed results from the direct interaction of salicylaldehyde and the corresponding alkylamine according to the general equation (4) regardless of the presence of metal ion in the reaction system.

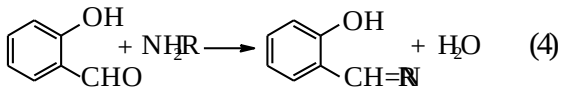

(4)

2) As a result of self-assembly, as a rule, we have the formation of tetradentate chelate ligand (and it is observed in all self-assembly processes in ***GIM*** described in the literature). In that case, two types of metal chelates – macrotricyclic (with three metalcycles), and macrotetracyclic (with four metal cycles) are theoretically possible. In this connection, it is worth entering special conventional signs of polycyclic metal complexes within the framework of analogous classification, namely to indicate for them, by means of figures in brackets, the number of atoms in metal cycles containing in these complexes. The number of these figures (three or four) will show the total number of metal cycles in this complex. The cycle numbering will be started from the leftmost one and then move clockwise along the cyclic loop perimeter. In addition, metal cycles formed as a result of "cross-linking", will be indicated on the second position (in the case of macrotricyclic complexes) and on the second and fourth positions (in the case of macrotetracyclic complexes). For example, complex having structural formula **I** will be marked as (**545**), complex having structural formula **II,** as (**565**), complex having structural formula **III,** as (**5656**), etc. (M – 3*d*-element atom).

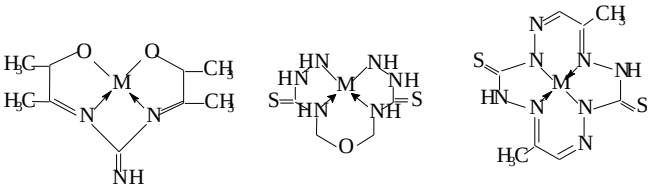

I II III

Self-assembly of aza- and azathiamacrocyclic metal chelates with the participation of (N,S)-ligsones and monocarbonyl compounds

The first experimentally observed case of self-assembly in MHF-**GIM** is the template process at the contact of $Ni_2[Fe(CN)_6]$-**GIM** with a water–alkaline (pH 12) solution containing dithiooxamide and formaldehyde leading to the formation of the diamagnetic brown (**565**)macrotricyclic compound Ni(II) with 2,8-dithio-3,7-diaza-5-oxanonan-dithioamide-1,9 [Ni**L**^{1}].[40] On the basis of data of the chemical analysis, mathematically treating the kinetic curves, UV–VIS, and IR spectroscopy in this and later works,[41–45] it has been shown that in this case the process (5) takes place.

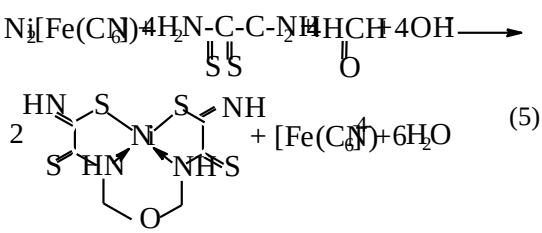

(5)

[Ni**L**^{1}]

Note that dithiooxamide in the water-alkaline solution does not interact with formaldehyde (at least at room temperature), therefore process (6) **can be** qualified as the template synthesis. In[43,45], it has been postulated that it proceeds according the following mechanism: at first, dithiooxamide is coordinated to Ni(II) via the donor N and S atoms, then formaldehyde comes into play as a "stitching agent":

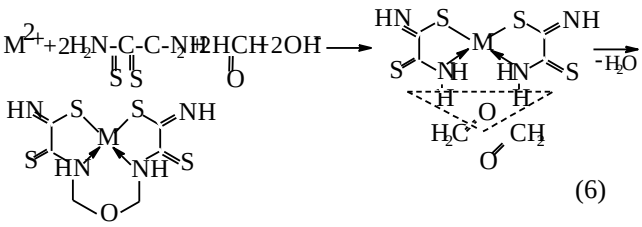

(6)

The fact that the "template" complex obtained under scheme (**5**) is not formed at the contact between any Ni(II) chelate with dithiooxamide and formaldehyde either at the complex formation in **GIM** or at the complex formation in the solution or the solid phase[43] serves as an indirect confirmation in favor of such mechanism, A process similar to (**5**) is implemented at the complex formation in the Cu(II)-dithiooxamide-formaldehyde system into a $Cu_2[Fe(CN)_6]$-**GIM**.[41,44,46,47] In the case of the Co(II)-

dithiooxamide-formaldehyde system at the complex formation into a $Co_2[Fe(CN)_6]$-**GIM**, the cobalt(II) complex formed according to the analogous reaction is only an intermediate and is immediately oxidized according to the reaction (**7**) into the heteroligand Co(III) complex containing the $\mathbf{L^1}$ chelant along with H_2O and the OH– group in the inner coordination sphere[44,48,49]

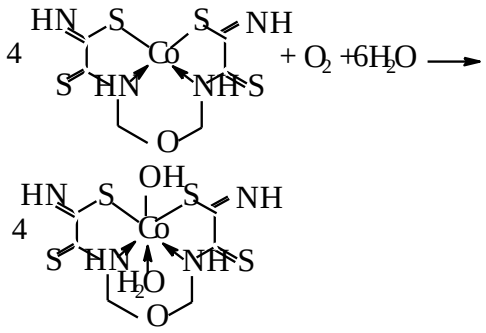

(7)

$[Co\mathbf{L^1}(H_2O)(OH)]$

In the Co(III)- dithiooxamide- formaldehyde system at the complex formation into a $KCo[Fe(CN)_6]$-**GIM**, the coordination compound with the composition of $[Co\mathbf{L^1}(H_2O)(OH)]$ is formed in one stage according to the scheme (**8**):[50]

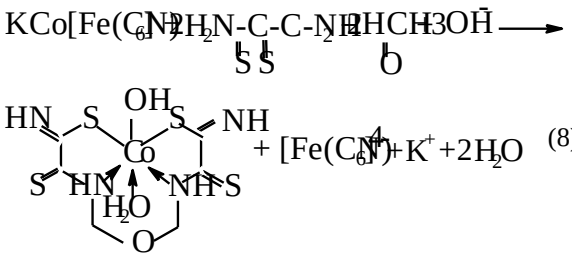

(8)

Processes analogous to (**5**) and (**7**) are implemented in the Fe(II)- dithiooxamide- formaldehyde system into a $KFe[Fe(CN)_6]$-**GIM**,[51] however, they have not yet been studied in more detail.

In the works[52,53] molecular structures of series of $M\mathbf{L^1}$ metalcomplexes have been determined. The typical examples of molecular structures of such metalchelates are presented in Figure 2. As you can see, the structures of Co(II), Ni(II) and Cu(II) macrotricyclic complexes with 2,8-dithio-3,7-diaza-5-oxanonandithio-amide-1,9 are extremely similar to each other. What puts of each of these complexes in a class by itself is that they, contrary to expectations, are non-coplanar; besides, both 5-numbered and 6-numbered chelate cycles having in their compositions, are non-coplanar, too. Among their number, the sum of valence angles in 6-numbered chelate cycle in the Co(II) complex is 620.8°, in the Ni(II) complex – 629.8°, in the Cu(II) complex– 623.0°, and these values differ strongly from sum of inner angles in the plane hexagon (720°).

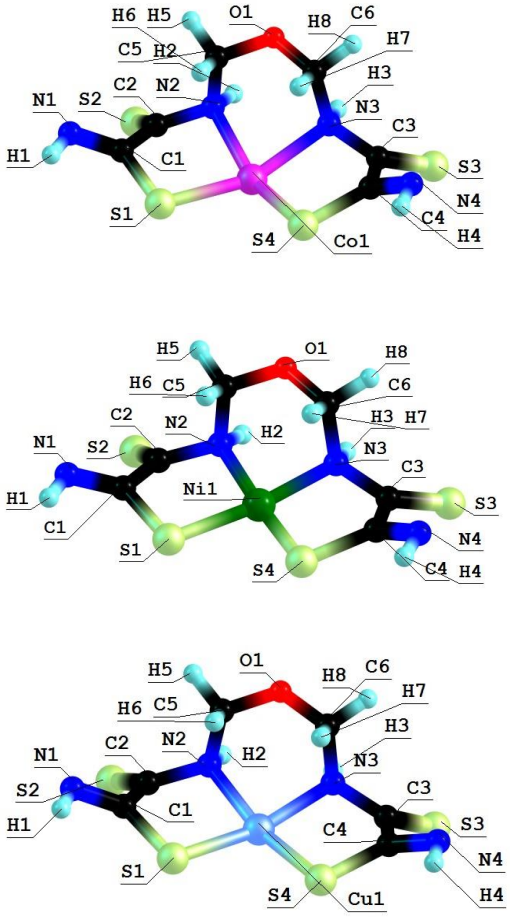

Figure 2. Molecular structures of $Co\mathbf{L^1}$ (on top), $Ni\mathbf{L^1}$ (in centre) and $Cu\mathbf{L^1}$ (on the bottom).

As for metal chelate MN_2S_2 cycle, it is practically plane in the case of $Ni\mathbf{L^1}$ and $Cu\mathbf{L^1}$ complexes whereas in the case of $Co\mathbf{L^1}$, there are only donor atoms in one plane [sum of valence angles between metal atom and donor atoms (SMN), (NMN), (NMS) and (SMS) is 358.2° (Ni), 356.8° (Cu), 353.9° (Co); sum of non-valence angles (SNN), (NNS), (NSS) and (SSN) in the each of these complexes is 360.0°].

The molecular structures of the $M\mathbf{L^1}(H_2O)(OH)$ complexes (M=Fe, Co) were determined in,[51,54] they are shown in Figure 3. To a certain extent, they resemble the structures of the $M\mathbf{L^1}$ complexes, since additional six-numbered metal cycle formed as a result of template "cross-linking", as in $M\mathbf{L^1}$, is not in the same plane with the MN_2S_2 grouping but, on the contrary, is very strongly declined [63.7° in the case of the Fe(III) complex and 55.5° in the case of Co(III)]. In this case, four atoms of six, contained in this cycle, namely two nitrogen and two carbon atoms, are in one plane; the plane (C)(O)(C) forms with (N)(C)(C)(N) plane the angle of 76.4° in the case of $Fe\mathbf{L^1}(H_2O)(OH)$ and 75.8° in the case of $Co\mathbf{L^1}(H_2O)(OH)$. For the Fe(III) complex as well as for the Co(III) complex, coplanar orientation of ligand $\mathbf{L^1}$ donor atoms, relative to corresponding metal ion, is energetically most favourable. In this case, the metal ion is located in one plane with $\mathbf{L^1}$ donor atoms [sum of angles (SMN), (NMS), (SMS) and (NMN) is very close to 360°].

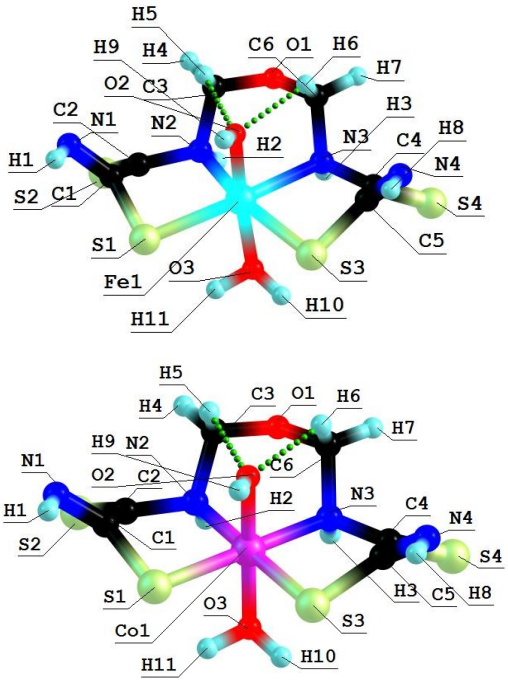

Figure 3. Molecular structures of Fe**L**^{1}(H_2O)(OH) (on top) and Co**L**^{1}(H_2O)(OH) (on the bottom)

It should be noted that in both M**L**^{1}(H_2O)(OH) complexes indicated, the values of the above-mentioned angles are rather close to each other. As for M–O bonds with H_2O and hydroxide-anion molecules, they, as it should be expected *a priori*, are a slightly different in their length from each other; in addition, the length of M–O bond for H_2O [~231.0 pm in the Fe(III) complex, ~204.8 pm in the Co(III) complex] is more than the length of M–O bond for OH^- [~183.8 pm in the Fe(III) complex, ~182.9 pm in the Fe(III) complex].

In[45,47,54–59], the possibility of implementing the "soft" template synthesis has been shown at the contact of MHF-**GIM** with the water-alkaline solutions containing dithiooxamide and such homologues of formaldehyde as acetaldehyde and acetone (M=Co, Ni, Cu). The kinetic curves and data of various physical and chemical methods indicate that, in the case of acetaldehyde, regardless of the template nature, the process proceeds according to the scheme (**9**) and is accompanied by the formation of the (**565**)macrotricyclic compounds with 4,6-dimethyl-2,8-dithio-3,7-diaza-5-oxanonandithioamide-1,9 **L**^{2}**.**

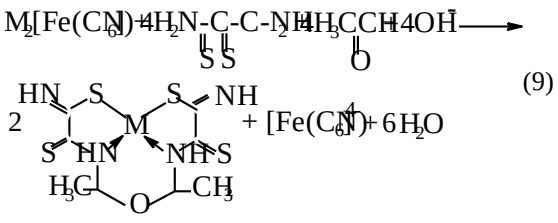

(9)

M**L**^{2}

In the case of acetone, according to the scheme (**10**) with the formation of (**565**) compounds with 4,4,6-trimethyl-2,8-dithio-3,7-diazanonendithioamide-1,9 **L**^{3}

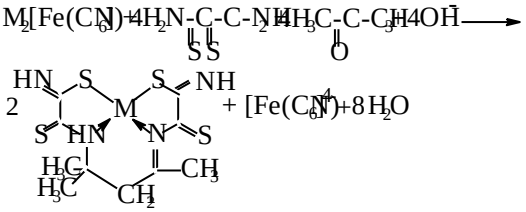

(10)

M**L**^{3}

Note that, in the case of formaldehyde and acetaldehyde, the (N,S,S,N)-donor chelant formed as a result of self-assembly contains oxygen, whereas in the case of acetone it does not. In[45,47], the possible mechanism of the reaction of the template synthesis in the M(II)-dithiooxamide- acetone system shown in the scheme (**11**) was proposed

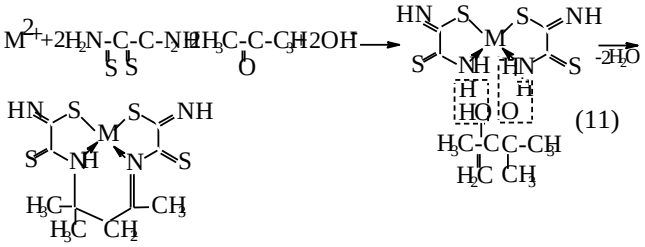

(11)

Molecular structures of complexes M**L**^{2}, as it should be expected, are extremely similar to ones of corresponding complexes M**L**^{1}. At the same time, molecular structures of M**L**^{3} complexes, according to data,[53,60,61] rather strongly differ from M**L**^{1} ones; they are shown in *Fig.4*.

In KFe[Fe(CN)$_6$] and KCo[Fe(CN)$_6$] **GIM**, the processes of self-assembly (**12**) are implemented. On the one hand, they are reminiscent of the general processes of (**8**),

and on the other hand, they are reminiscent of the general processes (**10**); therefore, similar [M**L**^{3}(H_2O)(OH)] (M = Fe, Co) complexes are formed[62,63]

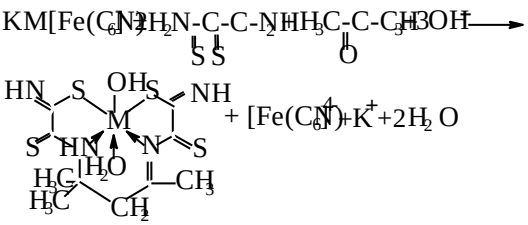

(12)

[M**L**^{3}(H_2O)(OH)]

Rather recently in[64–69], the "soft" self-assembly in the Cu(II)–dithiomalonamide– formaldehyde, Cu(II)–dithiomalonamide– acetone, and Cu(II)–thiocarbohydrazide–acetone systems was observed.

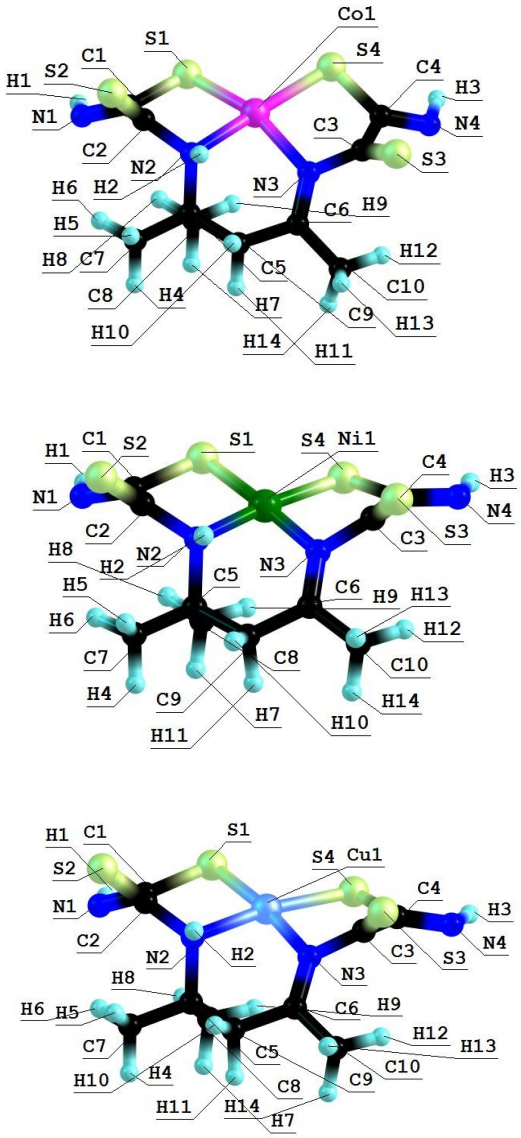

Figure 4. Molecular structures of Co**L**^{3} (on top), Ni**L**^{3} (in centre) and Cu**L**^{3} (on the bottom).

According to the data of works cited above, in the first of these systems the process according to the scheme (**13**) with the formation of the Cu(II) (**666**) complex with 3,9-dithio-4,8-diaza-6-oxaundecadithioamide-1,11 **L**^{4} occurs;

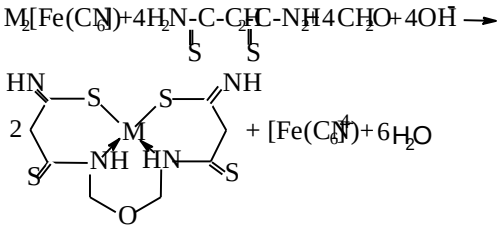

(13)

[M**L**^{4}]

in the second system, the process according to the scheme (**14**) with the formation of the Cu(II) (**666**) complex with 5,5,7-trimethyl-3,9-dithio-4,8-diaza-undecene-7-dithioamide-1,11 **L**^{5} occurs; and in the third system, with the formation of the heteroligand copper(II) (**565**) complex with 4,4,6-trimethyl-2,3,7,8-tetraazanonen-6-dithiohydrazide-1,9 **L**^{6} according to the scheme (15), takes place.

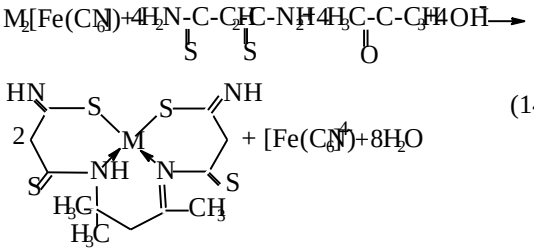

(14)

[M**L**^{5}]

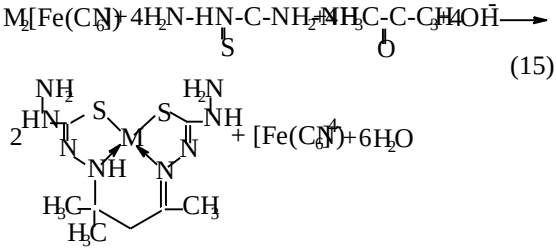

(15)

[M**L**^{6}]

It should be noted in this connection that for Ni(II)–thiocarbohydrazide– acetone systems at the complexing in solutions, two other processes, namely (**16**) and (**17**), occur (M = Ni):

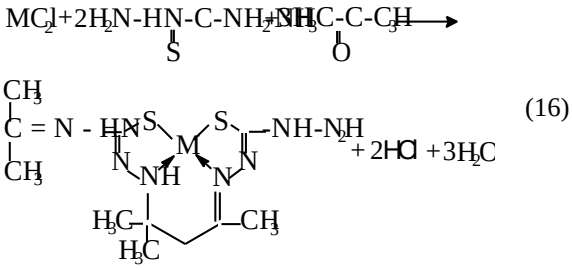

(16)

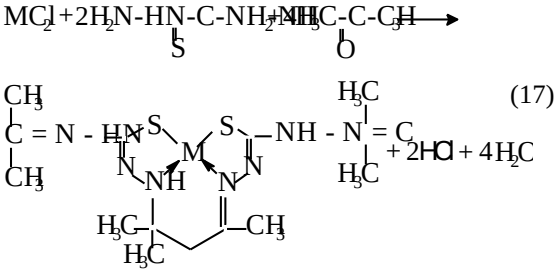

(17)

Note that, in the case of Cu(II), the processes of self-assembly are preceded by the alkaline destruction of $Cu_2[Fe(CN)_6]$ to $Cu(OH)_2$ hydroxide, which further reacts with the corresponding combination of ligsons. In the case of Ni(II), such process does not occur and $Ni_2[Fe(CN)_6]$ itself is apparently a stronger compound than the macrocyclic compounds which, in principle, could be

formed in the above triple systems. Most likely, this is the reason that when copper(II) hexacyanoferrate (II) is replaced by the nickel(II) compound of a similar structure, no process of self-assembly (**13-15**) is implemented. When Co(II) plays the role of the template, the character of the proceeding processes is apparently somewhat different, but no detailed information on this subject is available in the literature[69].

In the works[70,71] molecular structures of some M**L**^{6} complexes were determined; two such structures are presented in Fig. **5**. In the full harmony with theoretical expectations, these complexes as well as other above-mentioned (**565**)macrotricyclic compounds, are non-coplanar and have quasi-pyramidal orientation of N and S donor atoms to M(II).

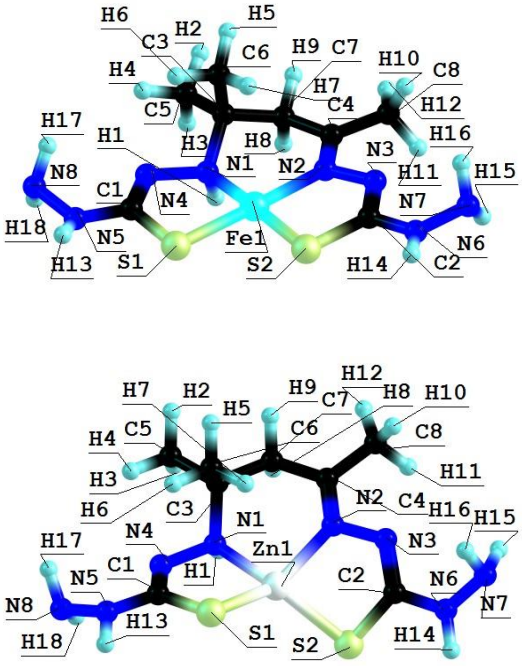

Figure 5. Molecular structures of Fe**L**^{6} (on top) and Zn**L**^{6} (on the bottom)

In the work,[72] the opinion about of possibility of self-assembly in the M(II)–thiooxamide–formaldehyde systems according to scheme (**18**) was voiced and mole-cular structures of a series 3*d*-elements M**L**^{7} (**565**)macrotricyclic complexes formed as a result of this process, were determined; some of them are presented in Fig. 6.

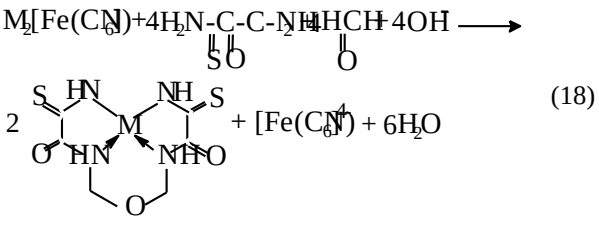

M**L**^{7}

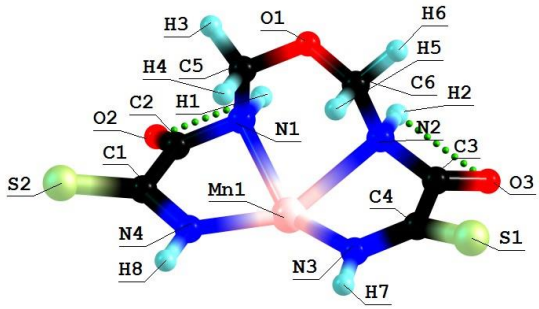

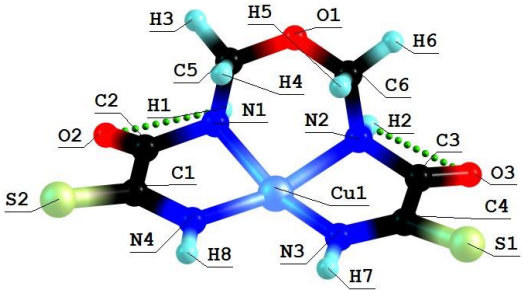

Figure 6. Molecular structures of Mn**L**^{7} (**on top**) and Cu**L**^{7} (**on the bottom**)

It should be noted in this connection that in[73] self-assembly in the cobalt(II), nickel(II) and copper(II) hexacyanoferrate(II) **GIM** has been fixed at its contact with the water-alkaline solution containing three reagents: dithiooxamide, formaldehyde and ammonia. In a similar system, not triple but fourfold (as each of these reagents performs the function of a ligson), the process of the complex formation proceeds according to the general equation (**19**) with the formation of the (**565**)macrotricyclic compound of M(II) ion with the 2,8-dithio-3,5,7-triazanonandithioamide-1,9 M**L**^{8} where M= Co, Ni, Cu

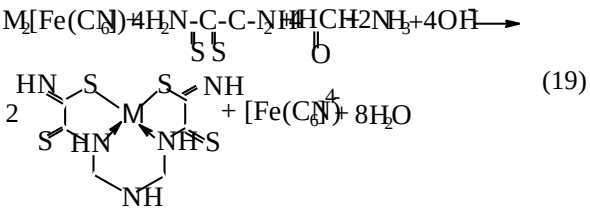

[M**L**^{8}]

The molecular structures of M**L**^{8} complexes were considered in[74]; as it was noted in the given article, these chelates are similar with M**L**^{1} ones. These structures for Co(II), Ni(II) and Cu(II) complexes are shown in Figure 7.

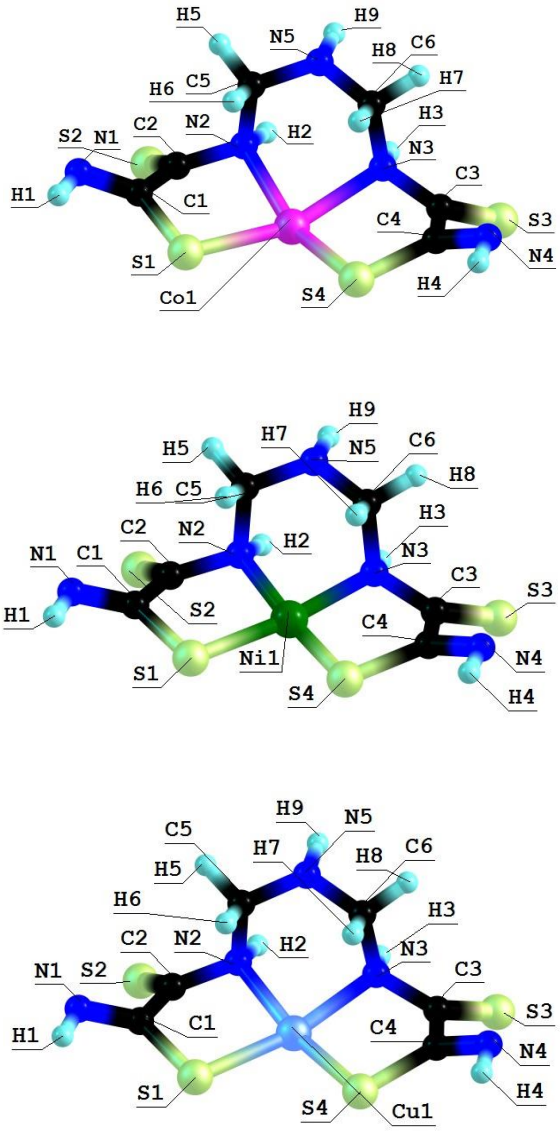

Figure 7. Molecular structures of Co**L**[8] (**on top**), Ni**L**[8] (in centre) and Cu**L**[8] (**on the bottom**).

As can be seen, molecular structures of these complexes, in whole, are like M**L**[1], M**L**[3] and M**L**[7] complexes and, also, are non-coplanar. In this connection, this non-coplanarity could be considered as general peculiarity of aza- and azathiatricyclic 3*d*-element complexes.

One can easily see that, in all the above cases, as a result of self-assembly in MHF-**GIM**, the macrotricyclic metal complexes with two five-member and one six-member cycles (**565**) or with three six-member cycles (**666**) are formed. There are some data that self-assembly with the formation of macrotetracyclic complexes of the (**5656**) type, for example M**L**[9], M**L**[10] and M**L**[11], according to the schemes (**20**-**22**), is possible,[75-77] molecular structures of some of them are shown in Fig. 8-10.

It should be noted in this connection that no of these macrotetracyclic complexes is plane; moreover, no of 5-numbered and 6-numbered cycles having in them, is not plane, too.[75-77]

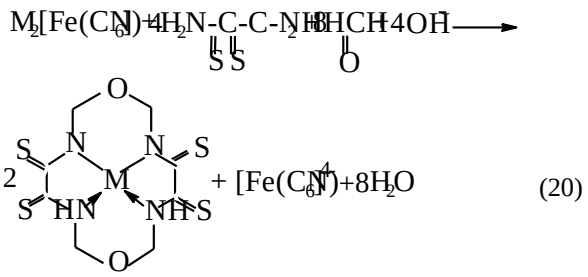

(20)

M**L**[9]

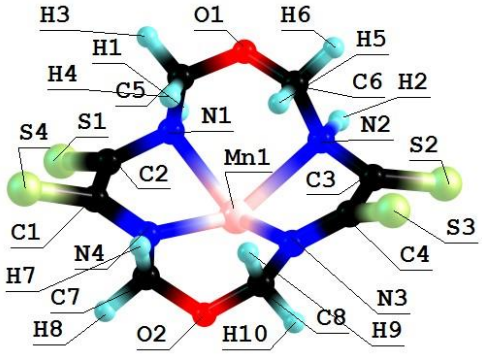

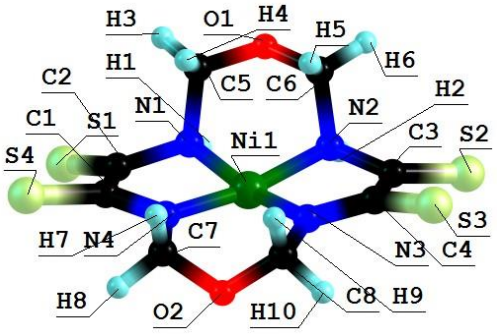

Figure 8. Molecular structures of Mn**L**[9] (**on top**) and Ni**L**[9] (**on the bottom**)

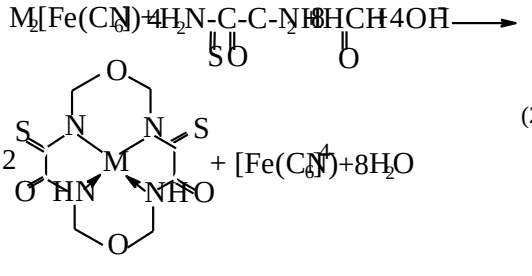

(21)

M**L**[10]

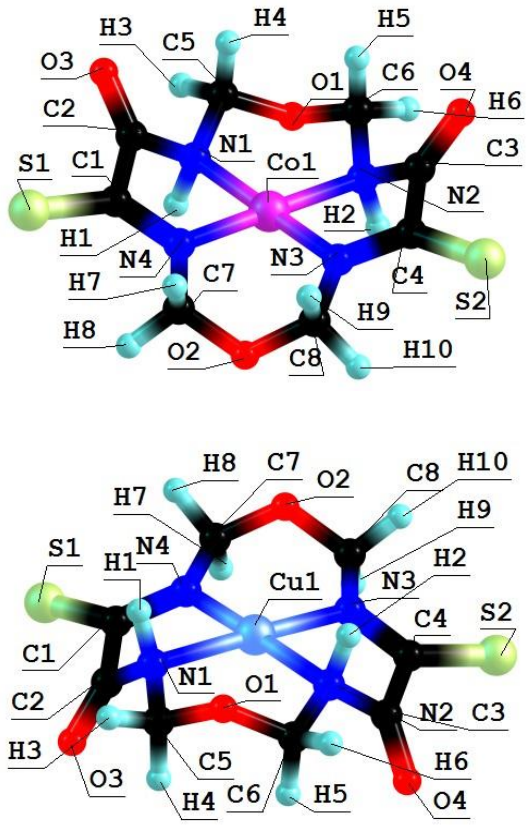

Figure 9. Molecular structures of Co**L**^{10} (**on top**) and Cu**L**^{10} (**on the bottom**)

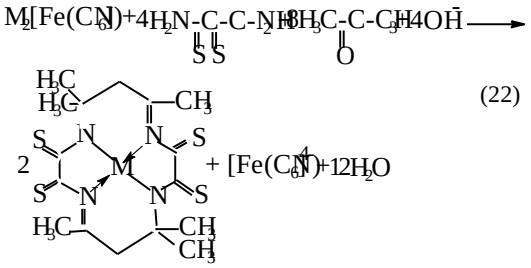

(22)

M**L**^{11}

The kinetic curves $D^{\blacktriangledown} = f(C_F, C_L^0, t)$, where C_F is the MHF concentration in the gelatinous matrix, C_L^0 is the (N,O,S) ligson concentration in the contacting **GIM** solution, and t is the time of the contact **GIM**/solution for all the above M(II) ion–(N,S)-ligson– monocarbonyl ligson systems, are simple enough and are characterized, as a rule, by the monotonous increase in the optical density values $D^{\blacktriangledown}$ with the increase in C_F, C_L^0 and t in the all systems considered. The examples of such curves are given in Figure 11.

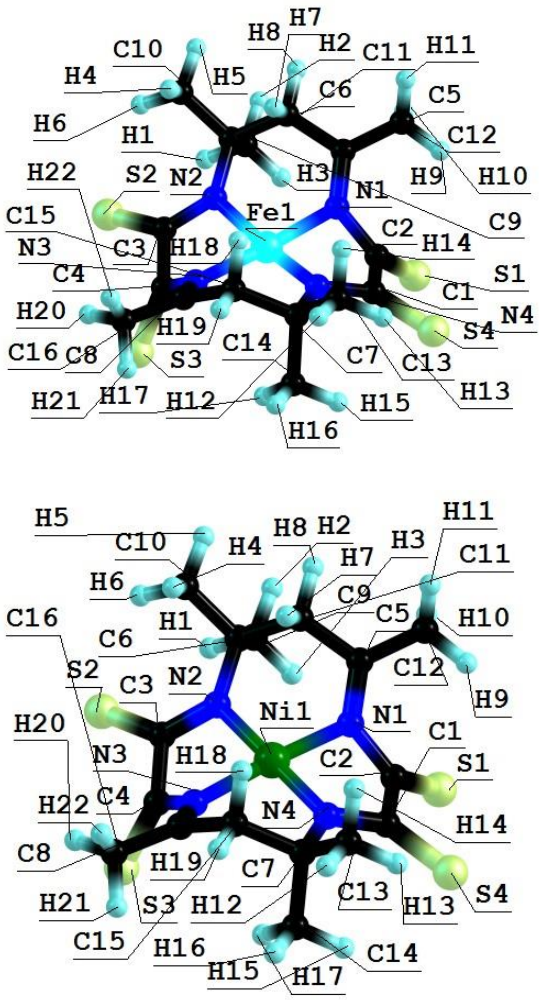

Figure 10. Molecular structures of Fe**L**^{11} (**on top**) and Ni**L**^{11} (**on the bottom**)

Self-assembly of aza- and azathiamacrocyclic metal chelates with the participation of (N,S)-ligsones and dicarbonyl compounds

It is easy to notice that, when monocarbonyl compounds are used for "stitching" the chelate cycles by the (N,S) ligson A in a single cyclic contour, at least two molecules of ligson B per one 3*d*-element atom are required. Thus, a certain structural reorganization occurs and, as a result, in some cases an oxygen atom appears in the additional chelate cycles (formaldehyde, acetaldehyde); in other cases this cycle contains only carbon and nitrogen atoms (acetone).

Interestingly, this additional cycle, as a rule, contains six atoms. The usage of dicarbonyl compounds in which the carbon atoms forming the C=O groups are close or separated by one, two, or three atoms, in the processes of self-assembly allows the implementation of one more possibility of "stitching" supposed theoretically when the additional cycle is formed at the participation of only one molecule of the carbonyl_containing ligson per one metal atom; in such a variant, this cycle can be both six-member and with another number of atoms (5, 7 or 8).

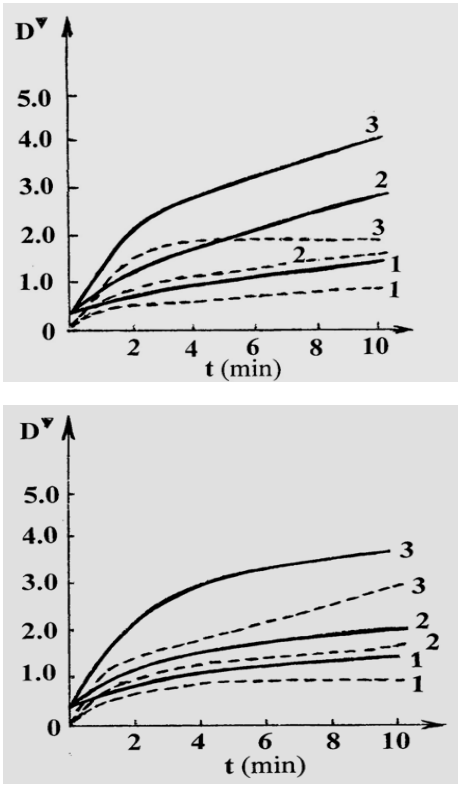

Figure 11. $D^{\blacktriangledown}$ = f(C_F,C_L^0,t) relationships in the Ni(II)–dithiooxamide– formaldehyde system in the coordinate section [C_F =constant, varied C_L^0, argument t] at dithiooxamide: formaldehyde molar ratio of 0.50 (left) and 1.00 (right) at C_F =0.60 (- - - - -) and 1.20 (——) mol•dm^{-3} and C_L^0 =5.0•10^{-2} (curves 1), 1.0•10^{-1} (curves 2) and 2.0•10^{-1} mol•dm^{-3} (curves 3). The optical densities of **GIM** ($D^{\blacktriangledown}$) were measured using a blue filter with a transmission maximum at 450 nm (adopted from work[43]).

The simplest dicarbonyl compound is known to be glyoxal HC(O)–CH(O). This compound has been used as a "stitching" ligson in a combination with the above-mentioned dithiooxamide in ref.[43,49,66–72] In this case, in $Ni_2[Fe(CN)_6]$- and $Cu_2[Fe(CN)_6]$-**GIM**, the process proceeds according to the generalized scheme (**23**)(see refs.[43,78–80] and refs.[78,79,81,84], respectively) and leads to the formation of the (**555**) macrotricyclic metal chelates with the (NSSN)-donor tetradentate chelant, 2,7-dithio-3,6-diazaoctadien-3,5-dithioamide-1,8 M**L**^{12}, where M = Ni, Cu.

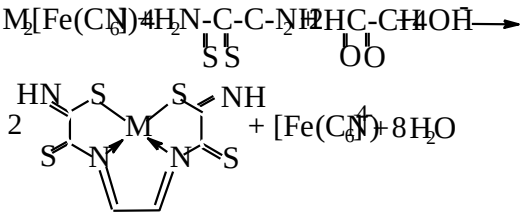

(23)

M**L**^{12}

In[43], the mechanism of this process described by the scheme (**24**) was proposed. In the case of $Co_2[Fe(CN)_6]$-GIM, self-assembly process proceeds in two stages; first is the reaction analogous to (**23**), and second is the oxidation of Co(II) to Co(III) according to the scheme (**25**) with formation of M**L**^{12}(H_2O)(OH) (where M= Co).[44,49,82]

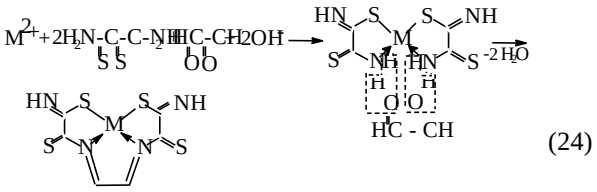

(24)

M**L**^{12}(H_2O)(OH)

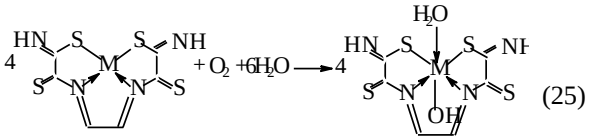

(25)

In KCo[Fe(CN)$_6$]-**GIM**, the process of self-assembly proceeds according to the scheme (**26**) and is accompanied by the formation of the same Co**L**^{12}(H_2O)(OH) macrotricyclic compound as in the Co(II)– dithiooxamide–glyoxal system[44,49,72,73] (M= Co)

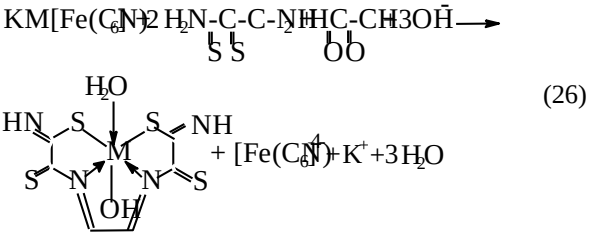

(26)

M**L**^{12} molecular structures were considered in[86]; for example, structures of Co**L**^{12}, Ni**L**^{12} and Zn**L**^{12} are shown in Fig. 12. One can easily note that this situation resembles the above situation in the Co(II)(Co(III))–dithiooxamide–formaldehyde systems.

Interestingly, in spite of the extensive literature on the processes of self-assembly of the metal macrocyclic compounds (for example, in[34,36] more than 1000 references to the publications on the this problem are given), no possibility of self-assembly even in one of the above systems in the solution or the solid phase is mentioned. Moreover, dithiooxamide, in spite of the availability of four mobile hydrogen atoms, has been never used as a ligson for template synthesis up until now. Apparently, this is due to the rather low proton donor ability of both dithiooxamide and its coordination compounds (and, respectively, the low mobility of protons at the nitrogen atoms coordinated to the metal ions) which is considerably enhanced in the gelatin bulk in the alkaline medium where the molecules of the given polymer, as was mentioned above, get the negative charge.

Recently, the "soft" template synthesis in the Cu(II)–dithiomalonamide– diacetyl system[87,88] and Cu(II)–thiocarbohydrazide– diacetyl system[89] was observed. According to the published data, in the first of these systems, the process (**27**) with the formation of the macrotricyclic complexes of the (**656**) type with the (NSSN) donor

tetradentate chelant, 5,6-dimethyl-1,10-diamine-1,10-dimercapto-4,7-diazadecatetraen-1,4,6,9-dithione-3,8 M**L**[13] (M = Ni, Cu) takes place

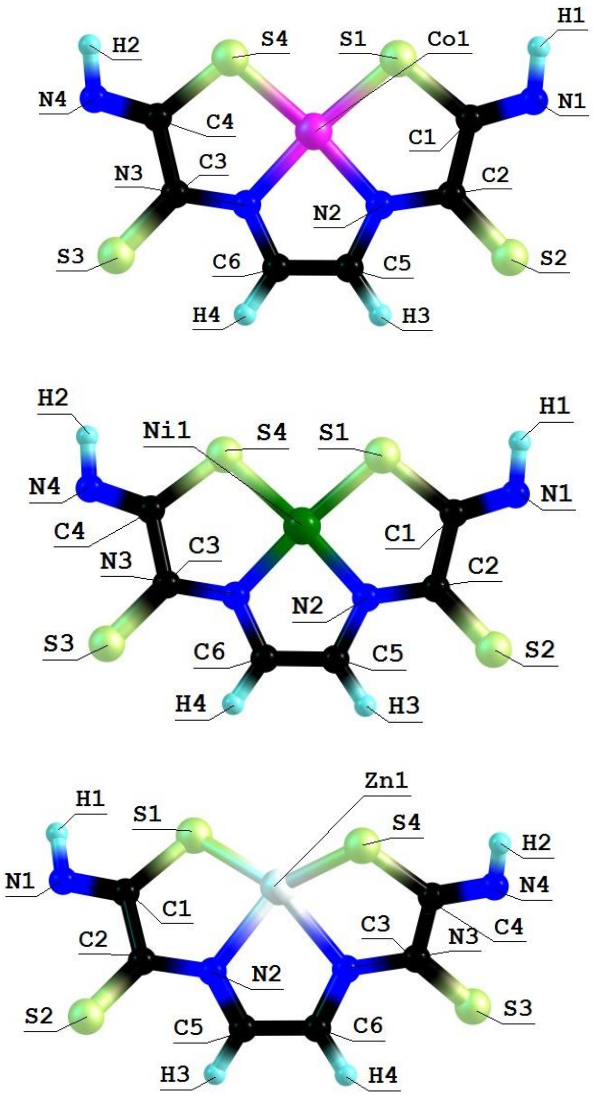

Figure 12. Molecular structures of Co**L**[12] (on top), Ni**L**[12] (in centre) and Zn**L**[12] (on the bottom).

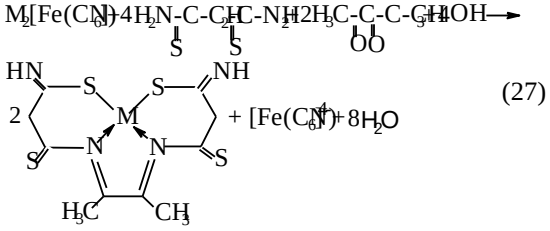

(27)

M**L**[13]

In the second of these systems, the formation of three complexes with two various chelants, namely two (**656**)macrotricyclic ones with 4,5-dimethyl-2,3,6,7-tetraazaoctadien-3,5-dithiohydrazide-1,8 **L**[14] and one (**5656**)macrotetracyclic ones with 3,10-dithio-6,7,13,14-tetramethyl-1,2,4,5,8,9,11,12-octacyclotetradecatetraene-1,5,7,12 **L**[15], according to the schemes (**4**.6, **4**.7) and (**4**.8), respectively[89], is observed (M= Cu)

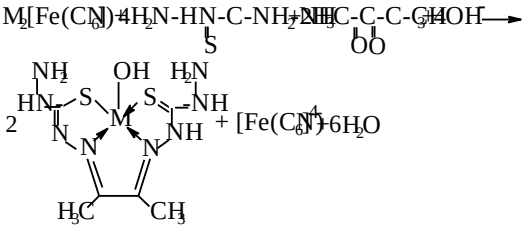

(28)

M**L**[14](OH)

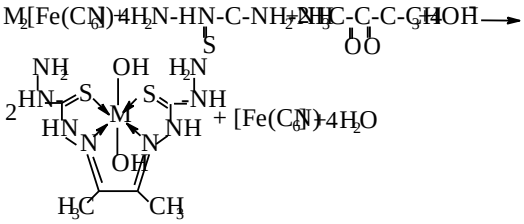

(29)

M(H**L**[14])(OH)$_2$

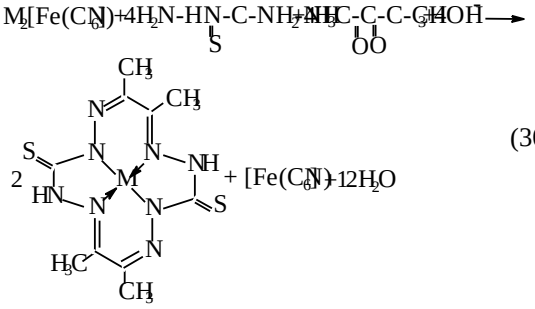

(30)

M**L**[15]

Molecular structure of M**L**[15] complexes was studied in ref.[90]; some of them are presented in Fig. 13. Because four non-planar methyl groups are the constituents of the test chelates, note that none of them can possess a fully coplanar structure.

Nevertheless, if we mentally remove these groups from the examination and take into consideration only chelate units and metal chelate rings for evaluating the structure coplanarity, we find that the complex of Cu(II) is ideally planar; the complexes of Fe(II), Co(II), and Ni(II) are almost ideally planar; and the complexes of Mn(II) and Zn(II) are noncoplanar only.

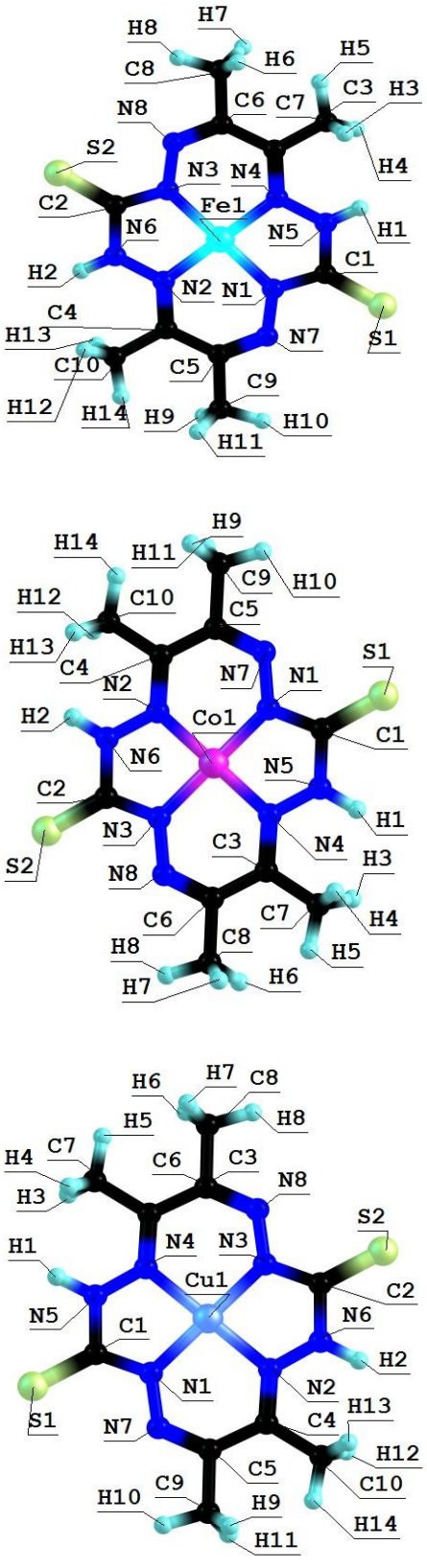

Figure 13. Molecular structures of Fe**L**[15] (on top), Co**L**[15] (in centre) and Cu**L**[15] (on the bottom).

Thus, a number of such complexes have a perfect or near perfect flat 14-membered macrocycle, which in itself is quite remarkable (if only because, even an 8-membered cycles, as it is well known in organic chemistry, are rarely flat).

Apart from glyoxal and diacetyl, as dicarbonyl ligson in the processes of self-assembly in the MHF-**GIM** has now tested only acetylacetone; this ligson was described in[91], where the process (**4**.9) with the formation of (**565**)macrotricyclic complexes M**L**[16] was realized

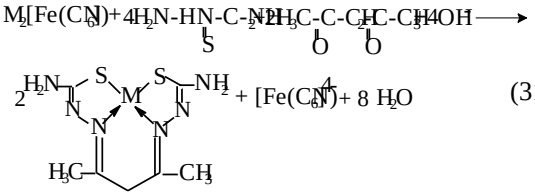

(31)

M**L**[16]

In ref.[92] the molecular structure of these complexes has been described in detail; some of them, namely the structure of the Ni(II) and Zn(II) chelates, are shown in Fig. 15. A very interesting feature of complexes considered in ref.[92], is that available in each of the 6-membered metal chelate cycle is essentially plane (sum of bond angles in them is different from the sum of the internal angles of the plane hexagon not more than 0.5°), although overall, they, like others previously considered (565)macrotricyclic metal chelates with N and S atoms in the macrocycle, are non-coplanar.

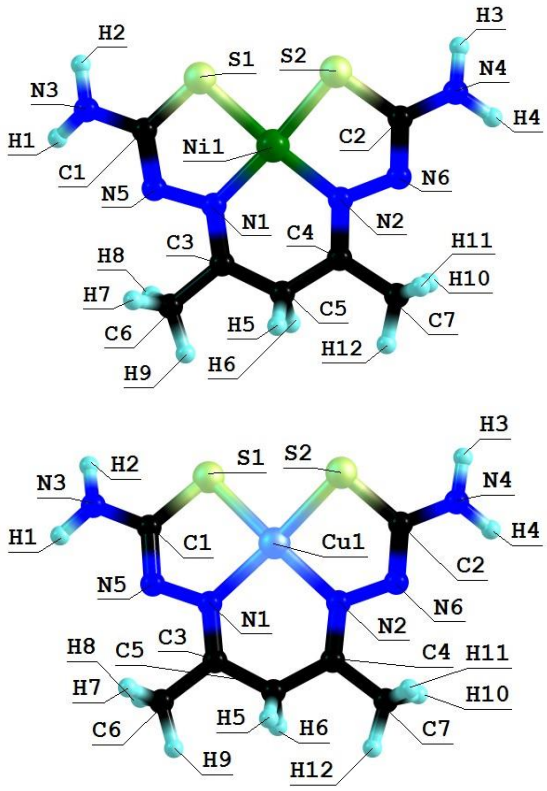

Figure 14. Molecular structures of Ni**L**[16] (left) and Cu**L**[16] (right)

As in the case of M(II) ion– (N,S)-ligson– monocarbonyl ligson systems, the kinetic curves $D^{\blacktriangledown} = f(C_F, C_L^0, t)$ for all the above M(II) ion–(N,S)-ligson– dicarbonyl ligson ones, are

simple enough and are characterized by the monotonous increase in the optical density values with C_F, C_L^0 and t increase in the all systems considered. The examples of such curves are given in *Fig. 16*.

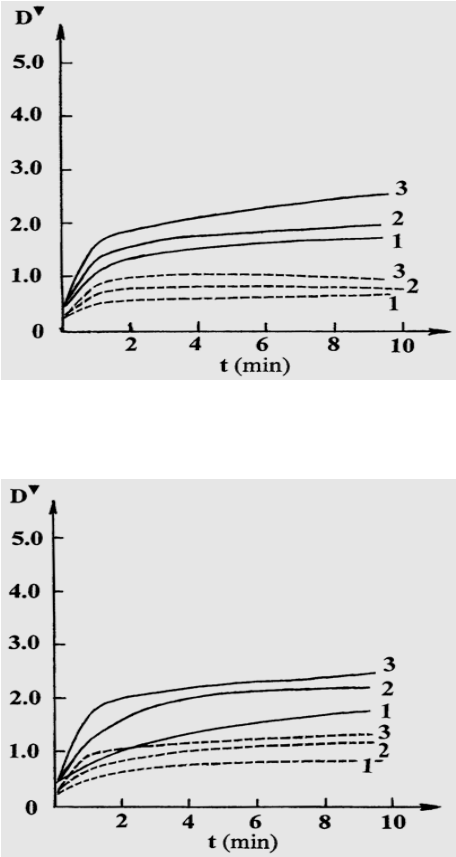

Figure 15. $D^{\blacktriangledown}$= f(C_F, C_L^o,t) relationships in the Co(II)-dithiooxamide-glyoxal system in the coordinate section [C_F =constant, varied C_L^o, argument t] at molar dithiooxamide: glyoxal ratio of 0.50 (**on top**) and 1.00 (**on the bottom**) at C_F =0.20 (- - - - -) and 0.40 (——) mol dm^{-3} and C_L^o=3.0•10^{-3} (curves 1), 6.0•10^{-3} (2) and 1.2•10^{-2} mol dm^{-3} (3). The optical densities of **GIM** ($D^{\blacktriangledown}$) were measured using a blue filter with a transmission maximum at 450 nm (adopted from work[49]).

It should be noted that the processes of self-assembly are implemented in a number of other triple systems containing dithiooxamide, dithiomalonamide, and thiocarbohydrazide as a (N,S)-ligson; however, the composition and the molecular structure of the metal complexes formed and chelants in their internal coordination sphere has to be specified.

At the present time, there is a lot of publications in literature where self-assembly processes of azamacrocyclic and thiaazamacrocyclic chelates were described (see, for example,[34,36,93-104]; in this connection, there are strong reasons to believe that the possibilities of the template synthesis in thin films of MHF **GIM** are high enough and the above list of triple metal ion– ligand synthon A– ligand synthon B systems in which it is implemented can be considerably expanded.

Conclusion

The information available at present, some fragments of which are presented in this review, allows one to state that one more "branch" in molecular nanotechnology, self-assembly, and the template synthesis of metal macrocyclic and supramolecular compounds in the biopolymer-immobilized matrix systems at the rigid fixation of a metal ion and the relatively high mobility of the organic compounds participating in self-assembly is being established. This field of nanochemistry operates with own objects and is based on constructive principles and methodical and methodological approaches. The present stage of its development, however, is rather far from its apogee regarding both the accumulation of the experimental data and their theoretical understanding, generalization, and systematization. In this field, in fact, only the first (though appreciable enough) steps are being made and the circle of the researchers working there is extremely limited. It is difficult to say what the reason for this is: whether no "initial raw material" necessary for the implementation of the processes of self-assembly in **GIM** is available to the majority of researchers, the researchers are inert, there is difficulty in understanding and quantitatively interpreting the experimental data obtained in these specific conditions, or it is simply an unwillingness to shift from the "traditional" conditions of the chemical experiment. Anyway, at the present stage of the development of this field of molecular nanotechnology, a lot of problems have appeared vividly. It would be good to mention some of them.

In the fundamental theoretical aspect, first of all, this includes improving the model for a description of the kinetics of self-assembly in MHF **GIM**. One "sketch" of such model has been given already by the author of this review in the book[5]. However, this model and its mathematical apparatus in fact do not consider the chemical nature of the metal ion M in MHF, let alone the nature of ligsons interacting with it. In addition, these reagents are actually considered particles with sizes extremely small if compared with the sizes of the pores of the polymeric bulk in which they diffuse during self-assembly. From the physical and chemical points of view, neither the first nor the second approximation can be considered completely correct (though on the whole this model yields quite good results when applied in practice). Another problem is to reveal the role of the gelatin molecules in the "choice" of the actual mechanism of the self-assembly processes happening in **GIM**, their function in the formation of the gelatin matrix as an organizing medium, and the transformations of the gelatin molecules in these processes (which are related, in particular, to a certain structural reorganization due to the rotation of all regions of each α-chain with respect to the axial line of the gelatin molecule).

The problem of the considerable expansion of the variety of metal complex **GIM** used in the processes of self-assembly is one of the fundamental pragmatic problems. First of all, it is the development of technologies of the immobilization of various metallorganic compounds containing both inorganic (CO and NO) and organic (allyl and cyclopentadienyl_anions, arenes) π-acceptor ligands in their structure which are now a considerable part of modern inorganic chemistry.

There are no obstacles in this respect from the theoretical point of view (except for the substance immobilized in **GIM** not having a low enough solubility in water). From our point of view, in the near future, self-assembly with the participation of the gelatin-immobilized heteronuclear and cluster metal complexes, in particular heterobinuclear and heteropolynuclear MHF various ions of the *p*-, *d*- and *f*-elements, may get an considerable impetus for development. The expansion of the variety of the solvents which are a part of the solutions of ligsons in contact with **GIM** during self-assembly belongs to the same category of problems, because the conformation of the gelatin molecules and the charge arising on them affecting the character and the results of the process under consideration strongly depend on the solvent nature. Although it is rather probable that their list will be limited only to those liquids which are liophilic with respect to gelatin and those liquids which form homogeneous systems with water, even in view of such restrictions it should be rather long.

As to the problems of the particularly pragmatic aspect, revealing the possibilities of the practical use of **GIM** containing metal macrocyclic compounds formed in the processes of self-assembly is undoubtedly of highest priority. Thus, it is rather probable that such systems will be effective catalysts of a number of practically important processes both in "conventional" chemical technology and in nanotechnology. Since gelatin refers to the category of the hydrophilic biopolymers, it is doubtless that similar **GIM** in the future can find their niche in biochemistry and biophysics and medicine and pharmacology. Revealing the particular possibilities of the gelatin-immobilized metal macrocyclic compounds could be considered one of the current problems of modern molecular nanotechnology.

Acknowledgments

Russian Foundation for Basic Research (RFBR) is acknowledged for the financial support of this research (grant No. **09-03-97001**).

References

[1]Thomas, A. L., *Phthalocyanines,* Research & Applications, CRC Press, **1990**.

[2]Hoss, R., Fogtle, F., *Angew. Chem*., **1994**, *106*, 389-398.

[3]*Synthetic Coordination and Organometallic Chemistry*, Ed. by Garnovskii, A. D. and Kharisov, B. I., Marsel-Dekker, New York – Basel, **2003**.

[4]Vigato, P. A., Tamburini, S., *Coord. Chem. Rev*., **2004**, *248*, 1717-2128.

[5]Mikhailov, O. V., *Gelatin_Immobilized Metal Complexes,* Scientific World, Moscow, **2005**.

[6]*The Science and Technology of Gelatin*, Ed. by Wird, A. G. and Courts, A., Academic Press, New York, **1977**.

[7]*Encyclopedia of Polymers*, Ed. by Kargin, V. A., Soviet Encyclopedia, Moscow, **1972**, Vol. 1.

[8]*Encyclopedia of Polymers*, Ed. by Kabanov, V. A., Soviet Encyclopedia, Moscow, **1977**, Vol. 3.

[9]Ramachandran, G. N., In: *Treatise on Collagen*, Academic, New York, **1967**, Vol. I, pp. 187-188.

[10]Boedker, H., Doty, P., *J. Phys. Chem*., **1954**, *58*, 968–983.

[11]James, T. H., Mees, C. E., *The Theory of the Photographic Process*, Macmillan, New York, **1972**.

[12]James, T. H., *The Theory of the Photographic Process*, Macmillan, New York, **1977**.

[13]*Photographic Gelatin*, Ed. by Cox, R. J., Academic Press, London, **1972**, Vol. I.

[14]*Photographic Gelatin*, Ed. by Cox, R. J., Academic Press, London, **1976**, Vol. I.

[15]Veis, A., Anesey, J., Cohen, J., *Arch. Biochem. Biophys*., **1961**, *94*, 20–31.

[16]Veis, A., Drake, M. P., *J. Biol. Chem*., **1963**, *238*, 2003–2011.

[17]Rich, A., Crick, F. H. C., *Nature*, **1955**, *176*, 915–916.

[18]Cowan, P. M., McGavin, S., North, A. C. T., *Nature*, **1955**, *176*, 1062–1066.

[19]Ferry, J. D., *Advances in Protein Chemistry*, Academic Press, New York, **1948**, Vol. 4.

[20]Chen, J. M., Kung, C. E., Feairheller, S. E., Brown, E. M., *J. Protein Chem*., **1991**, *10*, 535–552.

[21]Fridman, R., Fuerst, T. R., Bird, R. E., Hoyhtya, M., Oelkuct, M., Kraus, S., Komarek, D., Liotta, L. A., Berman, M. L., Stetler-Stevenson, W. G., *J. Biol. Chem*., 1992, *267*, 15398–15405.

[22]Banyai, L., Tordai, H., Patthy, L. J., *J. Biol. Chem*., **1996**, *271*, 12003–12008.

[23]Tordai, H., Patthy, L., *Eur. J. Biochem*., **1999**, *259*, 513–518.

[24]Caldararu, H., Timmins, G. S., Gilbert, B. C., *Phys. Chem. Chem. Phys*., **1999**, *1*, 5689–5695.

[25]*Handbook of Hydrocolloids*, Ed. by Phillips, G. O., Williams, P. A., Woodhead, London, 2000.

[26]Lin, W., Yan, L., Mu, C., Li, W., Zhang, M., Zhu, O., *Polym. Int*., **2002**, *51*, 233–238.

[27]Pickford, A. R., Potts, J. R., Bright, J. R., Han, I., Campbell, I. D., *Structure*, **1997**, *5*, 359–370.

[28]Gehrmann, M. L., Douglas, J. T., Banyai, L., Tordai, H., Patthy, L., Llinas, M., *J. Biol. Chem*., **2004**, *279*, 46921–46930.

[29]Trexler, M., Briknarova, K., Gehrmann, M., Llinas, M., Patthy, L., *J. Biol. Chem*., **2003**, *278*, 12241–12246.

[30]Groome, R. J., Clegg, F. G., *Photographic Gelatin*, Focal Press, London, **1965**, pp. 35-40.

[31]Pratt, W. B., Hackney, J. F., *Biochemistry*, **1971**, *10*, 3002–3008.

[32]Hulmes, D. J. S., Miller, A., Parry, D. A. D., *J. Mol. Biol*., **1973**, *79*, 137–148.

[33]Ramachandran, G. N., Kartha, G., *Nature*, **1955**, *176*, 593–597.

[34]Gerbeleu, N. V., Arion, V. B., *Template Synthesis of Macrocyclic Compounds*, Shtiintsa, Kishineu, **1990**.

[35]Lehn, J. M., *Supramolecular Chemistry: Concepts and Perspectives*, Wiley, Weinheim, **1995**.

[36] Gerbeleu, N. V., Arion, V. B., Burgess, J., *Template Synthesis of Macrocyclic Compounds*, Wiley, Weinheim, 1999.

[37]A.D. Garnovskii, A. D., Vasil'chenko, V. S., Garnovskii, D. A., *Contemporary Topics of the Synthesis of Metal Complexes: The Main Ligands and Techniques*, LaPO, Rostov, 2000.

[38]Mikhailov, O. V., *Russ. Chem. Rev*., **1995**, *64*, 657-671.

[39]Mikhailov, O. V., *Revs. Inorg. Chem*., **1997**, *18*, 287–332.

[40]Mikhailov, O. V., *Russ. Chem. Rev*., **1997**, *66*, 665-678.

[41]Mikhailov, O. V., Khamitova, A. I., *Mendeleev Commun*., **1998**, *3*, 96–97.

[42]Mikhailov, O. V., Khamitova, A. I., *Russ. J. Phys. Chem*., **1998**, *72*, 921–925.

[43]Mikhailov, O. V., Khamitova, A. I., Shigapova, L. S., Busygina, T. E., *Transition Met. Chem*., **1999**, *24*, 503–510.

[44]Mikhailov, O. V., Khamitova, A. I., Morozov, V. I., *Heterocyclic Commun*., **2000**, *6*, 137–142.

[45]Mikhailov, O. V., *Int. J. Inorg. Mater*., **2001**, *3*, 1053–1061.

[46]Mikhailov, O. V., Khamitova, A. I., *Russ. J. Coord. Chem*., **1999**, *25*, 795–799.

[47]Mikhailov, O. V., *Transition Met. Chem*., **2000**, *25*, 552–558.

[48]Mikhailov, O. V., Khamitova, A. I., *Russ. J. Gen. Chem*., **1998**, *68*, 1187–1193.

[49]Mikhailov, O. V., Khamitova, A. I., *Transition Met. Chem*., **2000**, *25*, 26–31.

[50]Mikhailov, O. V., Khamitova, A. I., *Russ. J. Coord. Chem*., **1998**, *24*, 807–810.

[51]Mikhailov, O. V., Chachkov, D. V., *J. Coord. Chem*., **2009**, *62*, 1058–1066.

[52]Chachkov, D. V., Mikhailov, O. V., *Russ. J. Inorg. Chem*., **2009**, *54*, 1952-1956.

[53]Chachlov, D. V., Mikhailov, O. V., *Macroheterocycles*, **2010**, *3*, 161-167.

[54]Mikhailov, O. V., *Russ. J. Gen. Chem*., **2002**, *72*, 1525–1530.

[55]Mikhailov, O. V., *Russ. J. Coord. Chem*., **2002**, *28*, 352–357.

[56]Mikhailov, O. V., *Russ. J. Coord. Chem*., **2002**, *28*, 32–38.

[57]Mikhailov, O. V., *Russ. J. Gen. Chem*., **2001**, *71*, 1676–1681.

[58]Mikhailov, O. V., Kazymova, M. A., Shumilova, T. A., Vafina, L. R., *Heterocycl. Commun*., **2000,** *6*, 357–362.

[59]Mikhailov, O. V., Chachkov, D. V., *J. Coord. Chem*., **2010**, *63*, 4309–4318.

[60]Chachkov, D. V., Mikhailov, O. V., *Russ. J. Inorg. Chem*., **2010,** *55*, 1243-1247.

[61]Chachkov, D. V., Mikhailov, O. V., *Russ. J. Gen. Chem*., **2008**, *78*, 1849-1861.

[62]Mikhailov, O.V., *Russ. J. Gen. Chem*., **2008,** 78, 82–89.

[63]Mikhailov, O.V., Kazymova, M. A., *Transition Met. Chem*., **2008,** *33*, 523–527.

[64]Mikhailov, O.V., Kazymova, M. A., Shumilova, T. A., Solovieva, S. E., Mannafov, T. G., *Transition Met. Chem*., **2003,** *28*, 592–594.

[65]Mikhailov, O.V., Kazymova, M. A., Shumilova, T. A., Solovieva, S. E., *Transition Met. Chem*., **2003,** *28*, 665–667.

[66]Mikhailov, O.V., Kazymova, M. A., Shumilova, T. A., *Heterocycl. Commun*., **2003,** *9*, 61–64.

[67]Mikhailov, O.V., Kazymova, M. A., Shumilova, T. A., *Russ. J. Gen. Chem*., **2008**, *78*, 258–263.

[68]Mikhailov, O.V., Kazymova, M. A., Shumilova, T. A., Solovieva, S. E., *Russ. J. Gen. Chem*., **2009**, *79*, 24–30.

[69]Mikhailov, O.V., Kazymova, M. A., Chachkov, D. V., *Macroheterocycles* **2008,** *1*, 90–97.

[70]Chachkov, D.V., Mikhailov, O.V., Astaf'ev, M. N., *J. Struct. Chem*., **2009,** *50*, 613-617.

[71]Chachkov, D.V., Mikhailov, O.V., *Russ. J. Phys. Chem*., **2011,** *85*, 152-155.

[72]Chachkov, D.V., Mikhailov, O.V., *Russ. J. Inorg. Chem*., **2011,** *56*, 1935-1942.

[73]Mikhailov, O.V., *Heterocycl. Commun*., **2001,** 7, 79–82.

[74]Chachkov, D.V., Mikhailov, O.V., *Russ. J. Inorg. Chem*., **2011,** *56*, 223-231.

[75]Mikhailov, O.V., Chachkov, D.V., *Macroheterocycles*, **2009,** *2*, 271–275.

[76]Chachkov, D. V., Mikhailov, O. V., *Russ. J. Inorg. Chem*., **2012,** *57*, 981-986.

[77]Mikhailov, O. V., Chachkov, D. V., *Eur. Chem. Bull*., **2014,** *3*, 515-519.

[78]Mikhailov, O. V., Khamitova, A. I., Morozov, V. I., *Int. J. Inorg. Mater.*, **2001,** *3*, 161–167.

[79]Mikhailov, O. V., Khamitova, A. I., Mingalieva, L. S., *Heterocycl. Commun*., **2001,** *7***,** 359–363.

[80]Mikhailov, O. V., Khamitova, A. I., *Russ. J. Coord. Chem*., **2000,** *26*, 804–808.

[81]Mikhailov, O. V., Khamitova, A. I., *Russ. J. Coord. Chem*., **1998,** *24*, 629–633.

[82]Mikhailov, O. V., Khamitova, A. I., *Russ. Chem. Bull*., **1999,** *48*, 1975–1981.

[83]Mikhailov, O. V., Khamitova, A. I., *Russ. J. Gen. Chem*., **1997,** *67*, 1913–1924.

[84]Mikhailov, O. V., Kazymova, M. A., Shumilova, T. A., *Transit. Met. Chem*., **2007**, *32*, 1056-1060.

[85]Mikhailov, O. V., Khamitova, A. I., Kazymova, M. A., *Transit. Met. Chem*., **2005,** *30*, 22–26.

[86]Chachkov, D. V., Mikhailov, O. V., *Russ. J. Inorg. Chem*., **2012,** *57*, 205-210.

[87]Mikhailov, O. V., Kazymova, M. A., Shumilova, T. A., Chmutova, G. A., Solovieva, S. E., *Transit. Met. Chem*., **2005,** *30*, 18–21.

[88]Kazymova, M. A., Shumilova, T. A., Mikhailov, O. V., Solov'eva, S. E., *Russ. J. Coord. Chem*., **2008**, *34*, 102–105.

[89]Mikhailov, O. V., Kazymova, M. A., Shumilova, T. A., Solovieva, S. E., *Transit. Met. Chem*., **2004,** *29*, 732–736.

[90]Mikhailov, O. V., Chachkov, D. V., *Russ. J. Inorg. Chem*., **2013,** *58*, 174-179.

[91]Kazymova, M. A., Makarova, L. A., Mikhailov, O. V., Shumilova, T. A., *Int. Symp. Adv. Sci. Org. Chem.* (Miskhor, Crimea, June 21-25, **2010**), Abstracts, **C-83**.

[92]Chachkov, D. V., Mikhailov, O.V., Shamsutdinov, T. F., *Russ. J. Inorg. Chem*., **2013,** *58*, 548-553.

[93]Tsymbal, L. V., Rosokha, S. V., Lampeka, Ya. D., *J. Chem. Soc., Dalton Trans*., **1995,** *16*, 2633-2637.

[94]Fabbrizzi, L., Liccelli, M., Manotti Lanfredi, A. M., Vassali, O., Ugozzoli, F., *Inorg. Chem*., **1996**, *35*, 1582-1589.

[95]Rudolf, M., Dautz, S., Jager, E. G., *J. Am. Chem. Soc*., **2000,** *122*, 10821-10830.

[96]Judele, R., Dix, M. J., Laschat, S., Baro, A., Nimtz, M., Menzel, D., Schoenes, J., Doll, K., Zwicknagl, G., Niemeyer, M., *Z. anorg. allgem. Chem*., **2008,** *634*, 299–310.

[97]Trommel, J. S., Marzilli, L. G., *Inorg. Chem*., **2001**, *40*, 4374-4383.

[98]Lu, X., Geng, Z., Wang, Y., Lu, B., Kang, J., *Synth. React. Inorg.-Met.-Org. Chem*., **2002,** *32*, 949-966.

[99]Garcia, K. W., Basinger, J., Williams, S., Hu, C., Wagenknecht, P. S., Nathan, L. C., *Inorg. Chem*., **2003,** *42*, 4885-4890.

[100]Singh, A. K., Singh, R., Saxena, P., *Transition Met. Chem*., **2004**, *29*, 867-869.

[101]Salavati-Niasari, M., *Inorg. Chem. Commun*., **2004**, *7*, 698-700.

[102]Ali Khan, T., Ghani, S. S., Shakir, M., Tabassum, S., *Synth. React. Inorg. Met. Org. Nano-Met. Chem*., **2005**, *35*, 509-513.

[103]Salavati-Niasari, M., Davar, F., *Inorg. Chem. Commun*., **2006**, *9*, 175-179.

[104]Fuliang Zhang, Liang Shen, *J. Chem. Cryst.*, **2010,** 40, 681-685.

Received: 28.07.2014.
Accepted: 11.10.2014.

IN VIVO TOXICITY OF NANOPARTICLES: MODALITIES AND TREATMENT

Sufia Naseem[a]*, Manzoor Ahmad Gatoo[a]#, Ayaz Mahmood Dar[b]§, and Khusro Qasim[c]

Keywords: nanoparticles; surface charge; aggregation; lymphatic, circulatory system and respiratory system.

In the present scenario, the burgeoning field of nanotechnology is playing central role in various real world applications. Researches engrossing nanoparticles are evolving at a rapid pace owing to which engineered nanomaterials are increasingly becoming part of daily life in the form of cosmetics, food packaging, drug delivery, therapeutics, biosensors, etc. It is intrigued that the properties of nanoparticles which bestow them their unique physicochemical characteristics could also lead to adverse biological consequences such as increased uptake and interaction with the biological systems. Nanomaterials, due to their small size could enter the body through various semi open anatomical interfaces and can penetrate through cells and organelles and disrupt their normal function, which could lead to tissue inflammation, altered cellular redox balance or even cell death. Nanoparticles unlike larger particles can transverse through the circulatory/lymphatic to various vital organs of the body including nervous systems and brain. Nanomaterials could lead to various allied illnesses including bronchitis, asthma, lung and liver cancer, Parkinson's disease, Alzheimer's disease, Crohn's disease, heart disease and colon cancer. Reckoning with the unprecedented applicability's of nanomaterials in daily life, avenues for direct or indirect exposures of nanoparticles to human beings increases, which raises concern about their role *in vivo* toxicity. This necessitates intensive research to have knowledge of the various routes of nanoparticle exposure and their effects upon the human health. This review is an attempt to evaluate the various modes of exposure of nanoparticles in human beings, mechanism of toxicity, their fate inside body and adverse health effects.

Corresponding Authors
E-mail: sufianaseem@gmail.com*, manzbio@gmail.com#, ayazchem09@gmail.com§
[a] Department of Biochemistry, Jawaharlal Nehru Medical College, Aligarh Muslim University, Aligarh, India
[b] Department of Chemistry, Aligarh Muslim University, Aligarh, India
[c] Department of Mechanical Engineering, Aligarh Muslim University, Aligarh, India

Introduction

Nanotechnology has been defined as the design, characterization, production and application of structures, devices and systems by controlling shape and size at nanometre scale while nanoparticles are classified as particles having one or more dimensions in order of 100 nm or less.[1] Research engrossing nanoparticles is currently an area of intense scientific interest due to their wide potential applications in diverse fields including biomedical, optical and electronics field. Semiconductors, metallic, magnetic and polymeric-nanosystems made possible the early diagnosis and new treatments for many diseases including multiple sclerosis, atherosclerosis and cancer.[2] For instance, super paramagnetic iron oxide NPs (SPIONs) have been used for magnetic labelling, cell isolation, hyperthermia, imaging and controlled drug release.[3] Nanomaterial based entities have potential applications in developing smart targeted drug delivery vehicles, biocompatible implants, sensor and diagnostic systems and besides biomedical applications, NPs are also used commercially in various products such as electronic components, scratch-free paint, sports equipment, cosmetics, food colour additives and surface coatings. Reckoning their potential applications, engineered nanomaterials with new chemical and physical properties are being produced on daily basis; resulting in increased exposure to environment and human beings, yet there is little understanding of the unique toxicological properties of NPs and their long-term impact on human health and infact there is considerable gap between the available literature on the nanomaterials production and toxicity evaluations.

Lately, air pollution studies have generated indirect evidence for the role of combustion derived nanoparticles (CDNP) in driving adverse health effects in susceptible groups. Reasonably, owing to the nano size, NPs are capable of entering the human body by exploiting various semi open anatomical surfaces of human beings viz. skin, respiratory tract and gastrointestinal tract (GIT). It has been evidenced that through inhalation they gain entry into the respiratory tract (most common route of exposure) and through ingestion or nasopharyngeal route they could enter the GIT. They could also breach the intact skin tissues and beside these, they could translocate the systemic circulation and through the blood stream could reach various organs of the body such as liver, spleen, bone marrow and nervous system including brain. Moreover, implants and injections also serve minor role for their entry into the body.

Since anquity, human beings have been directly or indirectly exposed to NPs. Particle toxicology and the consequent adverse health effects of asbestos fibres and coal dust, serve as landmark references to the development of nanotoxicologic concepts.[4] Nanomaterials owing to their diverse chemical, optical, magnetic and structural properties may display different toxicological profiles, thus generalization of potential toxicological effects is extremely difficult[5] and requires scruiting at individual level. Typical nanoparticles that have been studied in this regard include

titanium dioxide, alumina, zinc oxide, carbon black, and carbon nanotubes and "nano-C60". Nanoparticle overload can instigate stress reactions that could lead to inflammation and weaken the body's defence system. Non-degradable or slowly degrading nanoparticles not only accumulate in bodily organs but can also interact or interfere with biological processes inside the body.

Although size is the key factor in determining the potential toxicity of a particle, other properties including chemical composition, shape, surface structure, surface charge, aggregation, presence of functional group and solubility play their role in imparting toxicity. Chemical composition of nanoparticles is responsible for their reactivity while their surface charge is responsible for their electrostatic interactions. Surface area to volume ratio of these particles increases their interaction with the surrounding molecules. Of note, upon exposure to tissue and fluids, they could immediately adsorb onto their surface and affect their functionalities. Hydrophobicity and sometimes lipophilic groups of nanoparticles allows them to interact with proteins and membranes, respectively. Besides complementary nanostructure could cause inhibition of enzyme activity either competitive or noncompetitive while accumulation of an inert particle in the body could trigger tissue formation around the foreign entity leading to formation of a scar tissue.

Mechanism of nanoparticle toxicity in the body

Unlike larger particles, nanoparticles may be taken up by cell mitochondria and the cell nucleus and can cause DNA mutation and major structural damage to mitochondria, even resulting in cell death. Nanomaterials like silver-coated gold nanoparticles, fullerenes, block copolymer micelles and carbon nanotubes may be capable of localizing to mitochondria and inducing apoptosis, ROS formation, DNA damage, cell-cycle arrest, mutageneses which are possible intrigued as sources of *in vivo* toxicity.[6]

The toxicity of nanomaterials can occur through three different mechanisms in the body: *i*) dissolution process of nanomaterials in biological media, *ii*) catalyst properties of nanomaterials and *iii*) reduction and oxidation (Redox) evolution of the surfaces.[7] It has been demonstrated that nanoparticles could penetrate into cells and by transcytosis could transverse through epithelial and endothelial cells into the lymphatic circulation to reach various sensitive parts of the body, such as bone marrow, brain, spleen, heart and nervous system including brain.

In experimental models, it has been observed that nanomaterial exposure ensues in oxidative stress, ROS generation, mitochondrial perturbation, inflammation, brain and peripheral nervous system injury, enzyme activity loss, atherogenesis, thrombosis, stroke, myocardial infarction, autoimmunity and DNA damage leading to mutagenesis and carcinogenesis. Of note, nanoparticles can reach the cell mitochondria and cell nuclei, which in turn cause DNA mutation and induce major structural damage and cell death [8] but most intracellular and *in vivo* toxicities from NPs arise from the production of excess reactive oxygen species (ROS).[9,6]

The Figure 1 depicts the interaction of nanoparticles with the cell and various mechanisms involved in nanotoxicity.

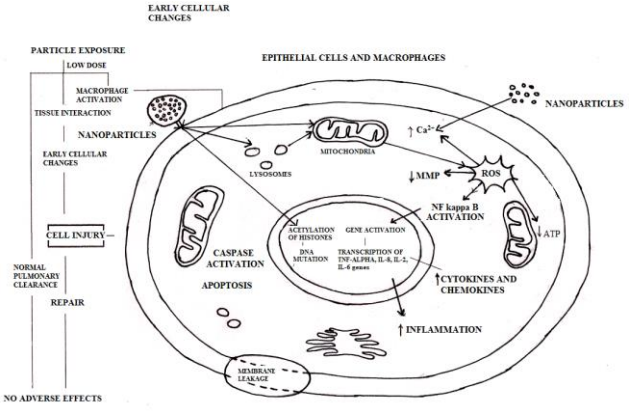

Figure 1. Nanoparticles interaction with the cell and various mechanisms involved in toxicity

Reactive oxygen species are both physiologically necessary and potentially destructive. Although moderate levels of ROS play specific roles in the modulation of several cellular events[10] but increased ROS levels is indicative of oxidative stress and can damage cells by peroxidizing lipids, altering proteins, disrupting DNA, interfering with signalling functions and modulating gene transcription[4,11,12] and finally ending up in cancer, renal disease, neurodegeneration, cardiovascular or pulmonary disease. Toxicity from ROS can be more pronounced in the central nervous system (CNS) due to the high content of unsaturated fatty acids, which are susceptible to peroxidation.[12] ROS also play a role in the development of vasculopathies, including those that define atherosclerosis, hypertension and restenosis after angioplasty.[13] Accumulation of NPs in the liver and spleen leads to imbalance in ROS homeostasis and antioxidant defences, making these organs main targets of oxidative stress.

Nel et al.,[14] described nanoparticle-induced oxidative stress affects cell signalling in three stages. A low level of oxidative stress enhances transcription of defence genes through transcription factor nrf2. A higher level of oxidative stress activates inflammation signalling through NFkB, and very high levels are connected with activation of apoptotic pathways and necrosis. Changing these signalling pathways in cells is associated with the carcinogenic effects of NPs. Peterson and Nelson[15] reviewed the ROS toxicity of NPs towards the cell nucleus and DNA material and observed that it leads to double strand breaks, which are considered the most lethal type of oxidative DNA damage. Damage to mtDNA due to excess amount of ROS is reported to be associated with several clinical syndromes such as neurogenic muscle weakness, ataxia and retinitis pigmentosa, mitochondrial encephalomyopathy, lactic acidosis, stroke like episodes, retinitis pigmentosa, cardiac conduction defect and elevated cerebrospinal fluid protein.[16]

Apart from ROS effects, certain physicochemical properties of NP can also induce toxicity. To mitigate ROS effects, some new steps have been taken in NP design. Recently, cerium oxide nanoparticles have been developed that incorporate oxygen defects which scavenge free radicals and prevent oxidative stress.

Nanoparticles: Routes of entry, translocation and their clearance from the body

Nanostructures can enter the body via six principle routes viz. intra venous, dermal, subcutaneous, inhalation, intraperitoneal, oral and through inhalation and amongst these airborne inhalation of nanosized particles (NPs) i.e. entry through the respiratory tract is the most likely route of exposure to nanoparticles. Exposure via other routes has not been studied in detail and is less plausible unless it is by direct ingestion through food or drug delivery, dermal contact through application of oils and skin creams, or as a contaminant in water through a nanoparticle-treated membrane system. Absorption can occur where the nanostructures first interact with biological components and then they can distribute to various organs in the body and may remain the same structurally, be modified, or metabolized and can reside in the cells for an unknown amount of time before leaving to move to other organs or to be excreted.[17] Figure 2 shows possible routes of entry of nanoparticles in the body and their adverse health effects.

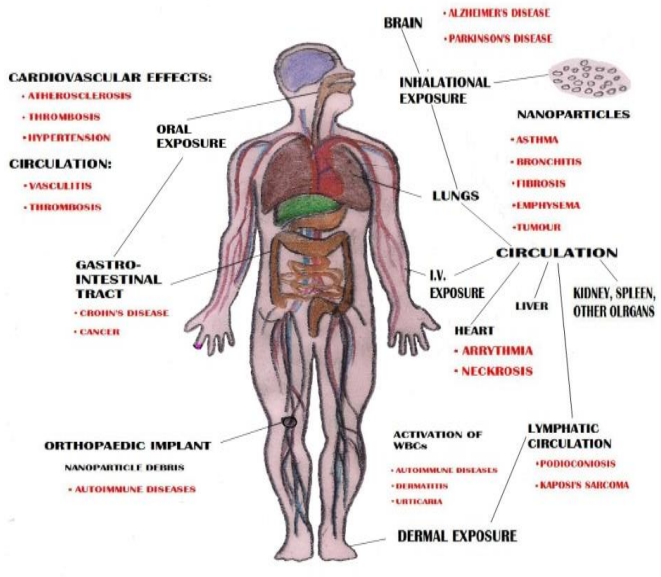

Figure 2. Possible routes of entry of nanoparticles in the body and their adverse health effects.

Respiratory uptake of nanoparticles

Inhalation of airborne nanoparticles through the respiratory tract is the most common means of entry in humans as mentioned above. Of note, lungs represent the primary entry port for inhaled particles. It has been shown that the inhaled nanoparticles are efficiently deposited by diffusional mechanisms in all regions of the lungs and with decrease in the particle size, notably below 500 nm, the deposition increases due to increasing diffusion mobility. Hoet et al.[18] summarized that most nanosized spherical solid materials easily enter the lungs. Particles of different sizes deposit differently in the airways, as well as the alveolar region so depict different effects in different parts of the lungs which is particularly important in children with developing lungs and in asthma and COPD patients. The smaller the particles, the higher the probability that the particle will hit the epithelium of a lung structure. Spherically shaped solid material with particle diameters less than 10 microns can reach the gas exchange surfaces. Larger diameter particles, with size and diameters of 10 microns or more tend to be deposited further up in the respiratory tract as a result of gravitational settling, impaction, and interception.[19] Many larger diameter fibres are deposited at "saddle points" in the branching respiratory tree. On the epithelium walls of the respiratory tract, particles contact first the mucous or serous lining fluid and its surfactant layer on top. Therefore, the fate of particle compounds soluble in this lining fluid of respiratory tract needs to be distinguished from slowly dissolving or even insoluble compounds.

The clearance of deposited particles in the respiratory tract is by physical translocation to other sites, and chemical clearance. Chemical dissolution in the upper or lower respiratory tract occurs for biosoluble particles in the intra-cellular or extra-cellular fluids, and they are sequestered to the circulatory and lymphatic systems. Slowly dissolving and insoluble NP deposited on the airway are cleared by means of mucociliary escalator and phagocytosis by alveolar macrophages. In the upper airways, particle clearance is performed mainly by the mucociliary escalator[20] into the gastrointestinal tract[21], lymphatic system[22] and circulatory systems.[4] From the gastrointestinal tract, nanoparticles are eliminated in the feces, while from the lymphatic and circulatory systems; they may be distributed to organs, including kidneys from where partial or total clearance may occur. The cilia of the bronchial epithelial cells move the sparingly soluble and insoluble particles which are covered and trapped in the mucous, away from the lungs into the pharynx and nasopharynx and are then removed by means of coughing and sneezing. Slowly dissolving and insoluble NP deposited in the alveolar region are only taken up and digested to a limited amount by alveolar macrophages which transport nanoparticles to the larynx where they are swallowed and excreted after passage through the gastro-intestinal tract. The remaining NP will interact with the cells of the epithelium such that NP will be taken up by those cells or transported into the interstitial spaces. As a result, most NP will be no longer retained as free particles on the epithelium while insoluble NP may stay for months and years in the lungs. Particles less than 10 microns can reach the lower airways.[23] The particle clearance from the lung alveoli occurs primarily through macrophage phagocytosis. If the particle is digested by lysosome enzymes, the residues are removed by exocytosis. If not, phagocytosis is followed by gradual movement of macrophages with internalized particles towards the mucociliary escalator, a process that can last up to 700 days in humans.[4] If the macrophage is unable to digest the particle and the particle produces damage to phagosomal membrane due to peroxidation, it will lead to reduced cell motility, impaired phagocytosis, macrophage death, and ultimately reduced clearance of particles from the lung.[24] If particles cannot be cleared by macrophages, they can kill successive macrophages attempting to clear them, and create a source of oxidative compounds, and inflammation with macrophage debris accumulation in form of pus. Oxidative stress is associated with various diseases, such as cancer, neurodegenerative, and cardiovascular diseases. This mechanism of alveolar clearance is not perfect, as it allows smaller nanoparticles to penetrate the alveolar epithelium and reach the interstitial space and from there, they may enter the circulatory and lymphatic systems and reach other sites throughout the body.[25] Phagocytosis occurs in different areas of the body having different names, according to their location, such as

alveolar macrophages, splenic macrophages and Kupfer cells, respectively. Translocation after inhalation of NP in the lung is not only towards the liver but also spleen, kidneys, brain and heart.[25]

Nervous system uptake of nanoparticles

Inhaled nanoparticles are shown to reach the nervous system via the olfactory nerves[26,4] or by breaching the blood-brain-barrier.[26,27] The nasal and tracheo-bronchial regions have many sensory nerve endings.[4] More recent studies confirm the uptake of inhaled nanoparticles from olfactory mucosa via the olfactory nerves.[4,26,28] Rat inhalation studies with 30 nm magnesium oxide[29] and 20-30 nm carbon[28] nanoparticles indicate that nanoparticles translocate to the olfactory bulb. [29]

The passage of nanoparticle to the nervous system is also possible via the blood-brain-barrier. Regarding the passage of nanoparticles, the blood-brain-barrier permeability is dependent upon the charge of nanoparticles[30] and allows a larger number of cationic nanoparticles to pass compared to neutral or anionic particles, due to the disruption of its integrity[30] Increased blood-brain-barrier permeability observed in hypertension, brain inflammation[26], respiratory tract inflammation[27] allows nanoparticles access to the nervous system.

Lymphatic systems uptake of nanoparticles

Translocation of nanoparticles to lymph nodes is a topic of intense investigation today for drug delivery and tumor imaging.[22] Several studies have shown that interstitially injected particles pass preferentially through the lymphatic system and not through the circulatory system, probably due to permeability differences[22] and get located in the lymph nodes.[22] The free nanoparticles reaching the lymph nodes are ingested by resident macrophages.[31] Nanoparticles that are able to enter the circulatory system can also gain access to the interstitium and from there could be drained through the lymphatic system to the lymph nodes as free nanoparticles and/or inside macrophages. [22, 31]

Circulatory system uptake of nanoparticles

Nanoparticles, unlike larger particles, are able to translocate across the respiratory epithelium after being deposited in the lungs.[4,32] Once, they have crossed the respiratory epithelium, they may persist in the interstitium for years, or they may enter the lymphatic system and circulatory system.[22] Inhalation or instillation studies in healthy animals have shown that metallic nanoparticles with size smaller than 30 nm pass rapidly into the circulatory system[4,22,32] while non-metallic nanoparticles with size between 4 and 200 nm pass feebly or do not pass at all.[33] In contrast, subjects suffering from respiratory and circulatory diseases have higher capillary permeability, allowing fast translocation of metallic or non-metallic nanoparticle into circulation.[33] From the circulatory system, long-term translocation to organs such as the liver, heart, spleen, bladder, kidney, bone marrow is possible, depending on the duration of exposure.[4] Evidence of rapid translocation of metal nanoparticles from lungs into the circulation and to organs has been provided by animal studies. These results have shown that nanoparticles with diameters of 30 nm (Au)[4], 22 nm (TiO2)[32] could be located in pulmonary capillaries; whereas particles of 15 nm (Ag)[25] and welding fumes[34] could be located in blood, liver, kidney, spleen, brain, and heart. Animal studies on rats with inhalation of titanium dioxide nanoparticles (22 nm diameter) have shown that they could translocate to the heart as evidenced by their presence in the heart connective tissue (fibroblasts).[32] Within 30 minutes post exposure, large quantities of intratracheally instilled gold nanoparticles (30 nm) has been found in platelets inside of pulmonary capillaries of rats.[4] On the contrary, there is no conclusive evidence for fast translocation of carbon-based non metal nanomaterials in systemic circulation.

Nanoparticle uptake by red blood cells is entirely dictated by size, due to absence of phagocytic receptors[27] while the nanoparticle charge or material type plays feeble roles. On the contrary, nanoparticle charge plays an essential role in their uptake by platelets; thereby influencing blood clot phenomena's.[35] Uncharged polystyrene particles do not have any effect on blood clots formation. Negatively charged nanoparticles significantly inhibit thrombi formation, while positively charge nanoparticles enhance platelet aggregation and thrombosis[35] due to interaction of the positively charged nanoparticles with negatively charged platelets leading to reduction of their surface charge, making them more prone to aggregation. Until now, it was thought that blood clots can be formed due to three main causes: when the blood flow is obstructed or slowed down, when the vascular endothelial cells are damaged, or due to the blood chemistry. However, it seems possible, in the view of recent findings that nanoparticles may act as nucleating centres for blood clots.[36] Microscopic and energy dispersive spectrometry (EDS) analysis of blood clots from patients with blood disorders revealed the presence of foreign nanoparticles.[36] Most notably, patients with the same type of blood disorder show fibrous tissue clots embedding nanoparticle with different composition.

Organ uptake of nanoparticles

Micro and nanoparticle debris has been detected by scanning electron microscopy in organs and blood of patients with orthopaedic implants[37], drug addiction[37], worn dental prostheses[38], blood diseases[36], colon cancer, Crohn's disease and ulcerative colitis.[39] The pathway of exposure most likely involves the translocation from lungs to circulation of the inhaled nanoparticles, followed by uptake by the organs. Rat inhalation studies with stainless steel welding fumes showed that manganese accumulates in blood and liver.[34] Rat inhalation studies with 4-10 nm silver nanoparticles have shown that within 30 minutes, the nanoparticles enter the circulatory system, and after a day can be found in the liver, kidney and heart, until subsequently cleared from these organs after a week.[25] Clearance from the liver can occur via biliary secretion into the small intestine. A case study shows that the wear of dental bridges leads to the accumulation of wear nanoparticles in liver and kidneys.[38] The maximum size of particles found in the liver (20 microns) was larger than in the kidneys (below 6 microns), suggesting that particles are absorbed by intestinal mucosa, translocate to liver before reaching the circulatory system and kidneys. After the removal of dental bridges, particles in stool are no longer observed.

Gastro-intestinal tract uptake of nanoparticles

Endogenous sources of nanoparticles in the gastro-intestinal tract are derived from intestinal calcium and phosphate secretion.[39] Exogenous sources are particles from food such as colorants – titanium oxide, pharmaceuticals, water, or cosmetics including toothpaste, lipstick, dental prosthesis debris[38] and inhaled particles.[25] The dietary consumption of nanoparticles in developed countries is estimated around 1012 particles/person per day[38] and mainly consists of TiO2 and mixed silicates. These nanoparticles do not degrade in time and accumulate in macrophages. A portion of the particles cleared by the mucociliary escalator can be subsequently ingested into the gastro-intestinal tract. Also, a small fraction of inhaled nanoparticles was found to pass into the gastrointestinal tract.[25] Particles that penetrate the mucus reach the enterocytes and are able to translocate further.[18] Diseases, such as diabetes, may lead to higher absorption of nanoparticles in the gastrointestinal tract. [18] The extent of particles absorption in the gastro-intestinal tract is affected by size, surface chemistry and charge, length of administration, and dose.[18] The absorption of particles in the gastro-intestinal tract decreases with increase in size of nanoparticles. For example study of polystyrene particles with size between 50 nm and 3 μm indicated that their uptake is 6.6%, 5.8%, 0.8% and 0% for nanoparticles of size 50 nm, 100nm, 1μm and 3 μm respectively.[40] The kinetics of particles in the gastro-intestinal tract depends strongly on the charge of the particles. Positively charged latex particles are trapped in the negatively charged mucus while negatively charged latex nanoparticles diffused across the mucus layer and became available for interaction with epithelial cells.[18]

It is generally assumed that nanomaterials do not remain in gastro-intestinal tract for indefinite periods.[18] Most of the studies of ingested nanoparticles have shown that they are eliminated rapidly; 98% in the faeces within 48 hours and most of the remainder via urine.[4] However, other studies indicates that certain nanoparticles can translocate to blood, spleen, liver, bone marrow, lymph nodes, kidneys, lungs, and brain, and can also be found in the stomach and small intestine.[40]

Dermal uptake of nanoparticles

The skin is composed of three layers; epidermis, dermis and subcutaneous and the outer portion of the epidermis is called stratum corneum.[18] As with many subjects involving nanoparticles, dermal penetration is still controversial.[26] Several studies have shown that nanoparticles are able to penetrate the stratum corneum.[4,26,41,42] Nanoparticles penetration through the skin typically occurs via the hair follicles[41], flexed[42] and broken skin.[4] Intracellular nanoparticles penetration is also possible, as demonstrated by in vitro experiments.[43] MWCNTs are internalized by human epidermal keratinocytes in cytoplasmic vacuoles and induce the release of pro-inflammatory mediators.[43] Spherical particles with diameter between 750 nm and 6 microns selectively penetrate the skin at hair follicles with a maximum penetration depth of more than 2400 microns (2.4 mm).[43] Broken skin facilitates the entry of a wide range of larger particles (500 nm - 7 μm).[4] Translocation of nanoparticles from skin into the lymphatic system occurs by soil particles found in lymph nodes as has been revealed in patients with podoconiosis. Neuronal transport of small nanoparticles along sensory skin nerves may also be possible, in a similar way to the proven path for herpes virus.[4] Penetration of the TiO2 nanoparticles (found in commercially available sunscreens) into the skin [44] is believed to depend on percentage of nanoparticles in the sunscreen. For example, the application of a sunscreen containing 8% nanoparticles (10-15nm) onto the skin of humans showed no penetration, while oil in water emulsions showed penetration.[44]

Dermal exposure is another important uptake source for NPs especially because of the increased interest in the use of TiO_2, ZnO and other nanoparticles for protection against ultraviolet rays in various dermal creams, lotions, and cosmetics. Nanosized particles can enter through the unbroken skin during the flexing of the wrist. [41] It has been observed that the flexing of the skin can lead to uptake of micrometer-long fluorescent beads. TiO_2 particles (5-20 nm) are able to penetrate into the skin cells and interfere with the immune system while anatase TiO_2 nanoparticles (10 nm and 20 nm) induced oxidative DNA damage, lipid peroxidation, and micronuclei formation.

Nanoparticle uptake via injection

Injectable nanoparticles are been involved in drug delivery studies. The translocation of nanoparticles following injection depends on the site of injection; intravenously injected nanoparticles quickly spread throughout the circulatory system, with subsequent translocation to organs such as liver, spleen, bone marrow, lymph nodes[4], small intestine, brain, lungs; whereas intradermal injection leads to lymph nodes uptake and intramuscular injection is followed by lymphatic and neuronal system uptake.[4] Nanoparticles injected intravenously are retained longer in the body than ingested ones. For example, 90% of injected functionalized fullerenes are retained after one week of exposure.[4] Coating nanoparticles with various types and concentrations of surfactants before injection significantly affects their distribution in the body.[45] For example, coating with polyethylene glycol or other substances almost completely prevents hepatic and splenic localization.[4,45] Similarly modification of nanoparticles surface with cationic compounds facilitates arterial uptake by up to 10 fold. A common side effect of injecting nanoparticles intravenously is hypersensitivity reaction.

Nanoparticle generation by implants

Nanoparticle debris produced by wear and corrosion of implants is transported to region beyond the implant and has been observed in liver and kidneys of diseased patients with implants and prostheses.[37] Implants release metal ions and wear particles and, after several years of wear, in some cases the concentration of metals in blood exceeds the biological exposure indices recommended for occupational exposure. Immunological responses and aseptic inflammation in patients with total hip replacement are a response to wear particles. Exposure to orthopedic wear-debris leads to inflammatory initiated bone resorption, implant failure, dermatitis, urticaria and vasculitis.[46]

Adverse Effects of Nanoparticles and their treatment

Recent researches has lead to changes in terminology of nanotechnological studies and brought about the realization that no particles are completely inert, and even low concentrations of particles could have negative health effects. It has been demonstrated the interaction of nanoparticles with biological systems can result in allergy[47], fibrosis, organ failure, Inflammation, cytotoxicity[48], ROS generation[49] and DNA/tissue damage.[50] Recent endeavours from the research fraternities has shown that nanoparticles inhalation can affect the immune system defence ability to combat infections[51] and are able to modulate the intrinsic defensive function of macrophages, affecting their reactivity to infections. Several types of nanoparticles (such as ZrO2) enhance the expression of some viral receptors leading to excessive inflammation[51] while exposure to other nanoparticles (SiO2, TiO2) leads to a decrease in the expression of some other viral and bacterial receptors, leading to lower resistance to some viruses or bacteria. Further, most human-made nanomaterials do not appear in the environment, so living organisms possibly do not embody an appropriate immune system to deal with these nanoscale products.

Adverse health effects of respiratory uptake of nanoparticles

The adverse health effects of nanoparticles uptake by respiratory system depend on the residence time in the respiratory tract[27] as well as genetic susceptibility and health status.[21] Smaller particles have a higher toxicological attributes than larger particles of the same composition and crystalline structure, and generates consistently higher inflammatory reaction in the lungs. Smaller nanoparticles are correlated with adverse reactions such as impaired macrophage clearance, inflammation, accumulation of particles, and epithelial cell proliferation, followed by fibrosis, emphysema, and the appearance of tumors.[20] Chronic (two year) high-dose inhalation exposures in rats with poorly soluble, low toxicity dusts can ultimately produce pulmonary fibrosis and lung tumours via an "overload mechanism" but same has not been reported in mice or hamsters, under similar chronic conditions. Treatments for nanoparticles inhalation include those that act to enhance mucociliary clearance, and those that reduce the effects of oxidation and inflammation. Anti-inflammatory medicine (sodium cromoglycate) was found to strongly reduce airway inflammation caused by diesel exhaust nanoparticles.[52] Antioxidant vitamins (particularly vitamin C)[53], rosmarinic acid[54] and a high intake of fresh fruit and some vegetables have a protective effect against lung diseases.[53]

Adverse health effects of neuronal uptake of nanoparticles

Experimental evidence suggests that the initiation and promotion of neurodegenerative diseases, such as Alzheimer's disease, Parkinson's disease, Pick's disease, are associated with oxidative stress and accumulation of high concentrations of metals (like copper, aluminum, zinc, but especially iron) in brain regions associated with function loss and cell damage.[55] However, it is not known if the presence of metals in brain of subjects with neurodegenerative diseases is due to nanoparticles themselves translocating to the brain or their soluble compounds.[34] Recent studies on DNA damage in nasal and brain tissues of canines exposed to air pollutants shows evidences of chronic brain inflammation, neuronal dysfunction, and similar pathological findings with those of early stages of Alzheimer's disease.[27] Epidemiological studies show a clear association between inhalation of dust containing manganese and neurological diseases in miners[56] and welders.[57] Some welders develop Parkinson's disease much earlier in their life, usually in their mid forties, compared to the sixties in the general population.[57]

Antioxidants and metal chelators are treatment options for the adverse health effects caused by the neuronal uptake of nanoparticles. Functionalized fullerenes[58] and nanoparticles made of compounds holding oxygen vacancies show great antioxidant properties.[59] It appears that the antioxidant properties depend upon the structure of the particle but they are independent of its size within 6-1000 nm.

Adverse health effects of circulatory system uptake

Translocation of nanoparticles into the circulatory system was correlated with the appearance of thrombi (or blood clots)[35,52] and cardiovascular malfunction.[60] Thrombosis occurs during the first hour after exposure of nanoparticles. There is a clear dose-dependent response correlating the quantity of pollutant administered and the observed thrombus sizes.[18,52] It is clear from clinical and experimental evidence that inhalation of nano and microparticles can cause cardiovascular effects.[60] Although causal link between the particles in the lungs and cardiovascular effects is not entirely understood but it is believed that the pulmonary inflammation caused by the particles triggers a systemic release of cytokines, resulting in adverse cardiovascular effects. However, recent studies on animals[25] and humans[61] have shown that nanoparticles diffuse from the lungs into the systemic circulation, and then are transported to the organs, demonstrating that cardiovascular effects of instilled or inhaled nanoparticles can arise directly from the presence of nanoparticles within the organism.

Adverse health effects of liver and kidney uptake

Translocation and accumulation of nanoparticles in liver and kidney causes potentially adverse reactions and cytotoxicity which may lead to diseases. Dental prosthesis debris internalized by intestinal absorption can lead to severe health conditions, including fever, enlarged spleen and liver, suppression of bile flow, and acute renal failure.[38] After the removal of dental bridges, and subsequent treatment with steroids, it has been observed that the clinical symptoms decline.[38] Slow clearance and tissue accumulation of potential free radical producing nanomaterials as well as prevalence of numerous phagocytic cells in the organs of the reticuloendothelial system (RES) makes organs such as the liver and spleen main targets of oxidative stress. In the liver, further metabolism of nanomaterials by cytochrome P450, may result in hepatotoxicity by reactive intermediates.[62]

Adverse health effects of gastro-intestinal tract uptake

In the intestinal tract there is a complex mix of compounds, enzymes, food, bacteria, etc., that can interact with ingested nanoparticles and reduce their toxicity.[18] Nanoparticles of carbon, ceramic filosilicates, gypsum, sulphur, calcium, silicon, stainless steel, silver, and zirconium[39] have been constantly found in colon tissue of subjects affected by cancer, Crohn's disease, and ulcerative colitis, while in healthy subjects they could not be traced.[38] Recently, it has been suggested that there is an association between high levels of dietary nanoparticles (100 nm-1μm) and Crohn's disease.[63] Exogenous nanoparticles were found in macrophages accumulated in lymphoid tissue of the human gut, the lymphoid aggregates being the earliest sign of lesions in Crohn's disease.[63] It is believed that genetic predisposition plays a role in development of Crohn's disease increasing risk of some members of the population after intake of nanoparticles.[11] Some evidence suggests that dietary nanoparticles may exacerbate inflammation in Crohn's disease.[64] The diseases associated with gastro-intestinal uptake of nanoparticles including Crohn's disease and ulcerative colitis have no cure and often require surgical intervention.

Adverse health effects of dermal uptake

Many manufacturing processes pose an occupational health hazard by exposing workers to nanoparticles and small fibres, as suggested from the intracellular uptake of MWCNTs by human epidermal keratinocytes.[43] This can explain beryllium sensitization in workers wearing inhalation protective equipment exposed to nanoparticulate beryllium.[42] Also, this may be relevant for latex sensitivity and other materials that provoke dermatologic responses. Lymphatic system uptake of nanoparticles via the dermis is shown to cause podoconiosis[65] and Kaposi's sarcoma.[66] Titanium dioxide commonly used as a physical sunscreen although reflects and scatters UVB and UVA light rays but can absorbs a substantial amount of UV radiation which in aqueous media leads to the production of reactive oxygen species which can cause substantial damage to DNA.[67] Reports regarding the toxicity of titanium dioxide nanoparticles in the absence of UV radiation are contradictory. Nanoparticles were seen to have no inflammatory effect or genotoxicity in rats[68] while several other studies reported that titanium dioxide caused chronic pulmonary inflammation in rats.[69]

It is known that silver has a beneficial antibacterial effect when used as a wound dressing, reducing inflammation and facilitating healing in the early phases[70] but the same property that bestow their antimicrobial attributes may render them toxic to human cells. It has been reported that the concentrations of silver that are lethal for bacteria are also lethal for both keratinocytes and fibroblasts[70] raising serious concerns on the applicabilities for human benefits.

Conclusion

With the rapid increase in the use of nanomaterials in everyday consumer products, manufacturing processes and medical products, it is obvious that people involved in production as well as consumers could have exposure to these potentially toxic nanoparticles. It is argued that the unusual physiochemical properties of nanomaterials that lead advancements in the field of nanotechnology could also be responsible for their potential toxicity to the system. Nanoparticles show varied adverse health effects in respiratory, circulatory, nervous, gastrointestinal and dermal systems. There are various possible routes for their toxicities, however, interactions with the mitochondria and cell nucleus are being considered as main sources of in vivo toxicity. Although in vivo toxicities can occur through diverse mechanisms but the main molecular mechanism involved is induction of oxidative stress which cause damages to biological components through oxidation of lipids, proteins and DNA. Increasing exploration of nanotechnology reveals newer and newer particles with many unique properties; however, there exist considerable wide gap between the available data on the nanomaterials production and in vivo toxicity evaluations which could possibly subjugate further fabrication of NPs owing to increasing health concern. This review indicates that only few specific nanoparticles have been investigated in a limited number of test systems and extrapolation of this data to other materials is not possible. Therefore, despite the existing research database on nanoparticles, no uniformly applicable reports about human toxicity can be given at this time. In addition, limited ecotoxicological data for nanomaterials precludes a systematic assessment of the impact of nanoparticles on ecosystems. The large number of variables influencing toxicity means that it is difficult to generalise about health risks associated with exposure to nanoparticles and each new nanoparticle must be assessed individually and all material properties must be taken into account. For nanomaterials to enjoy status of repute in the application arena, it is crucial to have thorough understanding of their *in vivo* toxicities and our attempt to shed light on some of their toxicological aspects is a step forward in this regard.

References

[1]Welsher, K., Yang H., *Nat. Nanotechnol.*, **2014**, *9*, 198-203

[2]Chauhan , A., Zubair , S., Tufail, S., Sherwani , A., Sajid , M., Raman , S. C., Azam, A., Owais, M., *Int. J. Nanomedicine*, **2011**, *6*, 2305-2319

[3]Hazra, S., Ghosh, N. N., *J. Nanosci. Nanotechnol*., **2014**, *14*, 1983-2000

[4] Oberdorster, G., Oberdorster, E., Oberdorster, J. *Environ. Health Perspect*., **2005**, *113*, 823-839

[5]Bakand, S., Haves, A., Dechsakulthorn, F., *Inhal Toxicol.*, **2012**, *24*, 125-135

[6]Unfried, K., Albrecht, C., Klotz, L. O., Von Mikecz, A., Grether-Beck, S., Schins, R. P. F., *Nanotoxicology*, **2007**, **1, *52-71***.

[7]Kumar, C., *Nanomaterials-Toxicity, Health and Environmental Issues*, *Wiley-VCH*, **2006**

[8]Alarifi, S., Ali, D., Ahamed, M., Siddiqui, M. A., Al-Khedhairy, A. A., *Int. J. Nanomedicine*, **2013**, *8*, 189-199

[9]Sabella, S., Carney, R. P., Brunetti, V., Malvindi, M. A., Al-Juffali, N., Vecchio, G., Janes, S. M., Bakr, O. M., Cingolani, R., Stellacci, F., Pompa, P. P. *Nanoscale*, **2014**, *6*, 7052-7061.

[10]Halliwell, B., Gutteridge, J. M. C., *Free Radicals in Biology and Medicine*, Oxford, University Press, Inc, New York, 4th edn, **2007**

[11]Jena, N. R., *J. Biosci.*, **2012**, *37*, 503-17

[12]Ray, P. D., Huang, B. W., Tsuji, Y., *Cell Signal.*, **2012**, *24*, 981-90

[13]Griendling, K. K., FitzGerald, G. A., *Circulation*, 2003, *108*, 1912-1916

[14]Rallo, R., France, B., Liu, R., Nair, S., George, S., Damoiseaux, R., Giralt, F., Nel, A., Bradley, K., Cohen, Y., *Environ. Sci. Technol*., **2011**, *45*, 1695-1702

[15]Petersen, E. J., Nelson, B. C., *Anal. Bioanal. Chem*., **2010**, *398*, 613-650

[16]Kirkinezos, G., Moraes, C. T., *Seminars in Cell and Developmental Biology*, **2001**, *12*, 449-457

[17]Arora, S., Raiwade, J. M., Paknikar, K. M., *Toxicol. Appl. Pharmacol.*, **2012**, *15*, 151-65

[18]Hoet, P. H. M., Brüske-Hohlfeld, I., Salata, O. V., *J. Nanobiotechnol.*, **2004**, *2*, 1-15

[19]Lippmann, M., *Environ. Health Perspec*., **1990**, *88*, 311-317

[20]Ferin, J., *Toxicol. Lett.*, **2004**, *72*, 121-125

[21]Semmler, M., Seitz, J., Mayer, P., Heyder, J., Oberdörster, G., Kreyling, W. G., *Inhalation Toxicol*., **2004**,*16*, 453-459

[22]Liu, J., Wong, H. L., Moselhy, J., Bowen, B., Wu, X. Y., Johnston, M. R., *Lung Cancer*, **2006**, *51*, 377-386

[23]Ng, A. W., Bidani, A., Heming, T. A., *Lung*, **2004**,*182*, 297-317

[24]Brown, D. M., Donaldson, K., Stone, V., *Respir. Res.*, **2014**, *5*, 29

[25]Takenaka, S., Karg, E., Roth, C., Schulz, H., Ziesenis, A., Heinzmann, U., Schramel, P., Heyder, J., *Environ. Health Persp*., **2001**, *109*, 547-551

[26]Borm, P. J. A., Robbins, D., Haubold, S., Kuhlbusch, T., Fissan, H., Donaldson, K.,Schins, R. P. F., Stone, V., Kreyling, W., Lademann, J., Krutmann, J., Warheit, D., Oberdorster, E., *Part. Fibre Toxicol*., **2006**, *3*, 11

[27]Peters, A., Veronesi, B., Calderon-Garciduenas, L., Gehr, P., Chen, L. C., Geiser, M., Reed, W., Rothen-Rutishauer, B., Schurch, S., Schultz, H., *Part. Fibre Toxicol.*, **2006**, *3*, 13

[28]Oberdörster, G., Sharp, Z., Atudorei, V., Elder, A., Gelein, R., Lunts, A., *J. Toxicol. Environ. Health A*, **2002**, *65*, 1531-1543.

[29]Elder, A., Gelein, R., Silva, V., Feikert, T., Opanashuk, L., Carter, J., Potter, R., Maynard, A., Ito, Y., Finkelstein, J., Oberdorster, G., *Environ. Health Perspect.*, **2006**, *114*, 1172-1178

[30]Lockman, P. R., Koziara, J. M., Mumper, R. J., Allen, D. D., *J. Drug Targ.*, **2004**, *12*, 635-641

[31]Shwe, T. T. W., Yamamoto, S., Kakeyama, M., Kobayashi, T., Fujimaki, H., *Toxicol. Appl. Pharmacol*., **2005**, *209*, 51-61

[32]Geiser, M., Rothen-Rutishauser, B., kapp, N., Schurch, S., Kreyling, W., Schultz, H., Semmler, M., Im Hof, V., Heyder, J., Gehr, P. *Environ. Health Perspect.*, **2005**, *113*, 1555-1560

[33]Chen, J., Tan, M., Nemmar, A., Song, W., Dong, M., Zhang, G., Li, Y., *Toxicol.*, **2006**, *222*, 195-201

[34]Donaldson, K., Tran, L., Jimenez, L. A., Duffin, R., Newby, D. E., Mills, N., MacNee, W., Stone, V., *Part. Fibre Toxicol*., **2005**, *2*, 10.

[35]Nemmar, A., Hoylaerts, M. F., Hoet, P. H. M., Dinsdale, D., Smith, T., Xu, H., Vermylen, J., Nemery, B., *Am. J. Respir. Crit. Care Med*., **2002**, 166, 998-1004

[36]Gatti, A. M. Montanari, S. Monari, E. Gambarelli, A. Capitani, F. Parisini, B., *J. Mater. Sci. Mater. Med.*, **2004**, *15*, 469-472

[37]Gatti, M., Rivasi, F., *Biomater.*, **2002**, *23*, 2381-2387

[38]Ballestri, M., Baraldi, A., Gatti, A. M., Furci, L., Bagni, A., Loria, P., Rapaa, M., Carulli, N., Albertazzi, A., *Gastroenterology*, **2001**,*121*,1234-1238

[39]Gatti, A. M., *Biomater.*, **2004**, *25*, 385- 392

[40]Jani, P., Halbert, G. W., Langridge, J., Florence, A. T., *J. Pharm. Pharmacol.*, **1990**, *42*, 821-826

[41]Toll, R., Jacobi, U., Richter, H., Lademann, J., Schaefer, H., Blume-Peytavi, U., *J. Invest. Dermatol.*, **2004**, *123*, 168-176.

[42]Tinkle, S. S., Antonini, J. M., Rich, B. A., Roberts, J. R., Salmen, R., DePree, K., Adkins, E. J., *Environ. Health Perspec.*, **2003**, *111*, 1202-1208.

[43]Monteiro-Riviere, N. A., Nemanich, R. J., Inman, A. O., Wang, Y. Y., Riviere, J. E., *Toxicol. Lett.*, **2005**, *155*, 377-384.

[44]Tsuji, J. S., Maynard, A. D., Howard, P. C., James, J. T., Lam, C. W., Warheit, D. B., Santamaria, A. B., *Toxicol. Sci.*, **2006**, *89*, 42-50

[45]Araujo, L., Lobenberg, R., Kreuter, J., *J. Drug Targ.*, **1999**, *6*, 373-385.

[46]Hasegawa, M., Yoshida, K., Wakabayashi, H., Sudo, A., *Orthopedics*, **2012**, *36*, 606-12

[47]Maynard, A. D., *Nature*, **2006**, *444*, 267-269

[48]Nel, Xia, T., Madler, L., Li, N. *Science*, **2006**, *311*, 622-627

[49]Manke, A., Wang, L., Rojanasakul, Y., *BioMed Res. Inter.*, **2013**, doi: 10.1155/2013/942916

[50]Singh, N., Manshian, B., Jenkins, G. J. S., Griffiths, S. M., Williams, P. M., Maffeis, T. G. G., Wright, C. J., Doak, S. H., *Biomaterials*, **2009**, *30*, 3891-3914

[51]Lucarelli, M., Gatti, A. M., Savarino, G., Quatronni, P., Martinelli, L., Monari, E., Boraschi, D., *Eur. Cytokin. Net.*, **2004**, *15*, 339-346

[52]Vermylen, J., Nemmar, A., Nemery, B., Hoylaerts, F., *J. Thromb. Haemost.*, **2005**, *3*, 1955-1961

[53]Romieu, *Int. J. Tuberc. Lung Diseases.*, **2005**, *9*, 362-374

[54]Risom, L., Moller, P., Loft, S., *Mutat. Res.*, **2005**, *592*, 119-137

[55]Liu, G., Mena, P., Harris, P. R. L., Rolston, R. K., Perry, G., Smith, M. A., *Neurosci. Lett.*, **2006**, *406*, 189-193

[56]Weiss, B., *Neurotoxicology*, **2006**, *27*, 362-368, 2006

[57]Antonini, J. M., Santamaria, A. B., Jenkins, N. T., Albini, E., Lucchini, R., *NeuroToxicol.*, **2006**, *27*, 304-310

[58]Bosi, S., da Ros, T., Spalluto, G., Prato, M., *Eur. J. Med. Chem.*, **2003**, *38*, 913-923

[59]Schubert, D., Dargusch, R., Raitano, J., Chan, S. W., *Biochem. Biophys. Res. Commun.*, **2006**, *342*, 86-91

[60]Schulz, H., Hardewr, V., Ibald-Mulkli, A., Khandoga, A., Koenig, W., Krombach, F., Radykewicz, R., Stampfl, A., Thorand, B., Peters, A., *J. Aerosol Med.*, **2005**, *18*, 1-22

[61]Nemmar, A., Hoet, P. H., Vanquickenborne, B., Dinsdale, D., Thomeer, M., Hoylaerts, M. F., Vanbilloen, H., Mortelmans, L., Nemery, B., *Circulation*, **2002**, *105*, 411-414,

[62]Lanone, S., Boczkowski, J., *Curr. Mol. Med.*, **2006**, *6*, 651- 663

[63]Lomer, M. C. E., Thompson, R. P. H., Powell, J. J., *Proc. Nutrition Soc.*, **2002**, *61*, 123-130

[64]Lomer, M. C. E., Hutchinson, C., Volkert, S., Greenfield, S. M., Catterall, A., Thompson, R. P. H., Powell, J. J., *British J. Nutrition*, **2004**, *92*, 947-955

[65]Ali, M., Afzal, M., Bhattacharya, S. M., Ahmad, F. J., Dinda, A. K., *Expert Opin. Drug. Deliv.*, **2013**, *10*, 665-678

[66]Montella, M., Franceschi, S., Geddes da Filicaia, M., De Macro, M., Arniani, S., Balzi, D., Delfino, M., Iannuzzo, M., Buonanno, M., Satriano, R. A., *Epidemiol. Prev.*,**1997**, *21*, 114-117

[67]Shi, H., Magaye, R., Castranova, V., Zhao, J., *Part. Fibre Toxicol.*, 2013, doi:10.1186/1743-8977

[68]Rehn, Seiler, F., Rehn, S., Bruch, J., Maier, M., *Toxicol. Appl. Pharmacol.*, **2003**, *189*, 84-95

[69]Oberdörster, G., Ferin, J., Gelein, R., Soderholm, S. C., Finkelstein, J., *Environ. Health Perspect*., **1992**, *97*, 193-199

[70]Poon, V. K., Burd, A., *Burns*, **2004**, *30*, 140-147

Received: 01.09.2014.
Accepted: 17.10.2014.

SYNTHESIS OF HYBRID MAGNETIC NANOMATERIAL BASED ON POLYDIPHENYLAMINE-2-CARBOXYLIC ACID AND Fe_3O_4 IN THE INTERFACIAL PROCESS

Galina Petrovna Karpacheva,[a]* Sveta Zhiraslanovna Ozkan,[a] Igor Sergeevich Eremeev,[a] Galina Nikolaevna Bondarenko,[a] Ella Leont'evna Dzidziguri[b] and Petr Aleksandrovich Chernavskii[c]

Keywords: interfacial polymerization *in situ*; core-shell; Fe_3O_4/polydiphenylamine-2-carboxylic acid hybrid nanoparticles; magnetic nanomaterials; magnetic fluids

Hybrid magnetic nanomaterial with core-shell structure, where particles of Fe_3O_4 form the core and polydiphenylamine-2-carboxylic acid is the shell, was obtained for the first time in the interfacial process. According to TEM data Fe_3O_4/polydiphenylamine-2-carboxylic acid nanoparticles have size $2 < d < 14$ nm. It was found by IR spectroscopy that the polymer shell is formed by C–C - joining into 2- and 4-positions of phenyl rings with respect to nitrogen. The obtained hybrid nanomaterial is superparamagnetic and thermally stable.

* Corresponding Authors
Tel: +74959554255
E-Mail: gpk@ips.ac.ru
[a] A.V. Topchiev Institute of Petrochemical Synthesis, Russian Academy of Sciences, 29 Leninsky prospect, Moscow 119991 Russia
[b] National University of Science and Technology "MISIS", 4 Leninsky prospect, Moscow 119049 Russia
[c] Department of Chemistry Lomonosov Moscow State University, 1-3 Leninskie Gory, Moscow 119991 Russia

Introduction

The modern level of development of science and technologies dictates the tasks of creating new advanced materials with a complex of necessary physical-chemical properties. Among these materials a special issue is given to the hybrid polymer nanomaterials[1-5] properties of which are defined not only by the constituent polymer and inorganic components, but also by the interaction between them at the molecular level. The grown up interest for the last ten years to hybrid nanomaterials, including polymers with a system of polyconjugation is associated with the fact that they are able to show excellent electric, magnetic and electrochemical properties. It makes them promising for the use in systems of magnetic information recording, organic electronics and electrorheology, medicine, while creating electromagnetic screens, microelectromechanic systems, rechargeable batteries, sensors and biosensors, supercapacitors, electrocatalysts, solar batteries, displays and other electrochemical devices.

A special place in this class of hybrid materials is held by magnetic nanomaterials with a core-shell structure, in which the core is the magnetic nanoparticle and the polymer shell plays the role of the stabilizer, preventing their aggregation. Such hybrid nanomaterials can be used as components of magnetic liquids – unique systems, combining properties of a magnetic material and a liquid.

The combination of these properties, that cannot be found in natural materials, provides a great potential for practical use of magnetic liquids (as contrast agents in magnetic resonance tomography, in hyperthermia, for sealing the gaps between the moving parts of devices (rotating shafts, pistons), in magnetic-hydrodynamic bearings, for ore beneficiation, in printing devices, for collecting oil products on the water surface, etc.).

In the known magnetic nanomaterials with core-shell structure the role of the polymer shell with a system of polyconjugated bonds, as a rule, is performed by polyaniline, which takes a special place among the conducting polymers, due to the simplicity of its synthesis, the ease of holding processes of doping-dedoping, stability of its properties. Such nanomaterials are obtained by *in situ* oxidative polymerization of aniline in presence of the magnetite nanoparticles introduced into the reaction mixture.

So, the magnetic dispersed Fe_3O_4/polyaniline nanomaterials with core-shell structure were obtained via aniline polymerization in an aqueous solution containing magnetic fluid, which is an aqueous suspension of Fe_3O_4 nanoparticles and the sodium salt of dodecylbenzenesulfonic acid with ammonium persulfate as an oxidizer.[6] Fe_3O_4 nanoparticles have spherical form with a diameter of 20–30 nm and aggregate easily due to magneto-dipole interaction. 70–80 % of nanoparticles have diameter from 70 to 100 nm.

The investigation of magnetic properties has shown that Fe_3O_4/polyaniline nanoparticles are ferromagnetic like bulk magnetite samples. Saturation magnetization and coercive force depend on the content of Fe_3O_4. Ferromagnetic nanoparticles with core-shell structure were obtained via emulsion polymerization of pyrrol in the presence of Fe_3O_4 nanoparticles. 80–90 % of obtained core-shell nanoparticles have size 30–40 nm.[7]

It was shown that because of the aggregation of magnetite nanoparticles the polyaniline shell is able to surround a cluster of size 50 nm including several Fe_3O_4 nanoparticles of size 10–15 nm.[8] To prevent the aggregation of Fe_3O_4 nanoparticles Lu et al. proposed to cover the Fe_3O_4 nanoparticles, preformed by hydrolysis of Fe(II)-Fe(III) chlorides, with a layer of molecules of the substituted aniline dimer synthesized via interaction of N-phenyl-1,4-phenylenediamine and succinic acid anhydride.[9] D. Chao et al. used anthranilic acid to modify Fe_3O_4 nanoparticles.[10] However, in both cases the authors did not manage to prevent the aggregation of nanoparticles completely due to the formation of hydrogen bonds and π-π interaction between the molecules of the modifier. Further polymerization of aniline in the presence of modified Fe_3O_4 nanoparticles leads to the formation of Fe_3O_4/polyaniline nanoparticles with the diameter of 10–20 nm. The obtained Fe_3O_4/polyaniline nanoparticles have core-shell structure as proved by TEM and XRD. These particles have superparamagnetic properties, saturation magnetization M_S = 21 emu g^{-1}.

Promising are the nanomaterials, in which the shell is a functionalized polymer with a system of polyconjugation, providing a stronger bond between the core and the shell, that should provide a high stability of the nanomaterial. Having said that, the creation of magnetic nanomaterials with a high degree of dispersion based on functionalized polymers with a system of polyconjugation seems to be an actual problem both in scientific and practical aspects.

Earlier hybrid dispersed magnetic nanoparticles with core-shell structure based on Fe_3O_4 and polydiphenylamine-2-carboxylic acid (PDPhAC) – new functionalized polymer with a system of polyconjugated bonds, the structure of which contains carboxylic groups, have been obtained homogeneously for the first time in ammonium hydroxide solution. In contrast to the papers described above where the previously obtained nanoparticles of magnetite are introduced into the medium of polyaniline synthesis, the *in situ* polymerization of diphenylamine-2-carboxylic acid (DPhAC) is carried out directly in the alkaline medium of Fe_3O_4 nanoparticles synthesis. It was shown that the obtained nanomaterial is superparamagnetic, saturation magnetization M_S = 33.5 emu g^{-1}.[11-13]

In this work the method of synthesis of hybrid nanoparticles based on Fe_3O_4 nanoparticles and DPhAC polymer in the interfacial process was developed. Magnetic and thermal properties of the obtained hybrid nanomaterials were studied.

Experimental

DPhAC (analytical grade), sulfuric acid (reagent grade), ammonia (reagent grade), ethyl alcohol (analytical grade), iron(II) chloride ("Acros Organics"), iron(III) chloride (high-purity grade) were used as received. Ammonium persulfate (analytical grade) was purified by recrystallization. Aqueous solutions of reagents were prepared using distilled water.

Fe_3O_4/PDPhAC hybrid nanomaterial was obtained as follows. Initially, Fe_3O_4 nanoparticles were synthesized via the hydrolysis of iron(II) and iron(III) chlorides mixed at the ratio 1 : 2 in ammonium hydroxide solution at 55 °C.[14]

$$FeCl_2 + 2FeCl_3 + 8NH_3 \cdot H_2O \rightarrow Fe_3O_4 + 8NH_4Cl + 4H_2O$$

To fix the monomer on the surface of Fe_3O_4 nanoparticles, the monomer solution in chloroform of the required concentration was added to the obtained aqueous-alkaline suspension. The process was conducted at 55 °C at a permanent vigorous stirring for 0.5 h.

In order to perform an oxidative polymerization of DPhAC on the surface of Fe_3O_4 nanoparticles, aqueous solution of ammonium persulfate was added dropwise to Fe_3O_4/DPhAC suspension preliminarily cooled down to 0 °C. Solutions of organic and aqueous phases were mixed immediately without gradual dosing of the reagents. The volume ratio of aqueous and organic phases was 1 : 1. The ratio [monomer] : [oxidizer] was 1 : 2. The synthesis was conducted at 0 °C for 3 h at a vigorous stirring. As the reaction was complete, the mixture was precipitated into two-fold excess of 1 M H_2SO_4, filtered, and washed with distilled water until the neutral reaction of the filtrate. The obtained product was dried in vacuum above KOH to a constant weight.

The magnetic fluid based on Fe_3O_4/PDPhAC nanoparticles suspension in ethanol was prepared. The suspension stability was observed for 8 months.

IR spectra of Fe_3O_4/PDPhAC nanoparticles were recorded on an IFS 66v FTIR spectrometer in the range 4000–400 cm^{-1}. The samples were prepared as KBr pellets. X-ray investigations of Fe_3O_4/PDPhAC nanoparticles were performed at room temperature on a Difrey X-ray diffractometer with Bragg–Brentano focusing using Cr*K*α-radiation. Microphotographs of Fe_3O_4/PDPhAC nanoparticles were taken on a JEM-2100 transmission electron microscope at the accelerating voltage 200 kV.

The metal content in Fe_3O_4/PDPhAC nanoparticles was determined quantitatively by the atom-absorption spectrometry method on an AAS 30 spectrophotometer (Carl Zeiss JENA). The accuracy of the determination of Fe was ± 1.0 %.

Magnetic characteristics of Fe_3O_4/PDPhAC nanoparticles were investigated on a vibrational magnetometer at room temperature.[15] The absolute magnetic moment value was determined using a cobalt standard with a mass of 2 mg.

Thermal analysis was carried out on a TGA/DSC1 device (Mettler Toledo) in dynamic regime in the range 30–1000 °C in air and in the flow of nitrogen. The loading of polymers was 100 mg, heating rate 10 °C min^{-1}, and the flow of nitrogen was 10 mL min^{-1}. Calcined alumina was used as a standard. The analysis of samples was conducted in Al_2O_3 crucibles.

DSC analysis was performed on a DSC823^e calorimeter (Mettler Toledo). The samples were heated at a rate of 10 °C min^{-1} in Ar flow of 70 mL min^{-1}. The measurement results were processed using STARe software supplied with the device. The measurement accuracies were ± 0.3 K for temperature and ± 1 J g^{-1} for enthalpy.

Results and discussion

The peculiarity of the developed method of synthesis of Fe_3O_4/PDPhAC composite nanoparticles in the interfacial process is that the *in situ* polymerization of DPhAC proceeds directly in the alkaline medium where Fe_3O_4 nanoparticles are obtained, as opposed to the case of pre-introduced magnetite nanoparticles described in the reference elsewhere. The formation of the hybrid dispersed nanomaterial Fe_3O_4/PDPhAC in the interfacial process includes synthesis of Fe_3O_4 nanoparticles via hydrolysis of a mixture of iron(II) and iron(III) chlorides in ratio 1:2 in the ammonium hydroxide solution,[14] immobilization of the monomer on the surface of Fe_3O_4 nanoparticles via the addition of monomer solution in chloroform with further polymerization *in situ* in the presence of ammonium persulfate. The monomer and oxidizer are distributed in two immiscible phases (Figure 1). Polymerization of DPhAC on the surface of Fe_3O_4 nanoparticles proceeds at the interface between the aqueous and the organic phases.

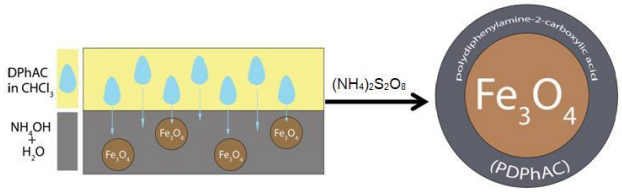

Figure 1. Scheme of Fe_3O_4/PDPhAC hybrid nanomaterial synthesis.

The formation of composite nanoparticles based on Fe_3O_4 was proved by XRD. Reflection peaks of Fe_3O_4 are clearly identified on the diffractogram in the range of scattering angles 2θ = 46.3°, 54.6°, 66.8°, 84.7°, 91.0°, 101.6° (Figure 2).

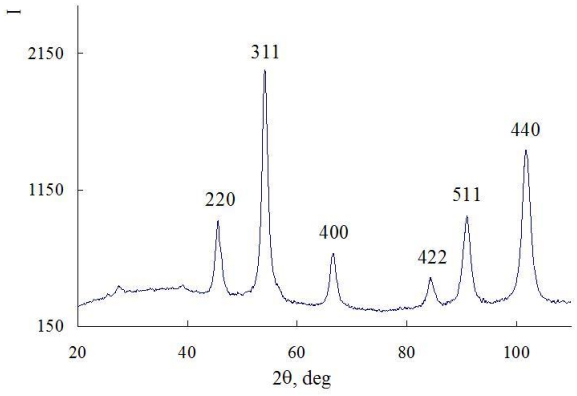

Figure 2. Fe_3O_4/PDPhAC hybrid nanomaterial diffractogram.

Electronic diffraction proves the crystalline nature and the phase content of nanoparticles (Figure 3a). According to TEM data Fe_3O_4/PDPhAC nanoparticles have size $2 < d < 14$ nm (Figure 3). According to atomic adsorption spectrometry data the content of Fe is 38.5 % wt. The obtained nanomaterial entirely consists of Fe_3O_4/PDPhAC hybrid nanoparticles. Fe_3O_4 nanoparticles without the polymeric shell are completely deleted after precipitation into sulfuric acid.

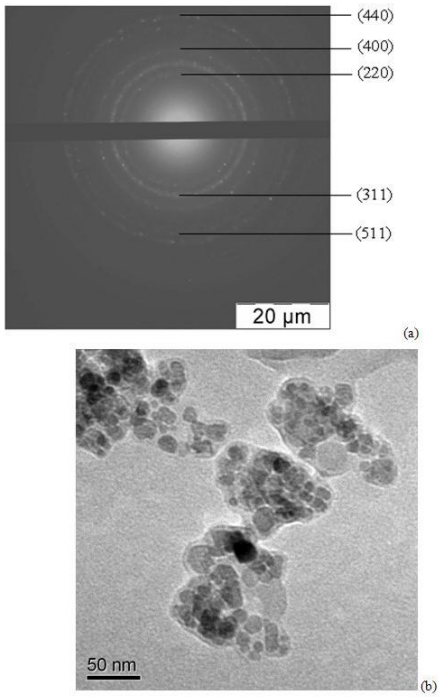

Figure 3. Fe_3O_4/PDPhAC hybrid nanomaterial diffraction image (a) and microphotograph (b).

According to the results of X-ray analysis the size distribution of coherent scattering regions (CSR) was calculated for Fe_3O_4/PDPhAC hybrid nanoparticles. Figure 4 depicts the volume size distribution of CSR in Fe_3O_4 nanoparticles. The size distribution curve of Fe_3O_4 crystallites is very narrow. About 90 % of crystallites have size up to 6 nm.

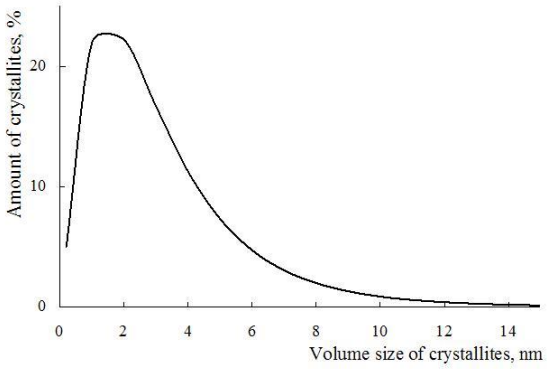

Figure 4. Volume distribution of crystallites by Fe_3O_4 size in Fe_3O_4/PDPhAC hybrid nanomaterial.

The IR spectroscopy data confirm the monomer immobilization on Fe_3O_4 nanoparticles via binding of the carboxylate-ion with iron with the formation of a coordination bond Fe---OOC. Absorption band at 572 cm^{-1}, corresponding to the stretching vibrations of ν_{Fe-O} bond, appears in IR spectra of composite nanoparticles (Figure 5).

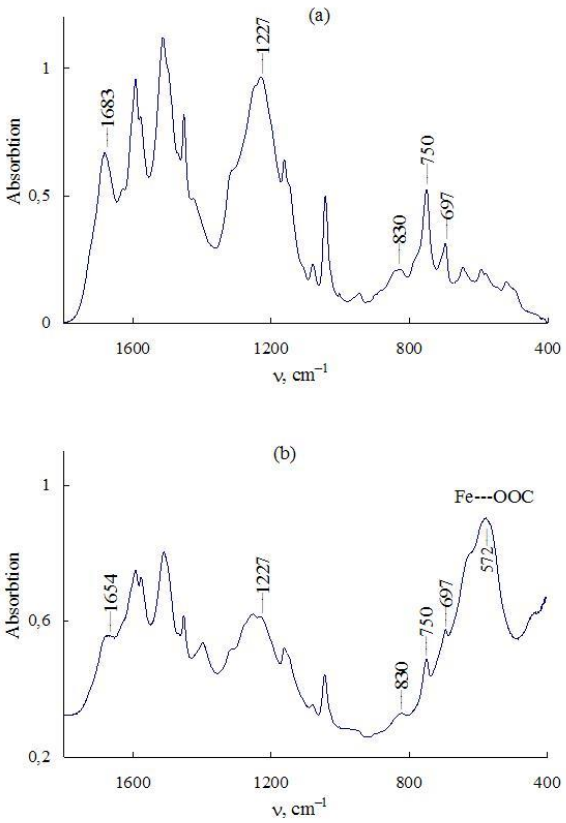

Figure 5. IR spectra of PDPhAC (a) and Fe_3O_4/PDPhAC hybrid nanomaterial (b).

The coordination bond Fe---OOC in hybrid nanoparticles appears as a result of redistribution of electronic density after an interaction between carboxylate-anion and iron.

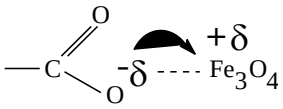

The positive charge appears on the polymer shell of hybrid nanoparticles due to the electronic interaction of delocalized π-electrons with free *d*-orbitals of iron.[16] The absorption band of valence vibrations of $\nu_{C=O}$ bond in carboxylic group appears at 1654 cm^{-1} in the IR spectra of hybrid nanoparticles; it is strongly shifted to longer wavelengths in comparison with the position of this band in the polymer at 1683 cm^{-1}. Such shift of $\nu_{C=O}$ bond simultaneously with the appearance of an intensive band at 572 cm^{-1} indicates that carboxylic groups of the polymer are immobilized on Fe_3O_4 nanoparticles with the formation of the polymeric shell, allowing to propose that Fe_3O_4/PDPhAC hybrid nanoparticles have core-shell structure where the core is the magnetite nanoparticle and the shell is the polymer of DPhAC. It is worth mentioning that there is no absorption band at 572 cm^{-1} in IR spectra of the nanocomposite, in which the Fe_3O_4 nanoparticles are dispersed into the polydiphenylamine matrix; the latter compound has no COOH groups in its structure.[17] Absorption bands of the valence vibrations of ν_{Fe-O} bond in magnetite are in the region of 440 and 480 cm^{-1} (shoulder).[18]

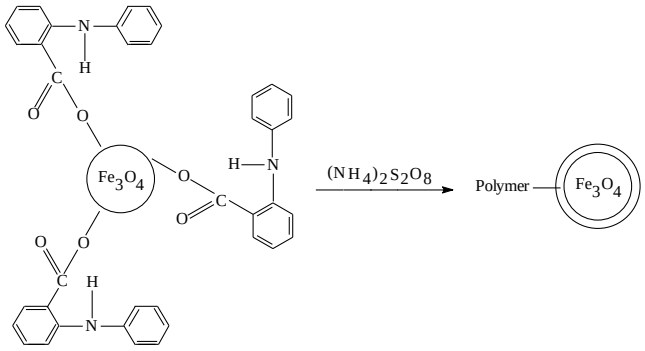

The presence of absorption bands in the region of 830 and 750 cm^{-1} in the IR spectra of composite nanoparticles, caused by the non-planar deformation vibrations of δ_{C-H} bonds of 1,2,4- and 1,2-substituted benzene ring, shows that the polymer shell around Fe_3O_4 nanoparticles is formed via C–C - joining into 2- and 4- positions of phenyl rings with respect to nitrogen.[19]

Analysis of the results of spectral studies allows to present the chemical structure of Fe_3O_4/PDPhAC hybrid nanomaterial as follows:

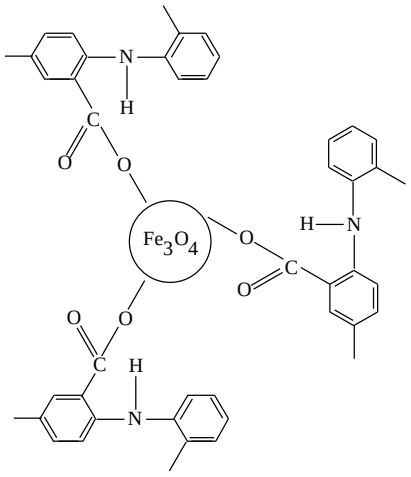

The study of the magnetic properties at room temperature showed that Fe_3O_4/PDPhAC hybrid nanomaterial has a hysteresis type of magnetization reversal. Figure 6 shows the composite nanoparticles magnetization dependence on the value of the applied magnetic field.

In Table 1, the values of the main magnetic characteristics of the Fe_3O_4/PDPhAC hybrid nanomaterial are listed. The magnetic characteristics of the dispersed material obtained in the ammonium hydroxide solution are given for comparison.[12,13] As it can be seen from the Table, regardless of the synthesis method, values of the squareness coefficient of the hysteresis loop $k_S = M_R/M_S$ indicate the superparamagnetic behavior of the composite nanoparticles, which is characteristic of the uniaxial single-domain magnetic nanoparticles.[3-5,21,22] At the same time, the hybrid nanomaterial obtained under the conditions of the interfacial polymerization *in situ* is superparamagnetic with almost 100 % content of superparamagnetic nanoparticles.

Table 1. Magnetic characteristics of Fe_3O_4/PDPhAC hybrid nanomaterial

Synthesis method	H_C,[a] Oe	M_S,[b] emu g^{-1}	M_R,[c] emu g^{-1}	M_R/M_S
In interfacial process	1.6	27.5	0.19	0.007
In NH_4OH solution	76	33.5	5.0	0.15

a – coercive force; *b* – saturation magnetization; *c* – residual magnetization.

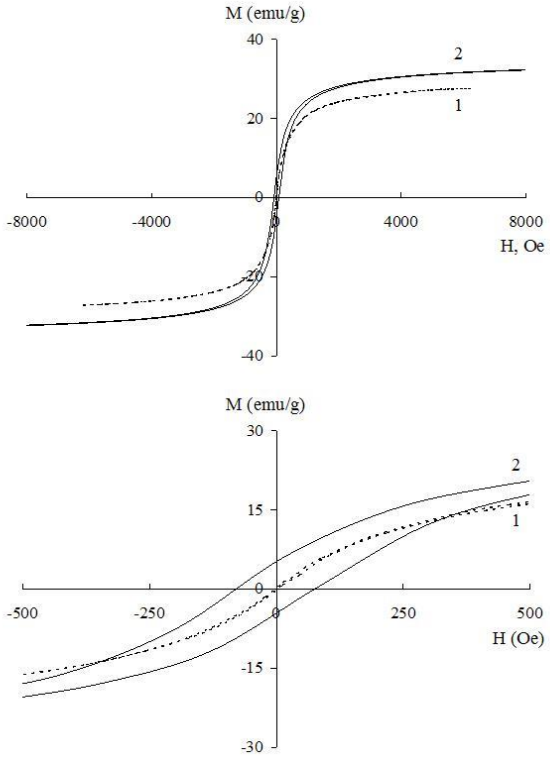

Figure 6. Magnetization of Fe_3O_4/PDPhAC hybrid nanomaterial obtained in the interfacial process (1) and in NH_4OH solution (2) as a function of the applied magnetic field at room temperature.

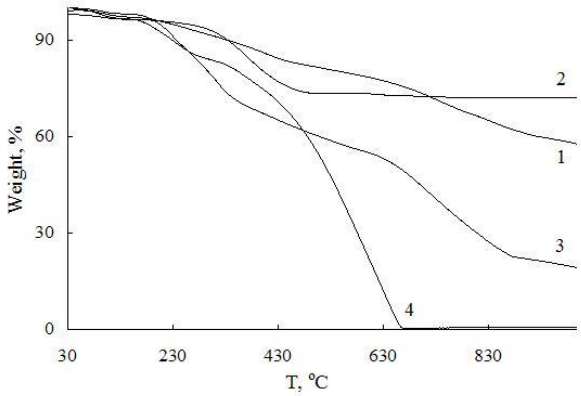

Figure 7. Weight dynamics of Fe_3O_4/PDPhAC hybrid nanomaterial (1, 2) and PDPhAC (3, 4) in heating to 1000 °C at heating rate 10 °C min^{-1} in nitrogen flow (1, 3) and in air (2, 4).

Thus, it is shown that the immobilization of the polymer on magnetite nanoparticles leads to an increase of the thermal stability.

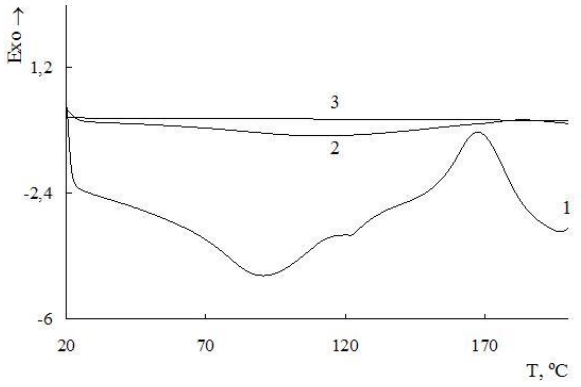

Figure 8. DSC thermograms of PDPhAC (1) and Fe_3O_4/PDPhAC hybrid nanomaterial (2, 3) in heating to 200 °C in nitrogen flow at heating rate 10 °C min^{-1} (1,2 – first heating, 3 – second heating).

TGA and DSC were used to study the thermal stability of the dispersed hybrid nanomaterial Fe_3O_4/PDPhAC in comparison with the polymer. The curves of weight loss have stepped nature (Figure 7). The weight loss at 168 °C in PDPhAC is caused by the removal of COOH groups.[19,23-25] There is an exothermic peak in this region of temperature in the DSC image (Figure 8), it is associated with decomposition.[26-28] The absence of weight loss in Fe_3O_4/PDPhAC hybrid nanomaterial at this temperature is described by the fact that the carboxylate groups of the polymer shell are immobilized on Fe_3O_4 nanoparticles with the formation of the coordination bond Fe---OOC.

As it is shown in Figure 6, 50 % weight loss in air for the PDPhAC obtained in the presence of the organic solvent is achieved at 520 °C. For the Fe_3O_4/PDPhAC hybrid nanomaterial obtained in the interfacial process, the residue at 520 °C is 73 %. In the inert atmosphere PDPhAC loses half of its initial weight at 660 °C. In the hybrid nanomaterial the residue at this temperature is 76 %.

The absence of weight loss in Fe_3O_4/PDPhAC hybrid nanomaterial in air above 500 °C is associated with complete thermal oxidative destruction of the polymer shell. Figure 9 shows the IR spectra of Fe_3O_4/PDPhAC composite nanoparticles before (a) and after heating in air up to 500 °C (b). In IR spectra of nanoparticles heated up to 500 °C there are no characteristic absorption bands corresponding to PDPhAC. After the completion of thermal oxidative destruction of the polymer shell, there was only magnetite left. Figure 10 shows diffraction images of Fe_3O_4/PDPhAC composite nanoparticles before and after heating in air up to 500 °C. In the diffraction images of composite nanoparticles heated up to 500 °C in air, reflection bands of Fe_3O_4 are clearly identified (Figure 10b). As it can be seen from Figure 7, there is a weight loss in Fe_3O_4/PDPhAC composite nanoparticles at T > 800 °C in inert atmosphere. It is associated with the partial reduction of Fe_3O_4 to Fe and FeO. Figure 10c shows the diffraction image of Fe_3O_4/PDPhAC composite nanoparticles after heating in nitrogen flow up to 800 °C.

 DOI: 10.17628/ecb.2014.3.1001-1007

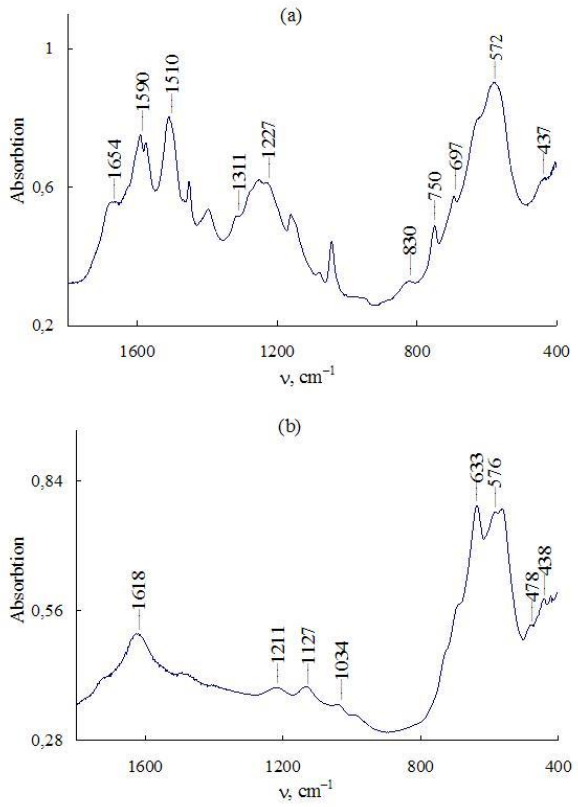

Figure 9. IR spectra of Fe_3O_4/PDPhAC hybrid nanomaterial before (a) and after heating in air to 500 °C (b).

Reflection bands of Fe are clearly identified in diffraction images along with Fe_3O_4 nanoparticles in the region of scattering angles 2θ = 68.7°, 106.1°, and with FeO in the region of scattering angles 2θ = 55.4°, 65.2°, 99.7°.

The hybrid dispersed nanomaterial Fe_3O_4/PDPhAC is a black powder, completely soluble in concentrated sulfuric acid and insoluble in concentrated hydrochloric acid and organic solvents.

The massive of varied experimental data (size of hybrid nanoparticles and their superparamagnetic behavior, indicating their single-domain structure; immobilization of polymer chains on magnetite nanoparticles with the formation of core-shell structure; the presence of the positive charge in the structure of the polymer shell due to electronic interaction of delocalized π-electrons with the free *d*-orbitals, defining the prevention of aggregation of nanoparticles; insolubility in aqueous and organic medium) gives a reason to suggest that the obtained hybrid dispersed nanoparticles can be used as active components of magnetic fluids, which are stable suspensions of magnetic particles in water or organic medium. To verify this assumption, aqueous and alcoholic suspensions of Fe_3O_4/PDPhAC hybrid nanoparticles were obtained. It was found that suspensions of Fe_3O_4/PDPhAC magnetic nanoparticles in ethanol and water are stable for at least 8 months, while Fe_3O_4 nanoparticles start to precipitate from the first minutes, as can be seen from Figure 11. Thus, due to the prevention of aggregation of nanoparticles by the polymer shell of PDPhAC, the stability of magnetic suspension can be provided for a long period of time.

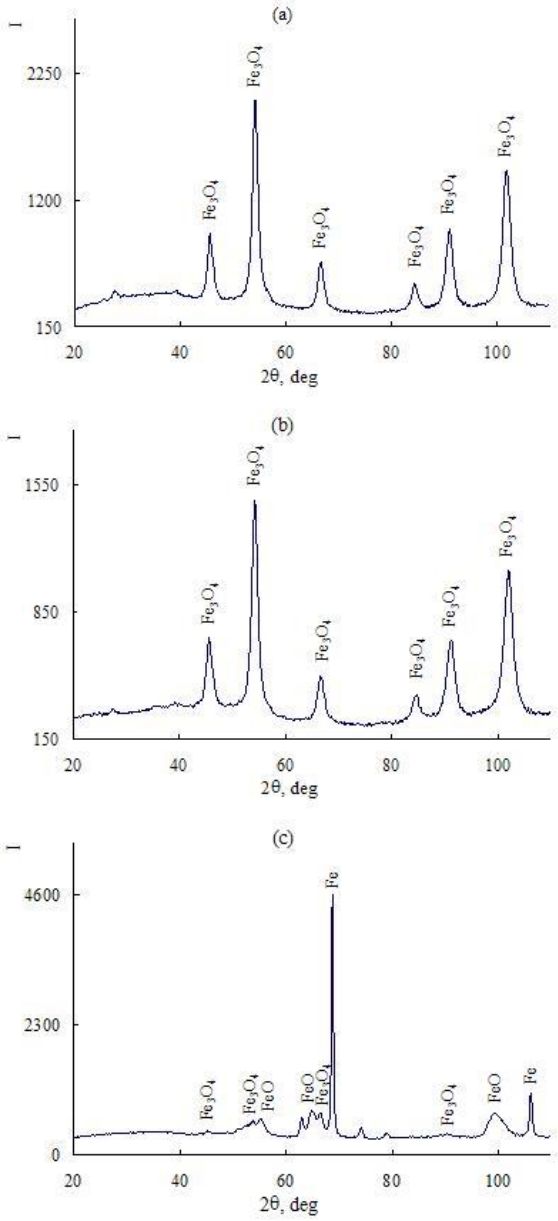

Figure 10. Fe_3O_4/PDPhAC hybrid nanomaterial diffractograms before (a) and after heating in air to 500 °C (b) and in nitrogen flow to 800 °C (c).

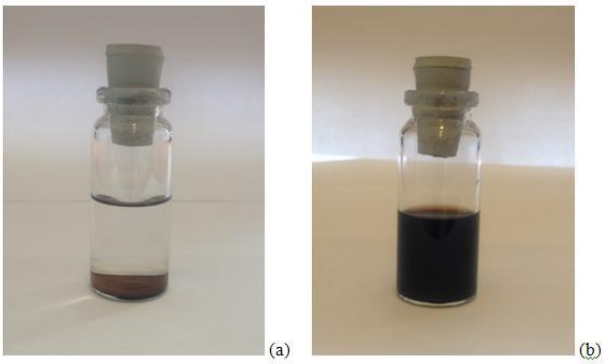

Figure 11. Suspension of Fe_3O_4 nanoparticles (a) and Fe_3O_4/PDPhAC hybrid nanomaterial (b) in ethanol. (a) – in 5 minutes, (b) – in 8 months.

Conclusions

Hybrid dispersed nanomaterial with core-shell structure, where Fe_3O_4 nanoparticles form the core and PDPhAC is the shell, were obtained for the first time in the interfacial process. The peculiarity of this method of synthesis of composite nanoparticles is the fact that polymerization *in situ* of DPhAC proceeds not in the presence of the magnetite nanoparticles introduced in the reaction medium, but directly in the alkaline medium of synthesis of Fe_3O_4 nanoparticles. The polymer shell effectively prevents the aggregation of composite nanoparticles. Size of Fe_3O_4/PDPhAC nanoparticles is $2 < d < 14$ nm. The obtained dispersed nanomaterial is superparamagnetic, $M_R/M_S \sim 0.007$. The shell (PDPhAC) is insoluble in water and organic solvents, which allows to use Fe_3O_4/PDPhAC hybrid nanoparticles for preparation of magnetic fluids. High thermal stability of the hybrid nanomaterial in air and inert atmosphere provides a possibility to use the obtained dispersed material in high temperature processes.

Acknowledgements

The work has been supported by the Russian Foundation for Basic Research, project № 11-03-00560-a.

Authors thank G.A. Shandryuk (TIPS RAS) for conducting the thermal analysis of the Fe_3O_4/polydiphenylamine-2-carboxylic acid hybrid nanomaterial.

References

[1]Sellinger, A., Weiss, P. M., Nguyen, A., Lu, Y., Assink, R. A., Gong, W., Brinker, C. J., *Nature*, **1998**, *394*, 256.

[2]Yamamoto, K., Sakata, Y., Nohara, Y., Takahashi, Y., Tatsumi, T., *Science*, **2003**, *300*, 470.

[3]Gerasin, V. A., Antipov, E. M., Karbushev, V. V., Kulichikhin, V. G., Karpacheva, G. P., Talroze, R. V., Kudryavtsev, Y. V., *Russ. Chem. Rev.*, **2013**, *82*, 303.

[4]Gubin, S. P., *Magnetic nanoparticles*. WILEY-VCH, Weinheim **2009**, 466 p.

[5]Gubin, S. P., Koksharov, Yu. A., Khomutov, G. B., Yurkov, G. Yu., *Russ Chem. Rev.*, **2005,** *74*, 489.

[6]Deng, J., He, C., Peng, Y., Wang, J., Long, X., Li, P., Chan, A., *Synth. Met.*, **2003**, *139*, 295.

[7]Deng, J., Peng, Y., He, Ch., Long, X., Li, P., Chan, A. S. C., *Polym. Int.*, **2003,** *52*, 1182.

[8]Khan, A., Aldwayyan, A. S., Mansour Alhoshan, M., Alsalhi, M., *Polym. Int.*, **2010**, *59*, 1690.

[9]Lu, X., Yu, Y., Chen, L., Mao, H., Gao, H., Wang, J., Zhang, W., Wey, Y., *Nanotechnology*, **2005**, *16*, 1660.

[10]Chao, D., Lu, X., Chen, J., Zhang, W., Wei, Y., *J. Appl. Polym. Sci.*, ***2006***, *102*, 1666.

[11]Karpacheva, G. P., Ozkan, S. Zh. **RU 2426188** "*Dispersed nanocomposite magnetic material and method of its obtaining*".

[12]Eremeev, I. S., Ozkan, S. Zh., Karpacheva, G. P., *J. Int. Sci. Publ. Mater., Methods, Technol.*, **2012**, *6*, 222.

[13]Eremeev, I. S., Ozkan, S. Zh., Karpacheva, G. P., Bondarenko, G. N., *Nanotechnol. Russ.*, **2014**, *9*, 38.

[14]Massart, R., *IEEE Trans. Magn.*, **1981**, *17*, 1247.

[15]Chernavskii, P. A., Khodakov, A. Y., Pankina, G. V., Girardon, J.-S., Quinet E., *Appl. Catal.*, **2006,** *306*, 108.

[16]Reddy, K. R., Lee, K.-P., Gopalan, A. I., *J. Appl. Polym. Sci.*, **2007**, *102*, 1181.

[17]Ozkan, S. Zh., Karpacheva, G. P. in: *Handbook of Organic Chemistry, Biochemistry, Biotechnology and Renewable Resources. Research and Development*, Ed. G. E. Zaikov, O. V. Stoyanov, E. L. Pekhtasheva, Nova Science Publishers, Inc. New York, **2013**, *2*, 93.

[18]Ivanovskaya, M. I., Tolstik, A. I., Kotikov, D. A., Pankov, V. V., *Russ. J. Phys. Chem. A.*, **2009**, *83*, 2081.

[19]Ozkan, S. Zh., Eremeev, I. S., Karpacheva, G. P., Prudskova, T. N., Veselova, E. V., Bondarenko, G. N., Shandryuk, G. A., *Polym. Sci. B.*, **2013**, *55*, 107.

[20]Madsen K. N., *J. Magn. Magn. Mater.*, **2002**, *241*, 220.

[21]Chernavskii, P. A., Pankina, G. V., Lunin, V. V., *Russ. Chem. Rev.*, **2011,** *80*, 579.

[22]Baranov, D. A., Gubin, S. P. IX International Scientific Conference «*Solid state Chemistry: Monocrystals, Nanomaterials, Nanotechnologies*», Kislovodsk, **2009**, p.12.

[23]Ogura, K., Shiigi, H., Nakayama, M., A. Ogawa, A., *J. Polym. Sci., Polym. Chem.*, **1999**, *37*, 4458.

[24]Ozkan, S. Zh., Bondarenko, G. N., Karpacheva, G. P., *Polym. Sci. B.*, **2010**, *52*, 263.

[25]Ozkan, S. Zh., Eremeev, I. S., Karpacheva, G. P., Bondarenko, G. N., *Open J. Polym. Chem.*, **2013**, *3*, 63.

[26]Ding, L., Wang, X., Gregory, R. V., *Synth. Met.*, **1999**, *104*, 73.

[27]Wang, X.-H., Geng, Y.-H., Wang, L.-X., Jing, X.-B., Wang, F.-S., *Synth. Met.*, **1995**, *69*, 265.

[28]Wen, T.-Ch., Chen, J.-B., Gopalan, A., *Mater. Lett.*, **2002**, *57*, 280.

Received: 12.09.2014.
Accepted: 16.10.2014.

HEAVY METAL ASSESSMENT IN INDUSTRIAL GROUNDWATER IN AND AROUND VIJAYAWADA, ANDHRA PRADESH, INDIA

T. Ravi Sankar and P. T. S. R. K. Prasada Rao

Keywords: Heavy metals, ground water, pollution, Vijayawada, industries.

Assessment of trace metals in ground water in industrial groundwater in and around Vijayawada, Andhra Pradesh, India was carried out. Samples were collected from 60 bore wells for this study. The present study was made assessing the impacts of industrial activities on the ground water quality in and around Vijayawada A.P. 60 ground water samples are collected from industrial areas of Vijayawada. The following metals, say, Pb, Cu, Ni, Fe, Ag, Zn, Mn, Cd, Cr and Co were analyzed in all the samples, The distribution maps served as important information to understand ecological status of the groundwater systems and for the identification of groundwater quality parameters with concentration above the allowable limits.

Corresponding Authors
Fax: 91 866 2881852
Tel: 91 866 2882911
E-Mail: posaniprasadrao@yahoo.co.in
[a] Department of Chemistry, Acharya Nagarjuna University, Nagarjuna Nagar, Guntur, Andhra Pradesh INDIA
[b] PG Department of Chemistry, P. B. Siddhartha College of Arts & Science, Moghalrajpuram, Vijayawada – 520010, Andhra Pradesh, INDIA

Introduction

The ground water is an important source for drinking water. It plays an important role in ecological functions in various eco systems. Due to increase of industrialization urbanization gradually decreases the ground water quality in some regions during some periods due to unsustainable use of water resources. However the problem is differ in some developing countries where in the latter the threat of unavailability of good quality ground water[1] is a life time threat problem. Water is also called elixir of life. About 71% of the earth surface covered by water mostly in oceans and other large water bodies 1.6% of water present in ground in aquifers and 0.001% in the air as vapour, clouds and precipitation. If 70%to 90% by weight in living organism. In urban area 50% of ground water is used in all developing countries derived wells bore holes and springs. 1000 millions in Asia and 150 million people in Latin America rely on sources. Over 97% of water present In the oceans and other water bodies and these water not useful for most of the purpose and in the remaining 3%, 2% % of water is present in icecaps and glaciers, 0.62% of water was present in ground water.

Water is dispersion medium in many biochemical reactions[2] which are responsible for the living process therefore without water life cannot survive. So water is essential for life not only for humans but all life plants and animal. Hence the quality of water plays an important role in human life. Generally ground water is much clean than surface[3] water but the abnormal growth of urbanization, Industrialization further affected the ground water quality due to increasing of resources and improper draining of wastage and effluents. One of another reason is large amount of wastage is concentrated in small area.

According to WHO 2.2 million people die from dieses causes from lake of safe drinking water[4].(Global Water Supply and Sanitation Assessment 2000 report). In general ground water is a suitable source for drinking water because of its high quality w.r.t others sources of water. Hence we need to protect and management of ground water quality[5]. The main aim of this study is to carry out the quality analysis of physicochemical parameters of selected groundwater industrial areas in around the Vijayawada. The result of the study increases to understand identification of ground water contamination and reliable management of groundwater quality.

Study Area

Vijayawada is a commercial city located on the bank of Krishna river in Krishna district of Andhra Pradesh, India. It is the third largest city in Andhra Pradesh, with an area of 261.88 km^2.

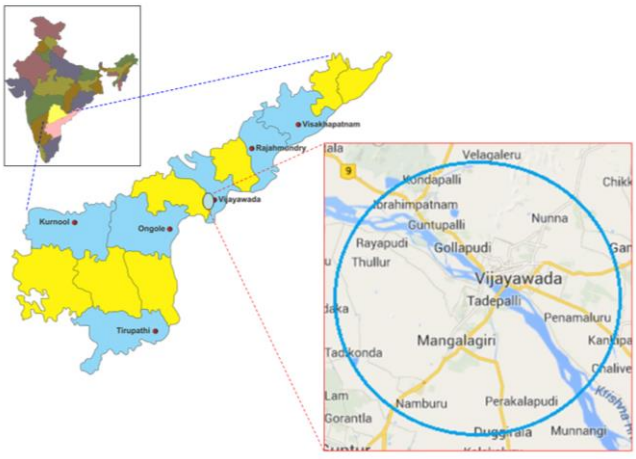

Figure 1. Location of the studied area

The city municipal limits has a population of 1,048,240 (2011 Census), while the population of the metropolitan area is 1,491,202. Located at 16.52° north latitude 80.62° east longitude and the average elevation of the land of the city of Vijayawada is about 39 feet above the sea level (Fig. 1). The northern, northwestern, and southwestern parts of the city are covered by a low range of hills, while the central, southwestern and northwestern parts are covered by rich and fertile agriculture lands with three major irrigation canals.

The main ground water recharging area in the study area is Krishna River and Eluru canal. The Krishna River passing on south side and Eluru canal passing on the North-East of our study area, Vijayawada. The ground water level in open-dug and bore wells are varying 2.5 to 3 meters below the ground level. The study area located North-East side of Vijayawada city (AutoNagar) south side (Morampudi and Pedavadlapudi, Atmakuru) and IDL (Ibrahimpatnam).

Geology and soil type in study area

The study area has changed lithological formations ranging in age from archaean crystallines to recent alluvium. Depending upon the occurrence of these rock formations the area can be divided into three lithological provinces. i) The north and western part occupied by crystalline group of rocks comprising of khondalites, peninsular gneisses, dharwars and Proterozoic group of rocks, ii) North-eastern and central part occupied by Sandstones of Gondwana group and iii) Eastern and southern part occupied by River and Coastal Alluvia. There are four types of soils in the area, viz., black cotton soils (57.6%), sandy clay loams (22.3%), red loamy soils (19.4%), and sandy soils (0.7%). The sandy soils form a fringe along the coast. The black cotton soil is most extensive and occurs in Western part. The sandy clay loam formed along river. The climate is an integral part of the geography of Vijayawada. Marked by hot summers, the temperature in the summer months goes on ascending and can even reach up to 50 °C. The winter months on the other hand are cool and pleasant and the temperature varies from 10 to 30 °C. The region experiences regular rainfall, (Fig. 2) caused by the south-west and north-east monsoons. The area is somewhat prone to cyclones which have resulted in the place being nicknamed as **"Blazewada".**

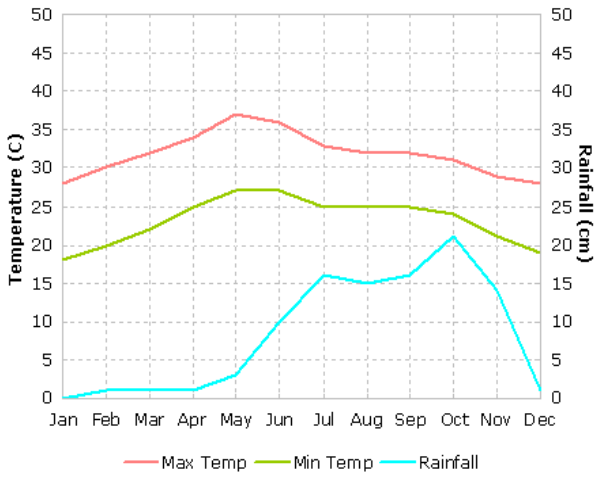

Figure 2. The average temperature and rainfall amount in a year

Materials and methods

The ground water samples are collected from bore and wells in the study area in the month of October 2012 .the sampling location are give table-1Deionised water used for the preparation of solution throughout the study. The samples are collected in clean HDPE bottles .the bottles are prewashed with laboratory grade detergent followed by adequate rinsing with deionized water. Two samples are collected in each sample site and the samples are acidified with 1.5ml of nitric acid per liter. And these samples are stored at 4°C before analysis.

Sample Analysis

Samples were categorized in five sections, as listed in Table 1. Samples were analyzed for trace metals[6] (Pb, Cu, Fe, Ag, Zn, Cd, Mn, Ni, Cd, and Co) using atomic absorption spectrophotometer (AAS, Shimadzu AA-6300). Analysis was carried out in triplicate and average values are reported.

Table 1. List of collected samples

S.No.	Industry type	No. of samples	Area/sample location
1	Chemical	13	Ibrahimpatnam, Vijayawada
2	Beverage/Diary	6	Morampudi, Vijayawada
3	Electroplating Alloys	20	Autonagar, Vijayawada
4	Power plants	4	Kondapally, Vijayawada
5	Automobiles and Mechanical works	17	Autonagar, Vijayawada

The AAS was calibrated with relevant Shimadzu AAS spectroscopic grade standards. Flame atomic absorption spectrophotometer (Shimadzu double beam Atomic Absorption Spectrophotometer) (Direct determination - Flame: Pb, 0.1ppm; Furnace: Pb, 0.3ppb)

Results and discussions:

All the 60 samples were labeled properly and analyzed for the metal content. Sample were analyzed 5 times (n=5) and their SUM, Max, Min, Mean, STDEV, % RSD and AveDEV were obtained. The minimum, maximum and average trace metal concentrations[7] in different parts of the Vijayawada region has been presented in Table 2.

Lead (Pb)

The minimum and maximum lead concentrations varied between 0.012-0.153 mg/l all of the samples exceeded the relevant prescribed limits for drinking water for that element. The major sources of lead in drinking water are corrosion of household plumbing systems; and erosion of natural deposits.

Table 2. The minimum, maximum and average trace metal concentrations in different parts of the Vijayawada region.

Sample Code	Location	Pb	Cu	Ni	Fe	Ag	Zn	Mn	Cd	Cr	Co
1	Continental Coffee	0.060	1.086	0.127	1.677	0.107	0.925	0.449	0.130	0.222	0.035
2	Continental Coffee	0.055	0.996	0.116	1.538	0.098	0.849	0.412	0.119	0.204	0.032
3	Coca-Cola Ind. Pvt Ltd	0.050	0.912	0.112	1.409	0.090	0.777	0.377	0.109	0.187	0.029
4	Coca-Cola Ind. Pvt Ltd	0.047	0.840	0.103	1.368	0.083	0.755	0.348	0.101	0.172	0.027
5	Coca-Cola Ind. Pvt Ltd	0.043	0.771	0.095	1.255	0.076	0.692	0.319	0.092	0.158	0.025
6	Viaya Milk Diary	0.060	1.099	0.091	1.634	0.113	0.714	0.072	0.127	0.245	0.035
7	Viaya Milk Diary	0.067	1.217	0.101	1.809	0.125	0.790	0.080	0.140	0.271	0.039
8	Lanco Industry	0.074	1.346	0.112	2.001	0.138	0.874	0.089	0.155	0.299	0.043
9	VTPS Industries	0.100	0.800	0.100	1.400	0.200	0.600	0.100	0.100	0.100	0.100
10	VTPS Industries	0.096	0.789	0.140	1.328	0.206	0.589	0.088	0.127	0.125	0.056
11	NTPS	0.093	0.761	0.135	1.281	0.199	0.569	0.085	0.123	0.120	0.054
12	Zenith Polymers	0.155	1.355	0.135	2.257	0.135	0.903	0.074	0.122	0.446	0.090
13	Lakshmi Electrodes	0.216	1.382	0.124	2.627	0.261	0.889	0.085	0.133	0.646	0.126
14	Lakshmi Synthons	0.198	1.265	0.114	2.406	0.239	0.814	0.077	0.122	0.591	0.116
15	Ida Main Road	0.182	1.163	0.104	2.210	0.231	0.788	0.071	0.112	0.543	0.106
16	Ida Main Road	0.167	1.067	0.096	2.028	0.212	0.723	0.065	0.103	0.498	0.098
17	R.K Industries	0.200	1.500	0.100	3.200	0.100	1.000	0.100	0.100	0.500	0.100
18	Alekhya Chemicals	0.234	1.825	0.159	2.467	0.128	1.219	0.068	0.137	0.409	0.137
19	Sandeep Chemicals	0.214	1.671	0.146	2.259	0.117	1.116	0.062	0.126	0.451	0.125
20	Godrej Agro Ltd	0.197	1.538	0.134	2.079	0.108	1.083	0.057	0.116	0.501	0.115
21	Post Office	0.191	1.488	0.130	2.011	0.104	1.047	0.050	0.112	0.484	0.112
22	Siris Chemical Industries	0.175	1.365	0.119	1.846	0.096	0.961	0.046	0.103	0.444	0.102
23	M.S Industries	0.169	1.315	0.115	1.778	0.087	0.926	0.044	0.099	0.428	0.099
24	KanuruAutomobile Works	0.155	1.209	0.105	1.634	0.085	0.851	0.041	0.091	0.394	0.091
25	S. Lakshmi Prsanna Paper Mill	0.142	1.109	0.097	1.500	0.078	0.781	0.037	0.083	0.361	0.083
26	Lakshmi Chaithanya Alloys	0.137	1.071	0.093	1.447	0.075	0.754	0.036	0.081	0.348	0.080
27	Agni Coals	0.155	1.468	0.124	2.246	0.079	0.945	0.087	0.122	0.432	0.090
28	Sri Sai Electrodes	0.112	0.896	0.142	1.599	0.140	0.620	0.095	0.131	0.111	0.065
29	Vardam Electrodes	0.108	0.865	0.137	1.544	0.135	0.599	0.092	0.126	0.107	0.063
30	Vardam Electrodes-2	0.105	0.837	0.133	1.495	0.130	0.580	0.089	0.122	0.104	0.061
31	Ratna Electrical Works	0.072	1.274	0.092	1.753	0.222	0.838	0.078	0.117	0.280	0.042
32	Ratna Electrical Works-2	0.100	1.200	0.100	1.700	0.200	0.800	0.100	0.100	0.300	0.000
33	Sree Sai Oil Works	0.155	1.537	0.155	2.030	0.187	0.994	0.076	0.130	0.329	0.090
34	Sahani Automobile Works	0.142	1.407	0.142	1.859	0.171	0.910	0.070	0.119	0.301	0.083
35	Sree Sai Durga Rubber Works	0.137	1.367	0.138	1.806	0.166	0.884	0.068	0.115	0.276	0.080
36	Asian Biochemical Industries	0.126	1.253	0.126	1.656	0.152	0.811	0.062	0.106	0.254	0.074
37	Visak Industries	0.100	1.100	0.100	2.100	0.100	0.700	0.100	0.100	0.500	0.100
38	Vinay Plastics	0.090	1.090	0.090	1.989	0.136	0.700	0.112	0.128	0.451	0.053
39	G.V.K Diesel Works	0.087	0.000	0.143	1.633	0.072	0.773	0.088	0.142	0.312	0.051
40	Azahar Radiators	0.100	1.100	0.100	2.000	0.100	0.700	0.100	0.100	0.400	0.100
41	Sai Sagar Industries	0.138	1.026	0.110	1.973	0.073	0.679	0.084	0.119	0.435	0.081
42	Ambica Chemcials	0.118	1.334	0.094	1.848	0.069	0.838	0.082	0.121	0.280	0.069
43	Ambica Chemcials -2	0.113	1.286	0.091	1.781	0.066	0.808	0.079	0.117	0.270	0.066
44	Ambica Chemcials -3	0.110	1.248	0.088	1.729	0.064	0.784	0.077	0.113	0.262	0.064
45	Sree Kanaka Durga Works	0.155	1.196	0.118	1.981	0.075	0.782	0.068	0.127	0.254	0.090
46	Sree Lakshmi Industries	0.150	1.158	0.114	1.918	0.073	0.756	0.066	0.123	0.246	0.088
47	Sri Gayatri Industries	0.145	1.119	0.111	1.854	0.070	0.731	0.063	0.118	0.238	0.085
48	Automobile Works	0.081	0.937	0.122	1.655	0.079	0.584	0.068	0.117	0.365	0.047
49	Swathi Gases	0.074	0.861	0.112	1.521	0.073	0.537	0.062	0.108	0.335	0.043
50	Lakshmi Timber Depot	0.068	0.790	0.103	1.396	0.071	0.493	0.057	0.099	0.308	0.040
51	Syshame Enterprises	0.066	0.762	0.100	1.347	0.065	0.475	0.055	0.096	0.297	0.039
52	Vijaya Lakshmi Diesel Agency	0.000	1.000	0.100	2.400	0.100	0.600	0.100	0.100	0.200	0.000
53	Siry Automobiles	0.012	0.925	0.118	2.213	0.057	0.567	0.085	0.113	0.184	0.007
54	Sri Rama Industries	0.012	0.894	0.114	2.138	0.056	0.548	0.082	0.109	0.178	0.007

55	Sree Uma Maheswara Mech.	0.013	0.826	0.161	3.889	0.139	0.509	0.114	0.133	0.102	0.008
56	Automobile Compacts	0.013	0.802	0.157	3.775	0.135	0.494	0.111	0.129	0.099	0.008
57	Krishan Moulds	0.013	0.776	0.152	3.655	0.130	0.479	0.107	0.125	0.096	0.007
58	Siva Sankar Casting Works	0.011	0.928	0.137	1.963	0.080	0.628	0.101	0.135	0.160	0.006
59	Sai DurgaTurning Works	0.222	1.713	0.158	2.597	0.045	1.508	0.243	0.133	0.342	0.130
60	Rockwell Industries	0.093	1.093	0.127	2.279	0.064	0.943	0.143	0.136	0.178	0.054

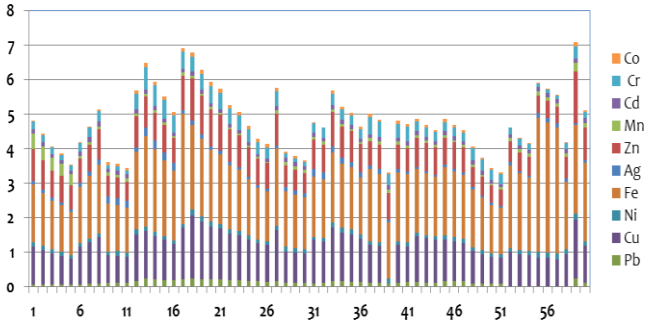

Figure 2. The heavy metal contamination of sample sites

Lead[8] enters the water ("leaches") through contact with the plumbing. Lead leaches into water through corrosion – a dissolving or wearing away of metal caused by a chemical reaction between water and your plumbing. Lead can leach into water from pipes, solder, fixtures and faucets (brass), and fittings. The amount of lead in your water also depends on the types and amounts of minerals in the water, how long the water stays in the pipes, the amount of wear in the pipes, the water's acidity and its temperature.

Copper (Cu)

The minimum and maximum copper concentrations were found to be ND and 1.85 mg/L respectively. Out of 60, 40 water samples exceeded the Cu maximum contaminant limits stipulated for drinking water. Cu enters the water system through mineral dissolution, industrial effluents, because of its use as algaecide, agricultural pesticide sprays and insecticide. Cu may be dissolved from water pipes and plumbing fixtures, especially by water whose pH is below 7. Cu salts are sometimes purposely added in small amounts to water supply reservoirs to suppress the growth of algae. Therefore Cu is more readily available for solution in surface and ground water than its low average abundance in rocks might imply

Iron (Fe)

The minimum and maximum iron concentrations varied between 1.347mg/l Measurable concentrations of the metal were found in all samples. However, all samples exceeded the relevant prescribed limits for drinking water Iron exists naturally in rivers, lakes, and underground water. It may also be released to water from natural deposits, industrial wastes, refining of iron ores, and corrosion of iron containing metals.

Silver (Ag)

The maximum and minimum concentration o f silver varied between 0.05- 020 mg/l. Measurable concentration of the metal was found in all samples. In some of the samples the concentration of the metal exceeds the limits. It released from a large area, such as an industrial plant or from a container, such as a drum or bottle, it enters the environment as a chemical emission.

Zinc (Zn)

The maximum and minimum concentration of zinc metal varied between the 0.05 -1.5 mg/l. In all samples measurable concentration of Zn is found. The metal concentration is not exceed the limits. Zn has lots of use like galvanization of steel, preparation of negative plates in electric batteries, vulcanization of rubber, wood preservatives and antiseptics and in rat and mouse poison (Zn-phosphide)17. Zn is also used extensively as a white pigment, zinc oxide (ZnO) in paint and rubber.

Manganese (Mn)

The minimum and maximum manganese concentrations varied between 0.02-0446 mg/l. Measurable concentrations of the manganese metal were found in all samples. However, only 15 of the samples exceeded the relevant prescribed limits for drinking water for that element. Mn is a very reactive element, found in nature and used extensively in industry for the manufacture of glass, ceramics, batteries, paints, varnishes, inks, dyes and fireworks14. However, in ground waters subject to reducing conditions Mn can be leached from the soil and occur in high concentrations

Cadmium (Cd)

All water samples had measurable concentrations of Cd metal. However, the samples concentration between 0.081 - 0.155 mg/l all samples exceeded the relevant maximum contaminant limits prescribed for Cd in drinking water. cadmium Is enter into drinking water because corrosion of galvanized pipes; erosion of natural deposits; discharge from metal refineries; runoff from waste batteries and paints.

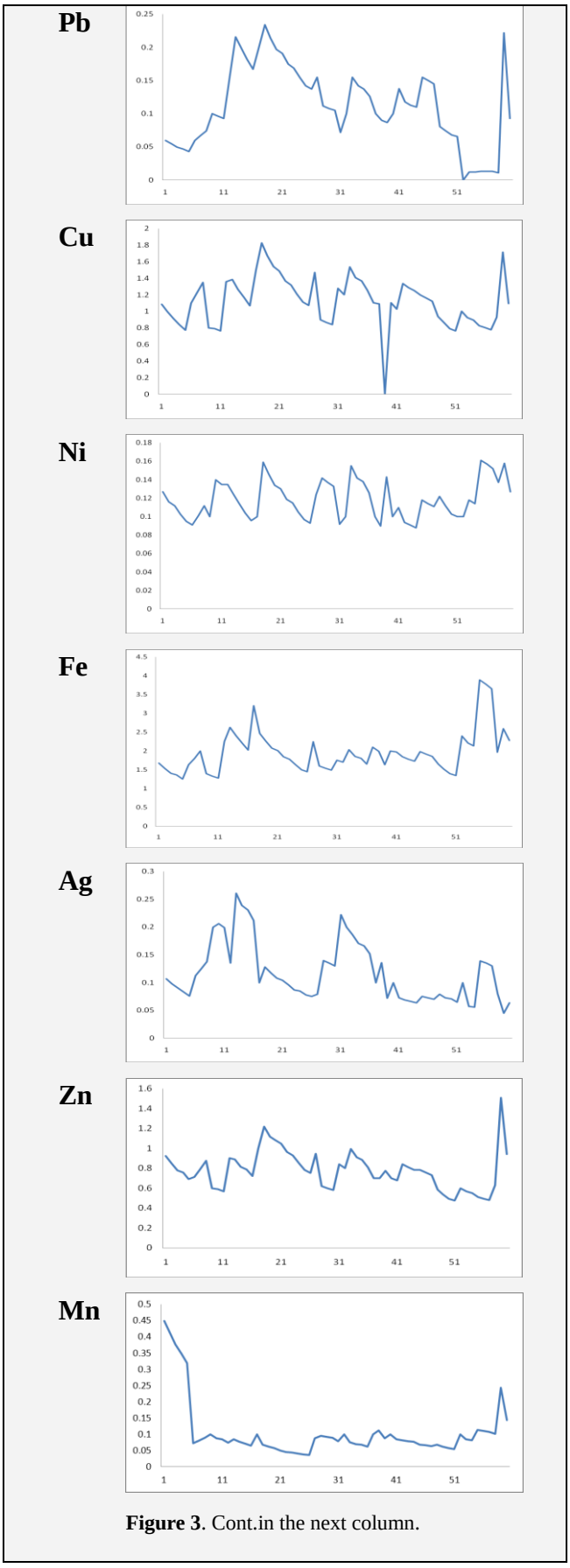

Figure 3. Cont.in the next column.

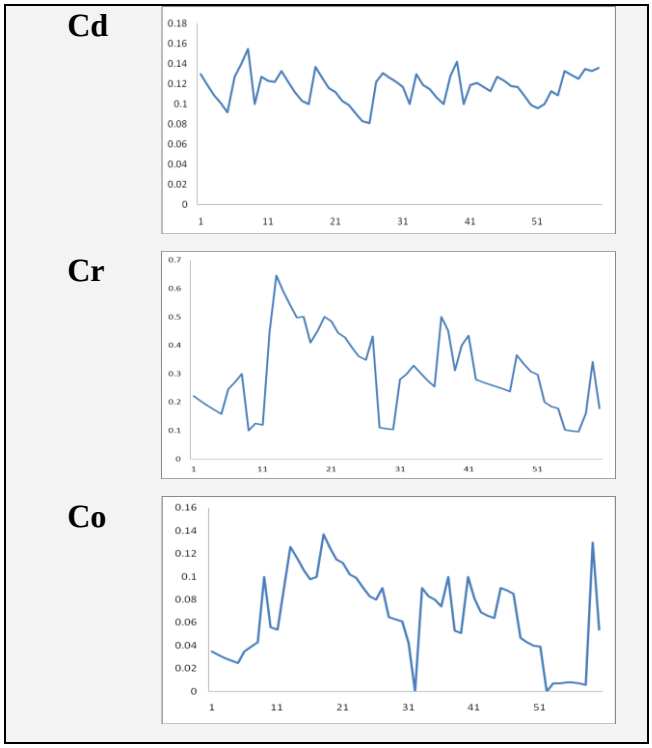

Figure 3. Distribution of heavy metal elements along the sample sites

Chromium (Cr)

The minimum and maximum Cr concentrations were found to be 0.096-0.646 mg/l respectively. Sixty water samples had measurable concentrations of Cr metal. However, the entire sample exceeded the Cr maximum contaminant limits stipulated for drinking water. Hexavalent chromium can enter water through industrial contamination from manufacturing facilities, including electroplating factories, leather tanneries and textile manufacturing facilities, or from disposal of fluids used in cooling towers before 1990. It also occurs naturally in some minerals. The commonly used tap water disinfectant chlorine can transform trivalent chromium into toxic hexavalent chromium. Chromium-6 is also produced by industrial processes and manufacturing activities including discharges from steel and pulp mills among others.

Nickel (Ni)

Sixty water samples had measurable concentrations of Ni between 0.093-0.157 mg/l However, none of the samples exceeded the Cr maximum contaminant limits stipulated for drinking water. Ni enters groundwater and surface water sources by dissolution from rocks and soils, from biological recycling, from atmospheric fallout and especially from industrial wastes. Through leaching from Ni-containing pipes

Cobalt (Co)

The minimum and maximum cobalt concentrations were found to 0.007-0.137 mg/l. Out of the 60 samples none of the samples are found to be exceeds the limits. The Sources of environmental cobalt are both natural and anthropogenic[13]. Natural sources include erosion (wind-blown continental dusts), weathering of rocks and soil, seawater spray, volcanoes, forest fires, extraction by plants, and continental and marine bionic emission.

Conclusions

The result shows that ground water quality assessment[9] helps to identify the significant parameters of water samples were collected from bore wells covering the Vijayawada industrial region. The minimum and maximum trace metals concentrations[10] in different areas for, Pb, Cu, Fe, Ag, Zn, Cd, Mn, Ni, Cd, and Co are 0.012-0.153 , 0.00 and 1.85, 0.00 -1.347, 0.05- 020, 0.05 -1.5, 0.2-0.446, 0.081 - 0.155, 0.096-0.646, .007-0.137, 0.093-0.157 mg/L respectively. Trace metals like Cd, Cr, Fe, Mn and exceeded the maximum limits according to WHO and IS10500 2012 for drinking water[11] in several sampled bore wells in the Vijayawada region. It is recommended to use some kind of inexpensive treatment to reduce the levels of trace metals[12] in areas supplying water directly to consumers without any treatment. From the obtained results it is evident that, at present the metal ion concentration is not at the levels which could be harmful for humans[13]. But still the study clearly points out that the concentrations of toxic metals are present in slight excess in some locations. It indicates precautionary measures should be immediately taken to avoid the consequences.

Acknowledgement

The authors express their deep sense of gratitude and sincere thanks to Mr. Sammaiah for assistance in water analysis in all these studies.

References

[1]Rizwan, U., Riffat, N. M., and Abdul,Q., *Afr. J. Env. Sci. Technol.*, **2009,** *3(12),* 429-446.

[2] Pacyna, J. M., Pacyna, E. G. and Asa, W., *Atm. Environ*., **2009**, *43(1),* 117-127.

[3] Satyanarayana, T. and Guru Prasad, B., *J. Nat. Environ. Pollut. Techn.* **2006**, *5(3),* 459-461.

[4] Schulze, E., WHO, Geneva **1984***(2),* 335.

[5] Chaitali V. M., Jayashree, D., *Int. J. Innov. Res. Sci. Eng. Tech.*, **2013**, *2(7),* 2992.

[6]Catherine, G., Richard, G., and Philippe Q., Ed(s), *Rapid Chemical and Biological Techniques for Water Monitoring*, **2009**.

[7] Ehi-Eromosele, C. O., Okiei, W. O., *Resourc. Environ.*, **2012**, *2(3),* 82. doi: 10.5923/j.re.20120203.01

[8]Clescexi, L. S., Arnold, E., Greenberg, R. and Rhodes, T., Standard methods for the examination of water and waste-water. *APHA*,Washington D.C. **2005**.

[9]Janardhana Rao, D., Hari Babu, B., Swami, A.V.V.S., and Sumithra, S., *Univ. J. Environ. Res. Tech.*, **2013**, *3(2),* 225.

[10]Shaheda, N., Swamy, A.V.V.S., Syamala Devi, K., *Int. J. Eng. Sci. Res.*, **2013**, *3(8),* 419.

[11]Hem, J. D., *Study and Interpretation of the Chemical Characteristics of Natural Water, 3rd Ed*., Scientific Publishers, Jodhpur 1991, 73-122.

[12]Borah, K. K., Bhuyan, B., and Sarma, H. P., *E-J. Chem.*, **2009,** *6(S1),* S501.

[13]Botkin, B. D., Keller, E.A., *Environmental Science: Earth as a Living Planet.* New York: Wiley; **2005**.

Received: 27.07.2014.
Accepted: 26.10.2014.

SYNTHESIS OF SILVER NANO PARTICLES USING PIPER BETLE AND ITS ANTIBACTERIAL ACTIVITY

P. Shanmuga Praba,[a] J. Jeyasundari[a]* and Y. Brightson Arul Jacob[b]

Keywords: *Piper betle*, Silver nanoparticles, antibacterial activity

Most of the researchers have been reported about the nontoxic biosynthesis of silver nanoparticles using several microorganism and plant extracts. This ecofriendly silver nanoparticles exhibit completely new or improved properties based on specific characteristics such as size, distribution, morphology and many applications. In this research the synthesis of silver nanoparticles using *Piper betle* has been investigated. We have synthesized silver nano particles using 1 mM silver nitrate solution into the plant extract and characterized by UV-vis absorption spectroscopy. The antibacterial efficacy also determined by disc diffusion method with *Bacillus cereus*, *Escherchia coli*, *Klebsiella pneumonia*, *Staphylococcus aureus* and it showed that high level of inhibition. The most outcome of this research will be suggested that biologically synthesized silver nanoparticle has more effective against various disease causing pathogens.

* Corresponding Authors
E-Mail:jjsundari16@gmail.com
[a] PG & Research Department of Chemistry, NMSSVN College, Nagamalai, Madurai-625019, Tamilnadu India.
[b] PG & Research Department of chemistry, The American College, Madurai-625002, Tamilnadu, India.

Introduction

Biological methods of synthesis have paved way for the "green synthesis" of nanoparticles and these have proven to be better methods due to slower kinetics, they often better manipulation and control over crystal growth and their stabilization. This has motivated an upsurge in research on the synthesis routes that allow better control of shape and size for various nanotechnological applications. The use of environmentally benign materials like plant extract,[1] bacteria,[2] fungi[3] and enzymes[4] for the synthesis of silver nanoparticles after numerous benefits of eco-friendliness and compatibility for pharmaceutical and other biomedical applications as they do not use toxic chemicals for the synthesis protocol. Green synthesis provides advancement over chemical and physical method as it is cost effective, environment friendly, easily sealed up for large scale synthesis and in this method there is no need to use high pressure, energy, temperature and toxic chemicals. Various approaches are available for the synthesis of silver. NPs include chemical,[5] electrochemical,[6] radiation,[7] photochemical methods,[8] Langmuir-Blodgett,[9,10] and biological techniques.[11]

Silver has long been recognized as having inhibitory effect on microbes present in medical and industrials process.[11,12] The most important application of silver and silver nanoparticles is in medical industry such as topical ointments to prevent infection against burn and open wounds.[13]

Existing literature also reports successful synthesis of silver nanoparticles through green route where the reducing and capping agent selected was the latex obtained from *Jatropha curcas*.[14] AgNPs were also obtained using *Aloe vera*,[15] *Acalyphaindica*,[16] *Garcinia mangostana*[17] as reducing agent.

Figure 1. Picture of *Piper betle* plant

Here we report green synthesis of silver nanoparticles using *Piper betle* extract which was confirmed by using various characterization techniques and application of antibacterial activity.

Materials and Methods

Reagents and chemicals: Silver nitrate was obtained from sigma Aldrich. Freshly prepared triple distilled water was used throughout the experiment.

Preparation of leaf extract by boiling method

Piper betle leaves were collected and washed several times with deionized water. 20 g of finely cut *Piper betle* leaves were taken and boiled in 200 ml of double distilled water for 3 min and filtered through Whatman No 1 filter paper. The filtrate was collected and stored at 4 °C for further use.

UV-Vis spectra Analysis

The reduction of pure Ag^+ ions was monitored by measuring the UV-Vis spectrum of the reaction medium at 3 hours after diluting a 1 ml of the sample into 4 ml of distilled water. UV-Vis spectral analysis was done by using UV-Vis spectrophotometer(Lambda 35).

FTIR analysis

For FTIR measurements, Silver nanoparticle solution was centrifuged at 12,000 rpm for 12 minutes. The pellet was washed three times with 20 ml of deionized water. The samples were dried and analyzed on IR-Prestige-21[SHIMADZU].

Antibacterial activity

The anti bacterial activity was done on human pathogenic *Bacillus cereus, Escherichia coli, Klebsiella pneumonia, Staphylococcus aureus* by the standard disc diffusion method. Nutrient agar (NA) plates were seeded with 8 h broth culture of different bacteria. In each of these plates, well were cut out using sterile cor borer. Using sterilized dropping pipettes, different concentrations (10, 20, 30, 40 µl/well) of sample was carefully added into the wells and allowed to diffuse at room temperature for 2 h. The plates were then incubated at 37 °C for 18-24 h. Gentamicin (10 µg) was used as positive control. The antibacterial activity was evaluated by measuring the diameter of inhibition zone.

Results and Discussion

Synthesis of silver nanoparticles

Piper betle extract is used to produce silver nanoparticles in this experiment Ag^+ ions were reduced to Ag nanoparticles when plant extract is mixed with $AgNO_3$ solution in 1:8 ratio reduction is followed by on immediate change in yellowish to brown color in the aqueous solution of the plant extract due to excitation of surface plasmon vibration in silver nanoparticle.[18] Further formation of AgNPs in aqueous extract can be monitored by color change. Fig. 1. Shows the color changes when the aqueous extract of *Piper betle* plant was mixed with a $AgNO_3$ solution. The mixture was kept at room temperature for 24 hours. The appearance of a yellowish-brown color in the reaction vessel indicated formation of AgNPs. AgNPs exhibit this yellowish-brown color in aqueous solution due to excitation of surface plasmon resonance in the AgNPs.

UV-Vis spectroscopy analysis

UV-Vis spectroscopy is most widely used technique for structural characterization of silver nanoparticles. This was confirmed by the UV-Vis spectroscopy of the colloidal solution of silver nanoparticles has been recorded. Fig. 3 shows that absorption spectra of silver nanoparticles formed in the reaction media has absorbance peak at 444 nm. Broadening of peak indicated that the particles are polydispersed.[19]

Figure 2. Color changes after the addition of leaf extract with aqueous silver nitrate solution: (A) silver nitrate solution (control), (B) silver nitrate with boiled leaf extracts

As shown in Fig. 3, the surface plasmon resonance of the AgNPs was centered at approximately 444 nm, indicating the presence of AgNPs in the solution.

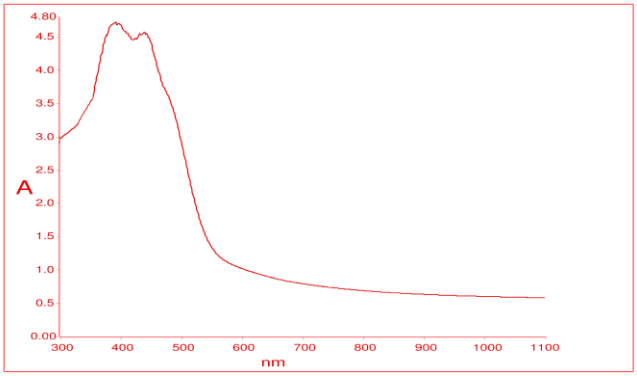

Figure 3. UV–Vis bioreduction kinetics in the range 300–700 nm for colloidal AgNPs solution with *Piper betle* leaf extract.

FTIR Spectroscopy Analysis

The FTIR spectrum of Ag nanoparticle is shown in Fig 4. The IR spectrum of Ag nanoparticles shown band at 3433 cm^{-1}, 1657 cm^{-1}, 2395 cm^{-1}, 1384 cm^{-1}, 1020 cm^{-1} corresponds to O-H stretching for alcohols and phenols, carbonyl stretching, N-H bond stretching of amines, C-N stretching of the aromatic amino group and C-O stretching of alcohols and ethers respectively. FTIR spectrum of Ag nanoparticles suggested that Ag nanoparticles were surrounded by different organic molecules such as terpenoids, alcohols, ketones, aldehydes and carboxylic acids. Fig. 4. Shows the plant *Piper betle* has been effectively involved in the antibacterial activity and also which is used in syntheses the silver nanoparticles.

Antibacterial activity

The anti bacterial activity was done on human pathogenic *Bacillus cereus, Escherchia coli, Klebsiella pneumonia, Staphylococcus aureus* by the standard disc diffusion method. (Fig. 5.)

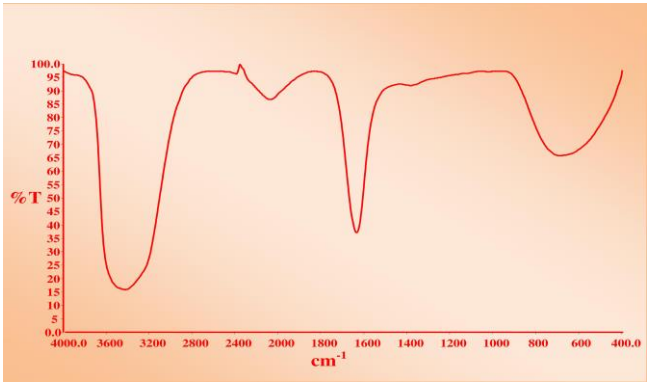

Figure 4. FTIR spectra of silver nanoparticles synthesized using *Piper betle* leaf extract

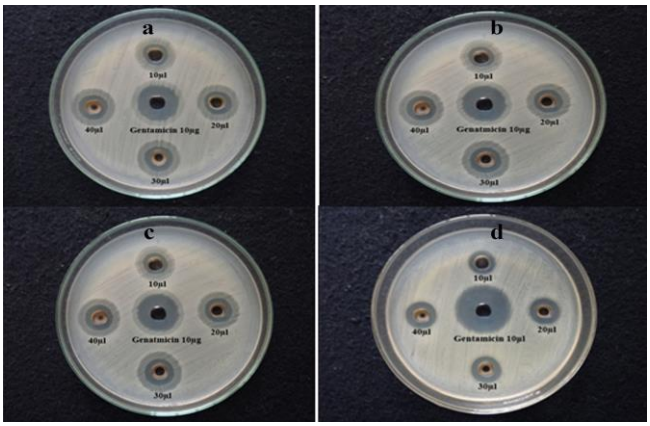

Figure 5. Antibacterial activity of synthesized silver nanoparticles (*Piper Betle* plant extract) on a) human pathogenic *Bacillus cereus*, b) *Escherchia coli*, c) *Klebsiella pneumonia*, d) *Staphylococcus aureus* by the disk diffusion method.

Table 1. Effect of silver nanoparticles on human pathogens

Pathogens	Zone of Inhibition	
	Plant silver	Gentamicin
Bacillus cereus	17mm	22mm
Escherchia coli	15mm	24mm
Klebsiella pneumonia	15mm	24mm
Staphylococcus aureus	16mm	26mm

Conclusion

We have demonstrated a good method for developing a simple, safe, cost-effective, and ecofriendly preparation of AgNPs in an aqueous extract of *Piper betle*. The present study concluded that the *Piper betle* plant extract can be used as an excellent source for synthesizing the silver nanoparticles. The primary confirmatory for the silver nanoparticles was color change of the solution, and UV-Vis absorption spectra of silver nanoparticles containing solution showed a peak at 444 nm, which confirms the presence of silver nanoparticles. FTIR spectrum of Ag nanoparticles suggested that Ag nanoparticles were surrounded by different organic molecules such as terpenoids, alcohols, ketones, aldehydes and carboxylic acids. The green synthesized nanoparticles have more effective antibacterial activity to the pathogens. So green synthesis of nanoparticles can be ecofriendly involved in the many applications of clinical, biomedical sectors and etc.

Acknowledgement

The authors are thankful to the management, principal and Head, chemistry department, NMSSVN College and The American College, Madurai, Tamilnadu, for their encouragement and necessary laboratory facilities

References

[1]Mukunthan, K. S., Elumalai, E. K., Patel, T. N., Ramachandramoorty,V., *Asian J. Trop. Biomed.*, **2011**, 270-274.

[2]Salata, O. V., *J. Nanobiotechnol*., **2004**, *2*, 3.

[3]Lu, J. M., Wang, X., Muller, C. M., Wang, H., Lin, P. H., Yao, Q., Chen, C., *Expert Rev. Mol. Diagn.*, **2009**, *9(4)*, 325-341.

[4]Satyavani, K., Gurudeepan, S., Balasubramanian, T. R., *J. Nanobiotechnol.*, **2011**, *9*, 43.

[5]Sharma, V. K., Yngard, R. A., Lin, Y., *Adv. Colloid Interface Sci.*, **2009**, *145*, 83-96.

[6]Yin, B., Ma, H., Wang, S., Chen, S., *J. Phys. Chem. B.*, **2003**, *107*, 8898–8904.

[7]Dimitrijevic, N. M., Bartels, D. M., Jonah, C. D., Takahashi, K., Rajh, T., *J. Phys. Chem. B*., **2001**, *105*, 954–959.

[8]Callegari, A., Tonti, D., Chergui, M., *Nano Lett*., **2003**, *3*, 1565–1568.

[9]Zhang, L., Shen, Y. H., Xie, A. J., Li, S. K., Jin, B. K., Zhang, Q. F., *J . Phys. Chem. B*., **2006**, *110*, 6615–6620.

[10]Swami, A., Selvakannan, P. R., Pasricha, R., Sastry, M., *J. Phys. Chem. B*., **2004**, *108*, 19269

[11]Naik, R. R., Stringer, S. J., Agarwal, G., Jones, S., Stone, M. O., *Nat. Mater*., **2002**, *1*, 169–172.

[12]Kemp, M. M., Kumar, A., Clement, D., Ajayan, P., Mousa, S., Linhard, R. J., *Nanomedicine*., **2009**, *4(4)*, 421-429.

[13]Safaepour, M., Shahverdi, A. R., Khorramizadeh, M. R., Gohari, A R., *Avicenna J. Med. Biotechnol.*, **2009**, *1(2)*, 111-115.

[14]Sankar, S. S., Rai, A., Anamwar, B., Singh, A., Ahmad, A., Sastry, M., *Nat. Mater*.,**2004**, *3*,482.

[15]Bar, H., Bhui, D. K., Sahoo, G. P., Sarkar, P., De, S. P., Misra, A., *Physicochem. Eng. Asp*., **2009**, *339*, 134–139.

[16]Chandran, S. P., Chaudhary, M., Pasricha, R., Ahmad, A., Sastry, M., Biotechnol. Prog., **2006**, *22*, 577–583.

[17]Krishnaraj, C., Jagan, E. G., Rajasekar, S., Selvakumar, P., Kalaichelvan, P. T., Mohan, N., *Biointerfaces*, **2010**, *76*, 50–56.

[18]Veerasamy, R., Xin, T. Z., Gunasagaran, S., Xiang, T. F. W., Yang, E. F. C., Jeyakumar, N., Dhanaraj, S. A., *J. Saudi Chem. Soc*., **2010**, *15*, 113-12.

[19]Jeevaa, K., Thiyagarajana, M., Elangovanb, V., Geethac, N., Venkatachalama, P., *Ind. Crops Prod*.**, 2014**, *52*, 714–720.

[20]Banerjee, P., Satapathy, M., Mukhopahayay, A., Das., P., *Biores. Bioprocess*., **2014**, *1*, 3.

[21]Ghaffari-Moghaddam, M., Hadi-Dabanlou, R., Khajeh, M., Rakhshanipour, M., Shameli, K., *Korean J. Chem. Eng.*, **2014**, *31*, 548–557.

Received: 23.08.2014.
Accepted: 26.10.2014.

CRYSTAL STRUCTURE OF 4-ETHYL-1,3-OXAZOLIDINE-2-THIONE

Hisako Okumura[a]*, Soh-ichi Kitoh[b], Mitsuhiro Suda[b], Mitsunori Honda[b] and Ko-Ki Kunimoto[b]

Keywords: Crystal structure; Hydrogen-bond; Oxazolidine thione; Thioamide; X-ray diffraction.

The crystal structure of 4-ethyl-1,3-oxazolidine-2-thione, C_5H_9NOS, has been determined from single crystal X-ray diffraction. This compound crystallizes in the monoclinic system, space group $P2_1/c$ with the unit cell parameters: a = 8.4988(17) Å, b = 10.2300(15) Å, c = 7.5192(19) Å, β = 96.8299(11) ° and four molecules in the unit cell. In the crystals, a pair of enantiomeric (*R*)- and (*S*)-molecules is connected *via* intermoleculer N1−H···S1 hydrogen bonds of the neighboring thioamide moieties to form a centrosymmetric dimer with an $R^2_2(8)$ graph-set motif.

* Corresponding Author
Fax: +81-258-34-9256
E-Mail: okumura@nagaoka-ct.ac.jp
[a] Department of Materials Engineering, National Institute of Technology, Nagaoka College, 888 Nishikatakai-machi, Nagaoka-shi, Niigata 940-8532, Japan
[b] Graduate School of Natural Science and Technology, Kanazawa University, Kakuma-machi, Kanazawa-shi, Ishikawa 920-1192, Japan

INTRODUCTION

Substituted 1,3-oxazolidin-2-one derivatives and their sulfur analogs, 1,3-oxazolidine-2-thione derivatives represent an important class of 5-membered heterocyclic compounds due to a range of potential applications in pharmacology, biochemistry and organic synthesis.[1,2]

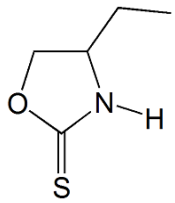

Figure 1. Chemical structure of the title compound.

Furthermore, these derivatives contain an amide or a thioamide group in the oxazolidine ring which may be involved in hydrogen-bonds. They can also act as ligands in coordination complexes. These structural features lead to capability of various hydrogen-bonding patterns and offer wide opportunities in crystal engineering.[3,4]

We have been studying crystal structures and hydrogen-bonding patterns of several 5-membered heterocyclic compounds containing the amide and/or thioamide group.[5-11] As an extension of our research, the present paper reports the crystal structure and hydrogen-bonding pattern of the title compound, 4-ethyl-1,3-oxazolidine-2-thione, C_5H_9NOS (Figure 1), determined from single crystal X-ray diffraction data analysis.

EXPERIMENTAL

Synthesis and Crystallization

The title compound was prepared by the reaction of hydrogen peroxide with a mixture of *DL*-2-amino-1-butanol, carbon disulfide and base in ethanol according to a reported procedure.[12] Single crystals suitable for X-ray diffraction were obtained from a mixed diethylether and hexane solution.

X-ray Data Collection, Structure Solution and Refinement

X-ray diffraction data was collected at 133(2) K by the ω scan technique on a Rigaku/MSC Mercury CCD diffractometer equipped with graphite monochromated MoK_α radiation (λ = 0.71070 Å) and processed using *CrystalClear*.[13] The data were corrected for Lorentz-polarization and absorption effects.[14]

These structures were solved by direct methods using *SIR2008* program[15] and refined by a full-matrix least-squares calculation on F^2 using *SHELXL-97*.[16] All calculations were performed using *CrystalStructure* software package.[17] Non-hydrogen atoms were refined anisotropically. The hydrogen atom bonded to nitrogen atom was located in a difference map and refined freely. The remaining hydrogen atoms were positioned geometrically (C–H = 0.98-1.00 Å) and refined using a riding model, with U_{iso}(H) = 1.2 U_{eq}(C). Structures were visualized using *ORTEP-3 for windows*[18] and *Mercury*.[19]

Crystallographic data for the title compound have been deposited with the Cambridge Crystallographic Data Centre [Deposition No. CCDC-1027326]. The data can be obtained free of charge *via* www.ccdc.cam.ac.uk/data_request/cif (or by contacting the Cambridge Crystallographic Data Centre, 12 Union Road, Cambridge CB2 1EZ, UK.; e-mail: data_request@ccdc.cam.ac.uk).

RESULTS AND DISCUSSION

Table 1 shows the crystal data, data collection and structure refinement parameters of the title compound. Figure 2 shows the molecular structure and atom-labeling scheme determined from single crystal X-ray diffraction analysis. Table 2 summarizes the selected geometric parameters. Figure 4 shows the crystal packing and hydrogen-bonding pattern.

As given in Table 1, the title compound crystallizes in the monoclinic system, space group $P2_1/c$ with the unit cell parameters: a = 8.4988(17) Å, b = 10.2300(15) Å, c = 7.5192(19) Å, β = 96.8299(11) ° and four molecules in the unit cell.

Table 1. Crystal data, data collection and structure refinement.

Crystal data	
Empirical formula	C_5H_9NOS
Formula weight	131.19
Crystal color, Habit	Colorless, Prism
Crystal dimensions	0.15 × 0.15 × 0.08 mm^3
Crystal system, Space group	Monoclinic, $P2_1/c$ (No. 14)
Unit cell dimensions	a = 8.4988(17) Å
	b = 10.2300(15) Å
	c = 7.5192(19) Å
	β = 96.8299(11) °
Volume, Z	649.1(2) Å^3, 4
Density (calcd.)	1.342 g cm^{-3}
F(0,0,0)	280
Absorption coefficient (MoK_α)	0.399 mm^{-1}
Data collection	
Diffractometer	Rigaku/MSC Mercury CCD
Radiation	MoK_α (0.71070 Å)
Temperature	133(2) K
Theta range for data collection	2.41 to 27.47 °
Index ranges	$-11 \le h \le 10$
	$-13 \le k \le 10$
	$-9 \le l \le 9$
Reflections collected	5774
Independent reflections	1396 [R_{int} = 0.0184]
Completeness to theta = 27.47 °	94.3 %
Absorption correction	Multi-scan[14]
Structure solution and refinement	
Structure solution	Direct methods using *SIR2008*[15]
Refinement method	Full-matrix least-squares on F^2 using *SHELXL-97*[16]
Data / Restraints / Parameters	1396 / 0 / 78
Final R indices [I > 2 sigma(I)]	R_1 = 0.0277, wR_2 = 0.0657
R indices (all data)	R_1 = 0.0317, wR_2 = 0.0674
Goodness-of-fit on F^2	1.094
Largest diff. peak and hole	0.240 and −0.200 e A^{-3}

As shown in Table 2 and Figure 2, the bond lengths and angles are normal, and comparable to those observed in 1,3-oxazolidine-2-thiones reported in the Cambridge Structural Database[20] Ver. 5.35. The 1,3-oxazolidine-2-thione moiety (O1/C1/S1/N1/C2/C3) is nearly planar, with maximum deviations of −0.0595(14) Å for C2 atom and 0.0448(14) Å for C3 atom.

Table 2. Selected geometric parameters (Å, °).

Bond lengths			
S1−C1	1.671(2)	O1−C1	1.340(2)
O1−C3	1.463(2)	N1−C1	1.318(2)
N1−C2	1.468(2)	C2−C3	1.538(2)
C2−C4	1.520(2)		
Bond angles			
C1−O1−C3	109.14(9)	C1−N1−C2	113.50(10)
S1−C1−O1	120.63(8)	S1−C1−N1	128.20(10)
O1−C1−N1	111.16(11)	N1−C2−C3	99.90(9)
N1−C2−C4	112.05(10)	C3−C2−C4	113.68(10)
O1−C3−C2	105.60(10)		
Torsion angles			
C1−O1−C3−C2	−6.75(11)	C3−O1−C1−S1	−178.63(8)
C3−O1−C1−N1	2.30(12)	C1−N1−C2−C3	−7.28(12)
C1−N1−C2−C4	113.43(10)	C2−N1−C1−S1	−175.42(9)
C2−N1−C1−O1	3.57(13)	N1−C2−C3−O1	7.96(10)
N1−C2−C4−C5	68.29(12)	C3−C2−C4−C5	−179.36(9)
C4−C2−C3−O1	−111.56(11)		

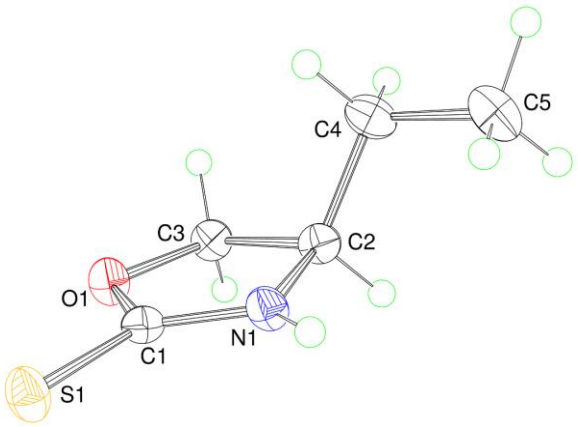

Figure 2. Molecular structure of the title compound. Anisotropic displacement ellipsoids are drawn at the 50% probability level.

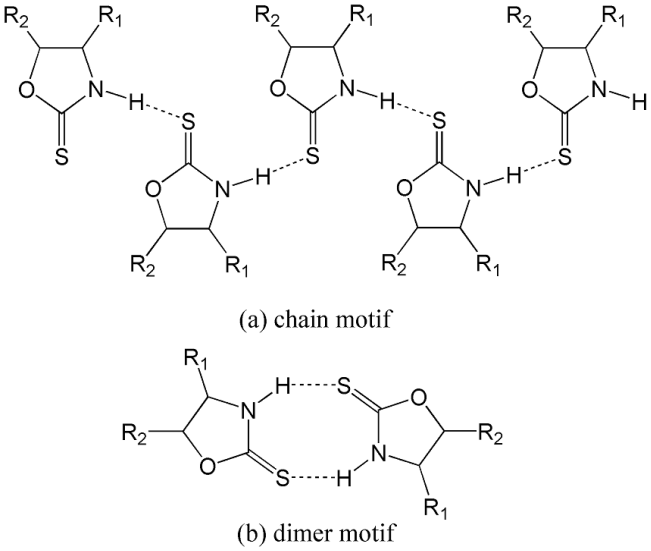

Figure 3. Possible hydrogen-bonding patterns of substituted 1,3-oxazolidine-2-thiones. Hydrogen-bonds are shown as dashed lines.

 DOI: 10.17628/ecb.2014.3.1017-1019

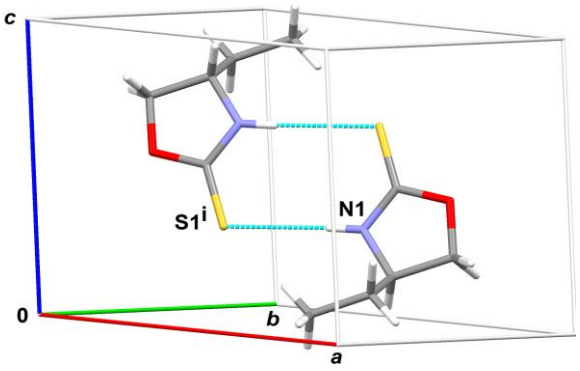

Figure 4. Crystal packing of the title compound. Hydrogen-bonds are shown as dashed cyan lines.

The Cambridge Structural Database survey indicates that substituted 1,3-oxazolidine-2-thiones form mainly two possible hydrogen-bonding patterns of the chain motif or the dimer motif (Figure 3).[5,6,21,22] In the crystals of the title compound (Figure 4), a pair of enantiomeric (*R*)- and (*S*)-molecules is connected *via* intermoleculer N1−H···S1 hydrogen bonds between the neighboring thioamide moieties to form a centrosymmetric dimer with an $R^2_2(8)$ graph-set motif[23] [N1···S1^{i} 3.3593(14) Å, N1−H···S1^{i} 177.0(15) °; symmetry code: (i) 1 − x, 1 − y, 1 − z].

Acknowledgement

We thank and acknowledge the technical assistance of Fukui Research Laboratory, Rengo Co., Ltd., 1-8-10 Jiyugaoka Awara-shi, Fukui 919-0604, Japan.

References

[1]Kaur, D., Sharma, R., *Struct. Chem.*, **2014**, *25*, 1111.

[2]Roux, M. V., Temprado, M., Jime´nez, P., Foces-Foces, C., Notario, R., Parameswar, A. R., Demchenko, A. V., Chickos, J. S., Deakyne, C. A., Ludden, A. K., Liebman, J. F., *J. Phys. Chem. A*, **2009**, *113*, 10772.

[3]Saxena, A., Pike, R. D., *J. Chem. Crystallogr.*, **2007**, *37*, 755.

[4]Tan, Y. S., Halim, S. N. A., Tiekink, E. R. T., *Z. Kristallogr. NCS*, **2014**, *229*, 55.

[5]Kitoh, S., Kunimoto, K.-K., Funaki, N., Senda, H., Kuwae, A., Hanai, K., *J. Chem. Crystallogr.*, **2002**, *32*, 547.

[6]Kitoh, S., Senda, H., Kunimoto, K.-K., *Anal. Sci.: X-ray Struct. Anal. Online*, **2003**, *19*, x15.

[7]Kunimoto, K.-K., Ichitani, M., Ogawa, T., Kitoh, S., Kuwae, A., Hanai, K., *Spectrosc. Lett.*, **2009**, *42*, 73.

[8]Ichitani, M., Kitoh, S., Fujinami, S., Suda, M., Honda, M., Kunimoto, K.-K., *Acta Cryst. E*, **2013**, *69*, o953.

[9]Kitoh, S., Feng, Y., Fujinami, S., Ichitani, M., Honda, M., Kunimoto, K.-K., *Acta Cryst. E*, **2013**, *69*, o1699.

[10]Ichitani, M., Kitoh, S., Tanaka, K., Fujinami, S., Suda, M., Honda, M., Kuwae, A., Hanai, K., Kunimoto, K.-K., *Eur. J. Chem.*, **2013**, *4*, 350.

[11]Ichitani, M., Kitoh, S., Tanaka, K., Fujinami, S., Suda, M., Honda, M., Kunimoto, K.-K., *Eur. J. Chem.*, **2014**, *5*, 6.

[12]Li, G., Ohtani, T., *Heterocycles*, **1997**, *45*, 2471.

[13]Rigaku, *CrystalClear*, Rigaku Corporation, Tokyo, Japan, **2006**.

[14]Rigaku, *REQAB*, Rigaku Corporation, Tokyo, Japan, **1998**.

[15]Burla, M. C., Caliandro, R., Camalli, M., Carrozzini, B., Cascarano, G. L., De Caro, L., Giacovazzo, C., Polidori, G., Siliqi, D., Spagna, R., *J. Appl. Cryst.*, **2007**, *40*, 609.

[16]Sheldrick, G. M., *Acta Cryst. A*, **2008**, *64*, 112.

[17]Rigaku, *CrystalStructure*, Rigaku Corporation, Tokyo, Japan, **2010**.

[18]Farrugia, L. J., *J. Appl. Cryst.*, **2012**, *45*, 849.

[19]Macrae, C. F., Edgington, P. R., McCabe, P., Pidcock, E., Shields, G. P., Taylor, R., Towler, M., van de Streek, J., *J. Appl. Cryst.*, **2006**, *39*, 453.

[20]Allen, F. H., *Acta Cryst. B*, **2002**, *58*, 380.

[21]Li, L., Zhong, H., *Jiegou Huaxue (Chin. J. Struct. Chem.)*, **1986**, *5*, 52.

[22]Gray, T., Laplaza, C. E., Staples, R. J., *Z. Kristallogr. NCS*, **1999**, *214*, 230.

[23]Etter, M. C., *Acc. Chem. Res.*, **1990**, *23*, 120.

Received: 07.10.2014.
Accepted: 31.10.2014.

SYNTHESIS OF NEW INTERCALATED QUINONES AND THEIR CYTOTOXIC EFFECTS ON CANCER CELL LINES

Feyriel Dridi,[a,b] Nathalie Bar,[a] Odile Sainte-Catherine,[c] Messaoud Hachemi,[b] Marc Lecouvey,[c] Didier Villemin[a]*

Keywords: naphthoquinone; benzofurane; benzodioxine; antitumor activity; cytotoxicity

Naphthoquinones with benzofuran or benzodioxan ring were obtained from dichloronaphthoquinone and were fully characterized. The new benzodioxanes were tested on 4 cancer cells and one of them, a derivative from methyl pyrogallate was found very cytotoxic for cancer cells.

* Corresponding Authors

E-Mail: villemin@ensicaen.fr

[a] Laboratoire de Chimie Moléculaire et Thio-organique, UMR CNRS 6507, INC3M, FR 3038, Labex EMC[3], Labex Synorg, ENSICAEN & Université de Caen, 14050 Caen, France

[b] Laboratoire de Chimie Moléculaire et Composites, Faculté des Sciences de l'Ingénieur, Université M' Hamed, Boumerdes, Algérie

[c] Université Paris 13, Sorbonne Paris Cité, Laboratoire de Chimie, Structure, Propriétés de Biomatériaux et d'Agents Thérapeutiques (CSPBAT), CNRS UMR 7244, 74, Rue Marcel Cachin F-93017

Introduction

Quinones are one of the largest classes of antitumor agents.[1] For example, among the drugs the most potent in cancer chemotherapy, there are the anthracycline antibiotics, Daunorubicin or Doxorubicin.[2,3]

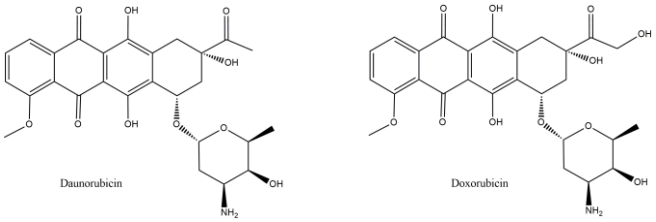

Figure 1. Structures of anthracycline Daunorubicin and Doxorubicin.

Quinoid antitumor agents generally give intercalation into DNA,[1,4] fitting themselves between base pairs of DNA which induce structural distortions due to the formation of stable intercaled complex (for example by alkylation) and it results in inhibition of human topoisomerases. The DNA topoisomerases do not indeed recognize DNA sequences anymore conducting to reading errors during the replication process, followed by cells apoptosis. The inhibition can be also due to the cleavage of DNA, which is sometimes induced by a proton-coupled electron transfer generally when photoexcitation takes place,[5,6] this is particularly the case when quinone or Psoralen derivatives are involved.[7]

DNA-intercalating molecules are usually aromatic, polycyclic and planar such as anthraquinones (as Doxorubicin, Saintopin),[8,9] coumarins[10] (as Elsamicin A[11]), or furanocoumarins (as Psoralen, Angelicin, Bergapten)[12-15] and benzodioxins.[16,17]

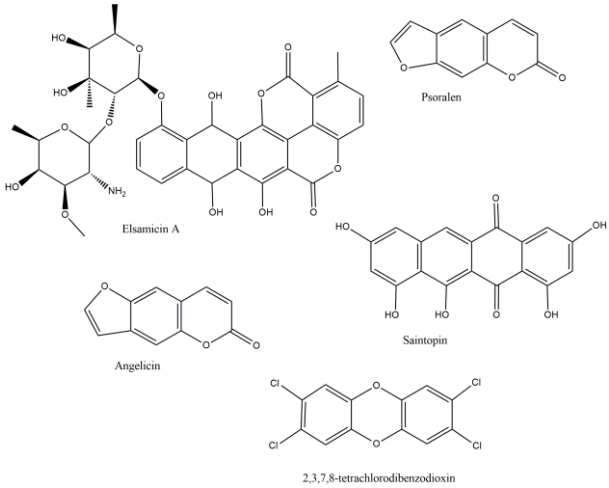

Figure 2. Structures of Psoralen, Saintopin, Elsamicin A, TCDD and Angelicin.

Results and Discussion

We have chosen to study naphthoquinone derivatives containing a naphthobenzofuran or a benzodioxin ring. These molecules are easily available from the reaction of dichloronaphthoquinone with phenols according to Lieberman reaction[18,19] and are well reported in literature.[20]

Synthesis

The reactions between a wide range of structurally varied phenols and 2,3-dichloro-1,4-naphthoquinone (2,3-DCNQ) **1** led to the formation of C-O and C-C bonds affording the derivatives of a variety of polycyclic quinones in good yields (Scheme 1).

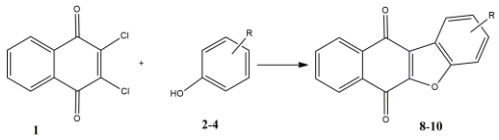

Scheme 1. Formation of benzofuranonaphthoquinones from DCNQ **1** and phenols **2-4**.

The products were obtained by the reaction of phenol derivatives with commercially available 2,3-DCNQ **1** under basic conditions. Resorcinol **2**, phloroglucinol **3** and Sesamol **4**, furnished [2,3]furan-4,9-dione (benzofurano-naphthaquinones) **8**, **9** and **10** respectively. The compounds **8**, **9** and **10** were previously prepared and described as cytotoxic for tumoral cells but not well characterised. In order to test in the future these compounds, we have fully characterised them by NMR (^{1}H, ^{13}C) and mass spectroscopy.

The reactions of 2,3-DCNQ **1** under basic conditions with catechol derivatives permit the formation of benzodioxin derivatives, through the formation of two C-O bonds.

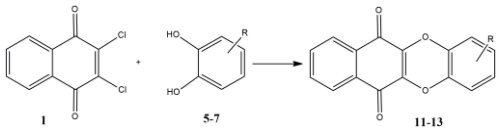

Scheme 2. Formation of benzodioxins from DCNQ **1** and catechols **5-7**.

With catechols like dihydroxycoumarin **5**, pyrogallate derivates **6** and **7**, we have obtained naphthoquinone benzodioxins respectively **11**, **12** and **13**. These compounds are not described in the literature. The reactions were simply performed by mixing reactants in the presence of potassium carbonate and acetone under reflux during several hours. All structures were fully characterized by standard spectroscopic methods (^{1}H, ^{13}C NMR, IR and MS data).

The results and the conditions of these reactions are reported in Table 1.

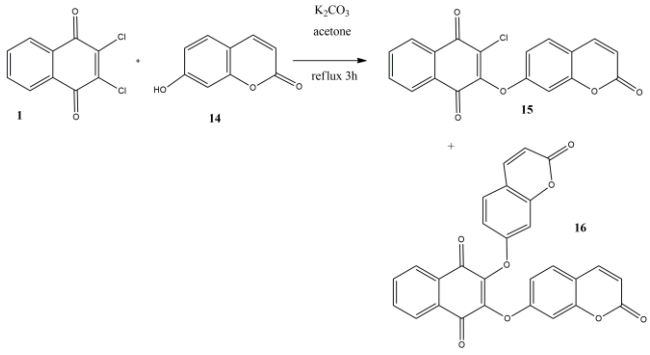

Scheme 3. Reaction of 2,3-DCNQ 1 with Umbelliferon **14**.

With 7-hydroxycoumarin (Umbelliferon) **14**, we are unable to obtain benzofuranonaphthoquinones but we have observed the formation of two products **15** and **16** (Scheme 3).

Clearly the phenol of Umbelliferon is desactivated and the formation of C-C bond does not occur. The attempts to obtain benzofuranonaphthoquinones with a Psoralen substructure, by ring closing of **15**, in the presence of hard or soft Lewis acid ($AlCl_3$ or $BiCl_3$) or palladium acetate oxidative coupling conditions were unsuccessful.

Finally, in order to raise the Psoralen pattern, we have performed the reaction between the compound **9** and malic acid under acidic conditions, according to Pechmann conditions.[21]

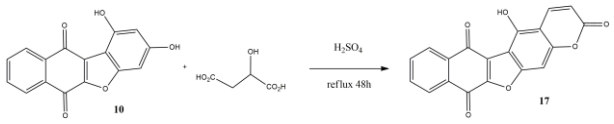

Scheme 4. Reaction of **9** in the Pechmann conditions.

We have obtained a mixture of three lactone compounds which we were not able to break up (**17**, **18**, **19**).

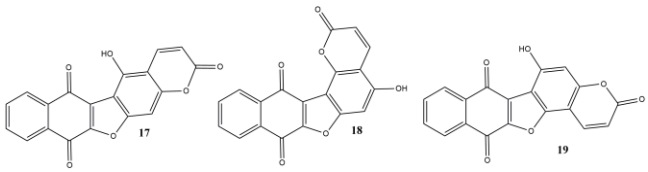

Figure 3. Mixture of products obtained from **9** in the Pechmann conditions.

Cytotoxic effects

Compounds **8,**[22] **9**[23] and **10**[22] have been already synthetized and were evaluated in vitro by Cheng et al.[22,24] for their inhibitory actions against cells line panel such as HL-60 (human promyelocytic leukemia) and SCLC (small cell lung cancer) cell lines. Compounds **8** and mainly **9** displayed the better cytotoxicity. The authors attributed this activity to the presence of hydroxyl group on aromatic cycle.

In this study, naphthoquinone benzodioxins were screened on a panel of four other cancer cell types corresponding to four types of cancer and isolated from four different cancer tissues.

The panel comprises human GBM cell line (U87MG); mouse melanoma cell line (B16F10); human epidermoïd cell line (A431); human breast adenocarcinoma (pleural metastasis) cell line (MDAMB231). Throughout our goal to identify new compounds active against cancer cell, three new compounds were evaluated for their antiproliferative activity using a MTT test.

Table 1. Reactions of 2,3-dichloronaphthoquinone **1** with phenols **2-4** and catechols **5-7** under basic conditions

DCNQ	Phenols, catechols	Reactions conditions	Products	Yield[a] %
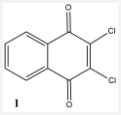	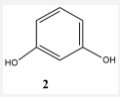	EtONa, RT, 12h	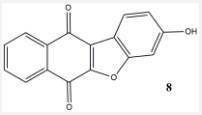	65
		KOH, MeOH 30°C, 3h		55
	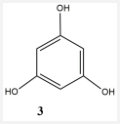	C_6H_5N, reflux 3h	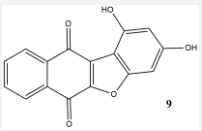	86
		K_2CO_3, acetone 60°C, 14h		90
	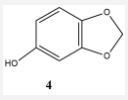	K_2CO_3, acetone 60°C, 14h	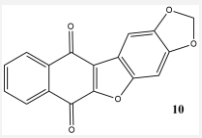	40
		K_2CO_3, acetone 60°C, 14h		90

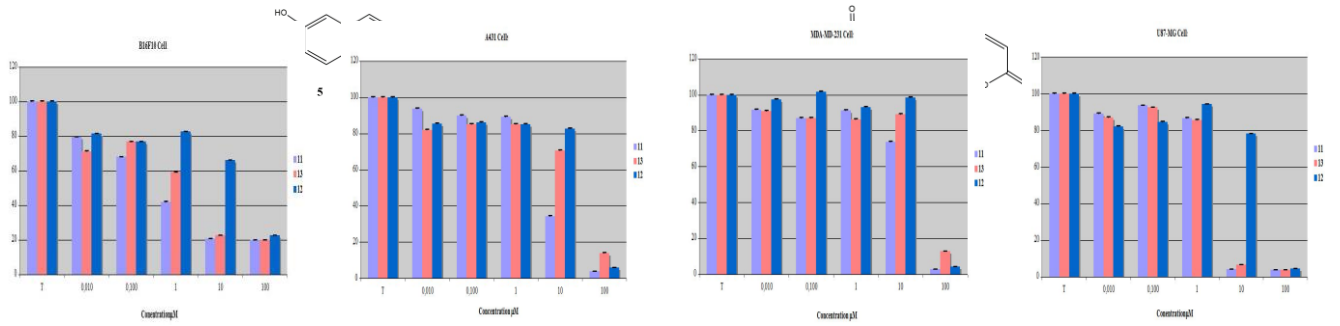

Figure 4. Comparative ef 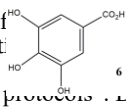 phthoquinone benzodioxins on B16F1 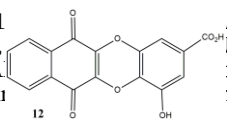 A), A431 cell proliferation (B), MDAMB231 cell proliferatU87MG cell proliferation (D). B16F10, U87MG cells were incubated with different concentrations of und. After 72 h, B16F10, A431, MDAell proliferation were assessed as described in "Experimental p. Data represent the mean value + SD of thnents.

Naphthoquinone benzodioxins **11**, **12**, **13** were evaluated on the U87MG, B16F10, A431, and MDAMB 231 cell viability (Figure 3). Cells were treated at concentrations ranging from 0.01 µM to 100 µM. Two compounds **11**, **13**, (Table 2) were identified with EC50 inferior to 10 µM on the GBM cell line (U87MG) and the mouse melanoma cell line (B16F10). Among the compounds showing an extended antiproliferative activity **11** was the only one to be active against cancer cell lines derived from epidermoïd cancer cell line (A431).

The differences of structure allowed us to establish structure activity relationships. Results showed that naphthoquinones benzodioxins have limited effect on MDAMB cell proliferation. In the other hand, the cytotoxicity is increased for the other cell models but depends on the structure of the heterocycles. The presence of free carboxylic group and hydroxyl group on the phenyl ring diminished drastically the cytotoxicity (compound **12**). Replacement by an ester group increased significantly the biological activity for three cell lines such as human GBM cell line (U87MG), mouse melanoma cell line (B16F10), human epidermoïd cell line (A431) (compound **11)** and two cell lines human GBM cell line (U87MG); mouse melanoma cell line (B16F10) (compound **13**). The nature of the ester function is an important factor to explain the biological activity differences. The presence of the ester with the free hydroxyl group on the phenyl ring did not increase the cytotoxicity. The lactone introduction leaded to the better results of cytotoxicity but the difference is weak.

Table 2. Antiproliferative values (EC50 µM) of the naphthoquinone benzodioxins on: A431- B16F10 (skin tissue), MDAMB231 (breast tissue), U87MG (brain tissue).

Compounds	U87MG	B16F10	A431	MDA-MB231
11	2 ± 0.9	0.4 ±0.2	9 ± 1	34 ± 2
12	20 ± 5	22 ± 5	18 ± 2	34± 5
13	2 ± 0.9	1.1 ±0.5	18 ± 2	35± 2

*Values are calculated from at least three independent experiments and for each set of experiments each point was repeated 3 times. **EC50 estimation was determined with XLSTAT software.

In conclusion, the compound **11** has given the best biological activity but the compound **13** could be interesting for in vivo biological evaluation. Naphthoquinones benzodioxins are very lipophilic. The presence of a free hydroxyl group should allow to increase the hydrophilicity and the solubilization in biocompatible medium.

Experimental

General

All commercial reagents were purchased from Acros, Aldrich, and Sigma and were used as recieved without further purification. Reaction times were monitored by TLC until no starting material remained. TLC was performed using Silica gel 60 F254 precoated aluminium sheets. Column chromatography was performed using Silica gel Si 60 (40-63 µm). ^{1}H,^{13}C, HMBC and HSQC NMR spectra were recorded on a Bruker AC 400 or Bruker AC 500 spectrometers. Chemical shifts (δ) are expressed in parts per million (ppm) and are referenced to the internal deuterated solvents with tetramethylsilane as the internal standard. Data are reported as follows: multiplicity (s = singlet, d = doublet, t = triplet, q = quartet, dd = doublet of doublet, dt = doublet of triplet, m = multiplet, brs = broad signal). Coupling constants are expressed in Hertz (Hz). Mass spectra were recorded on a QTOF Micro (Waters) spectrometer with electrospray ionization (ESI, positive mode), lockspray orthophosphoric acid, infusion introduction at 10 µL/min, a source temperature of 80°C and desolvation temperature of 120 °C.

Organic synthesis

Synthesis of 3-hydroxybenzo[d]naphto[2,3-b]furan-6,11-dione (8)

Sodium (1.6 g) is slowly added to ethanol (50 mL) into a 100 mL flask fitted with a reflux condenser, the mixture is stirred until total dissolution of sodium. The flask is then cooled to 0°C and 2,3-dichloro-1,4-naphthoquinone (M=227, 2.27 g, n=0.01 mol) is first introduced by small portions, followed by dropwise addition of resorcinol (M=110, 2.20 g, n = 0.02 mol) dissolved in 25 mL ethanol. The reaction is allowed to proceed under stirring overnight at room temperature. The next day, the mixture is acidified using a solution of HCl (1M). The formed precipitate is collected by suction filtration, washed successively with water, methanol and with diethylether affording the compound 8 as an orange solid. Yield = 65%. mp = 325°C (litt = 320°C [23]). IR ν (cm-1) = 1658, 1578, 1247, 993. NMR 1H (400 MHz, CDCl3) δ = 10.5 (s, 1H, OH), 8.09-8.13 (m, 2H, Hnapht), 7.99 (d, J = 8.5 Hz, 1H, CH-CH-COH), 7.87-7.91 (m, 2H, Hnapht), 7.19 (d, J = 2.0 Hz, 1H, CH-COH), 7.07 (dd, J = 2.0 Hz and J = 8.5 Hz, 1H, CH-CH-COH). NMR 13C (125 MHz, CDCl3) δ = 181.4, 174.0, 160.1, 157.6, 152.3, 134.2, 134.1, 132.7, 132.2, 126.2, 126.1, 123.1, 123.7, 116.5, 114.1, 98.4. MS m/z (% relative abundance): 263 (M-H, 100), 235 (10), 219 (20), 191 (18). Exact mass (ESI-TOF) calculated for $C_{16}H_7O_4$ [M-H] = 263.0344, found 263.0344.

Synthesis of 1,3-dihydroxybenzo[d]naphtho[2,3-b]furan-6,11-dione (9)

Potassium hydroxide (2.0 g; M = 56, n = 0,036 mol) is dissolved in methanol (50 mL) in a 100 mL flask fitted with a reflux condenser, at room temperature, under stirring until total dissolution of potassium hydroxide. The mixture is then heated under nitrogen to 30°C, 2,3-dichloro-1,4-naphthoquinone (M=227, 1.70 g, n = 7.5 10^{-3} mol) is introduced and the medium becomes turbid. 1.4 g of phloroglucinol (M=126, n=11 10^{-3} mole) previously dissolved in 20 mL of methanol, is added dropwise and the reaction is allowed to proceed under stirring during 3h. The formed precipitate is collected by suction filtration, washed with methanol. It is then dispersed in 50 mL of HCl (0.2 M) at 0°C, filtered, washed with ethanol affording **9** as a brown solid. Yield = 55 %. mp = 348°C (litt = 340-342°C [**Hiba! A könyvjelző nem létezik.**]). IR ν (cm^{-1}) = 3391, 1622, 1576, 1562, 1269, 1187, 1003. NMR ^{1}H (400 MHz, DMSO-d6): δ = 8.11-8.17 (m, 2H, Hnapht), 7.88-7.97 (m, 2H, Hnapht), 6.69 (d, *J*=1.8 Hz, 1H, CH-C-Ofuryl*)*, 6.40 (d, *J*=1.8 Hz, 1H, COH-CH-COH), 3.32 (s, 2H, 2 OH). NMR ^{13}C (DMSO-d6) δ = 183.3, 173.1, 162.4, 158.2, 152.6, 150.9, 135.1, 134.0, 132.3, 131.7, 126.7, 126.5, 125.7, 104.5, 99.9, 90.5. MS *m/z* (% relative abundance): 281 (M+H, 100), 253 (10), 225

(29), 183 (38). Exact mass (ESI-TOF) calculated for $C_{16}H_9O_5$ [M+H] = 281.0450, found 281.0439.

Synthesis of (methylenedioxy)benzo[b]naphtho[2,3-d]furan-7,11-dione (10)

0.73 g of Sesamol (M=138, n=5.28 10^{-3} mol), 1 g of 2,3-dichloro-1,4-naphthoquinone (M = 227, n=4.4 10^{-3} mol) and 10 mL of pyridine are introduced in a 50 mL flask fitted with a reflux condenser and the mixture is stirred and heated under reflux during 3 h. After cooling, acetic acid (6M) is added and the neutralisation reaction is allowed to proceed during 12h. Finally, the formed precipitate is collected by suction filtration, washed with water affording the compound **10** as a red-orange solid. Yield = 86%. mp = 309-310°C (lit. = 310°C[22]). IR (ν, cm^{-1}) = 3085, 3056, 2897, 1659. NMR ^{1}H (400 MHz, DMSO-d6) δ = 5.95 (s, 2H, OCH_2O), 6.72 (m, 1H, CH-C-Ofuryl), 6.85 (m, 1H, CH), 7.88 (m, 2H, Hnapht), 8.10 (m, 2H, Hnapht). NMR ^{13}C (125 MHz, $CDCl_3$) δ = 180.8, 174.0, 161.2, 153.0, 152.3, 144.0, 143.3, 134.3, 126.2, 118.6, 117.4, 106.6, 101.3, 97.8. Exact mass (ESI-TOF) calculated for $C_{17}H_8O_5$ [M] = 292.0346, found 292.0350.

Synthesis of 1H-benzo[b]pyrano[3,2-i]dibenzo[b,e][1,4]dioxine-2,7,12-trione (11)

2,3-dichloro-1,4-naphthoquinone (0.5 g, M=227, n = 2.2 10^{-3} mol), 4,5-dihydroxycoumarine (0.35 g, M=178, n = 2.10^{-3} mol), K_2CO_3 (0.61 g, M = 138, n = 4.4 10^{-3} mol) and 4 mL of anhydrous acetone are introduced in a 50 mL flask fitted with a reflux condenser and a $CaCl_2$ dying tube. The medium is under nitrogen stream and heated at 60°C using an oil bath during 14 hours. After cooling, the formation of a red precipitate is observed. It is then filtered, washed with sodium carbonate solution and water affording the compound **11** as a red solid. Yield = 90 %. mp > 399°C. IR ν (cm^{-1}) = 1668, 1656, 1567, 1284, 1265, 979. NMR ^{1}H (500 MHz, DMSO-d6, 40°C): δ = 8.04 -8.03 (m, 2H, Hnapht), 7.93 (d, *J* = 9.5 Hz, CH=CH-C=O), 7.90-7.88 (m, 2H, Hnapht), 7.53 (s, 1H, CH-C-CH=CH-C=O), 7.30 (s, 1H, CH-C-OCO), 6.46 (d, *J* = 9.5 Hz, CH=CH-C=O). NMR ^{13}C (125 MHz, DMSO-d_6, 40 °C): δ = 177.0 (1), 176.4 (2), 159.4 (3), 151.5 (4), 143.1 (5), 139.0 (6), 138.0 (7), 136.9 (8), 134.5 (9), 134.4 (10), 129.7 (11-12), 125.8 (13-14), 115.9 (15), 115.6 (16), 115.2 (17), 105.6 (18). MS *m/z* (% relative abundance): 333 (M+H, 100), 305 (8), 277 (28), 249 (20), 221 (10). Exact mass (ESI) calculated for $C_{19}H_9O_6$ [M+H] = 333.0399, found 333.0414.

Synthesis of 4-hydroxy-6,11-dioxo-6,11-dihydrobenzo[b]dibenzo[b,e][1,4]dioxine-2-carboxylic acid (12)

2,3-dichloro-1,4-naphthoquinone (0.5 g, M=227, n = 2.2 10^{-3} mol), gallic acid (0.37 g, M=170, n = 2.1 10^{-3} mol), K_2CO_3 (0.61 g, M = 138, n = 4.4 10^{-3} mol) and 6 mL of anhydrous acetone are introduced in a 50 mL flask fitted with a reflux condenser and a $CaCl_2$ dying tube. The medium is stirred under nitrogen stream and heated at 60°C using an oil bath during 14 hours. The formation of a precipitate is observed. It is then filtered, washed with sodium carbonate solution and the washing water layers are then acidified to pH = 3. They are then filtered, affording compound **12** as an orange solid. Yield = 40 %. mp > 399°C. IR ν (cm^{-1}) 3394, 1654, 1601, 1440, 1339, 1223, 1196. NMR ^{1}H (125 MHz, DMSO-d6, 40°C): δ = 10.38 (s, 1H, CO_2H), 8.05-8.01 (m, 2H, Hnapht), 7.89-7.85 (m, 2H, Hnapht), 7.28 (d, *J* = 2.0 Hz, 1H, CH-COH), 6.96 (d, *J* = 2.0 Hz, 1H, CH-C-CO_2H). NMR ^{13}C (500 MHz, DMSO-d6, 40°C): δ = 176.8 (CO), 176.7 (CO), 165.7 (CO_2H), 146.1 (COH), 141.1 (5), 138.9 (6), 138.8 (7), 134.3 (8), 134.3 (9), 132.5 (10), 129.7 (11-12), 127.4 (13), 125.7 (14-15), 115.4 (16), 107.8 (17). MS *m/z* (% relative abundance): 323 (M-H, 100), 279 (74), 251 (62), 235 (12). Exact mass (ESI) calculated for $C_{17}H_7O_7$ [M-H] = 323.0192, found 323.0204.

Synthesis of methyl 4-hydroxy-6,11-dioxo-6,11-dihydrobenzo[b]dibenzo[b,e][1,4]dioxine-2-carboxylate (13)

2,3-dichloro-1,4-naphthoquinone (0.5 g, M=227, n = 2.2 10^{-3} mol), methyl gallic ester (0.37 g, M=184, n = 2.10^{-3} mol), K_2CO_3 (0.61 g, M = 138, n = 4.4 10^{-3} mol) and 6 mL of anhydrous acetone are introduced in a 50 mL flask fitted with a reflux condenser and a $CaCl_2$ dying tube. The medium is stirred under nitrogen stream and heated at 60°C using an oil bath during 14 hours. After cooling, the formed precipitate is collected by suction filtration, and then recrystalised in glacial acetic acid affording compound **13** as a red solid. Yield = 90 %. mp > 399°C. IR ν (cm^{-1}) = 3312, 1717, 1676, 1665, 1649, 1595, 1507, 1449, 1370, 1351, 1184, 1004. NMR ^{1}H (500 MHz, DMSO-d6, 60°C): δ = 8.03-8.00 (m, 2H, Hnapht), 7.87-7.85 (m, 2H, Hnapht), 7.31 (d, *J* = 2.0 Hz, 1H, CH-COH), 6.97 (d, *J* = 2.0 Hz, 1H, CH-C-CO_2Me), 3.83 (s, 3H, Me), 3.10 (s, 1H, OH). NMR ^{13}C (125 MHz, DMSO-d6, 60°C): δ = 176.7 (1), 176.6 (2), 164.7 (3), 146.3 (4), 141.3 (5), 138.9 (6), 138.8 (7), 134.3 (8), 134.2 (9), 133.0 (10), 129.8 (11-12), 126.3 (13), 125.7 (14-15), 115.5 (16), 107.7 (17), 52.2 (18). MS *m/z* (% relative abundance): 339 (M+H (100), 243 (8), 214 (15). Exact mass (ESI) calculated for $C_{18}H_{11}O_7$ (M+H) 339.0505, found 339.0515.

Synthesis of 2-chloro-3-(2-oxo-2H-chromen-7-yloxy)naphtalene-1,4-dione (15)

2,3-dichloro-1,4-naphthoquinone (0.5 g, M=227, n = 2.2 10^{-3} mol), 7-hydroxycoumarine (0.39 g, M=162, n = 2.4 10^{-3} mol), K_2CO_3 (0.48 g, M = 138, n = 3.5 10^{-3} mol) and 15 mL of anhydrous acetone are introduced in a 100 mL flask fitted with a reflux condenser and a $CaCl_2$ dying tube. The medium is weakly stirred under a stream of nitrogen and heated under reflux with an oil bath, during 3 hours. After cooling, the formed precipitate is collected by suction filtration. A purification by chromatography (silica,) furnished the compound **15** as a yellow solid. Yield = 53 %. mp = 224°C (litt = 207°C.[25] IR ν (cm^{-1}) = 1724, 1668, 1575, 1251. NMR ^{1}H (400 MHz, $CDCl_3$) δ = 8.23-8.27 (m, 1H, Hnapht), 8.06-8.09 (m, 1H, Hnapht), 7.78-7.87 (m, 2H, Hnapht), 7.67 (d, *J = 9.5 Hz*, 1H, CH=CH-C=O), 7.47 (d, *J = 8.6 Hz*, 1H, CH-CH-C-Onapht), 6.98 (dd, *J = 2.5 Hz, J = 8.6 Hz*, 1H, CH-CH-C-Onapht), 6.92 (d, *J = 2.5 Hz*, 1H, CH-C-Onapht), 6.35 (d, *J = 9.5 Hz*, 1H, CH=CH-C=O). NMR ^{13}C (125 MHz, $CDCl_3$) δ = 178.1, 177.6, 160.4, 158.9, 155.5, 152.8, 142.9, 135.0, 134.9, 134.9, 131.3, 130.5, 129.4, 127.8, 127.5, 115.4, 115.3, 113.6, 104.9. MS *m/z* (% relative abundance): 375, (M+Na, 14), 355 (35), 353 (M+1, 100), 325 (39), 309 (12). Exact mass (ESI-TOF) calculated for $C_{19}H_{10}O_5Cl$ [M+H] = 353.0217, found 353.0232.

Synthesis of 2,3-bis(2-oxo-2H-chromen-7-yloxy)naphtalene-1,4-dione (16)

The compound **16** is isolated after chromatography as a second fraction. NMR ^{1}H (400 MHz, $CDCl_3$): δ = 8.12-8.16 (m, 2H), 7.82-7.87 (m, 2H), 7.63 (d, *J = 9.6 Hz*, 2Hb), 7.41 (d, *J = 8.5 Hz*, 2Hc), 6.91 (dd, J_1 *= 2.4 Hz*, J_2 *= 8.5 Hz*, 2Hd), 6.87 (d, *J = 2.5 Hz*, 2He), 6.32 (d, *J = 9.6 Hz*, 2Ha). Exact mass (ESI-TOF) calculated for $C_{28}H_{14}O_8Na$ [M+Na] = 501.0586, found 501.0582.

MTT assay

Cell lines

A431, MDA-MB-231, B16F10, and U87MG cells were purchased from American Tissue Culture Collection (Rockville, MD, USA). The cells were routinely grown in DMEM (Life Technologies Inc., Gaithersburg, MD, USA), supplemented with 10% FCS, 2 mM L-glutamine, 1 mM sodium pyruvate, 50U mL^{-1} penicillin and 50 mL^{-1} streptomycin (all obtained from Life Technologies Inc.), at 37°C in a 5% CO_2-humidified atmosphere.

Cell proliferation assay

Cell proliferation was assessed using a MTT-microculture assay[26] which is based on the ability of mitochondrial enzymes to reduce 3-(4,5-dimethylthiazol-2-yl)-2,5-diphenyltetrazolium bromide (MMT) (Sigma, LO, USA) into purple formazan crystals. Briefly, the cells were seeded in 10 % FCS-DMEM at a density of $5x10^3$ cells/well in 96-well tissue culture plates (Falcon, Strasbourg, France) and allowed to adhere for 24 h. Cells were washed and incubated in DMEM-2% FCS with various concentrations of naphthoquinone benzodioxins varying from 0.1 μM to 100 μM. After a 72 h incubation, cells were washed with PBS and incubated with 0.1 ml of MTT (2 mg mL^{-1}) for 4 h. Cells were lysed in 200 μL DMSO and absorbance corresponding to solubilized formazan pellet (which reflects the relative viable cell number) was measured in a Labsystem plate reader at 570 nm. Concentration-response curves were constructed and the EC_{50} values (concentration of the compound inhibiting 50% of cell proliferation) were determined using the XL STAT software (Addinsoft).

Conclusions

Benzofuran napthoquinones previously reported as cytotoxin on tumor cells were synthetized and fully characterized. The new benzodioxan naphthoquinones were tested on 4 cancer cell lines, two of them displayed antiproliferative activity, and the ester **11** was found to be the most promising. According to our knowledge the cytotoxicity on cancer cells of benzodioxan naphthoquinones has not been reported in literature yet.

Acknowledgments

We gratefully acknowledge the CNRS (National Center for ScientificResearch), the "Region Basse Normandie", the University of Boumerdes (Algeria), the Franco-Algerian program for the Superior Education (PROFS), and the Algerian-French cooperation for a BAF grant for Feyriel Dridi. Also the authors thank Rémy Legay and Baptiste Rigaud for NMR spectra and Mrs. Karine Jarsalé for ESIMS and HRMS analysis.

References

[1]Asche, C., *Mini-Rev. Med. Chem.*, **2005**, *5(5)*, 449-67.

[2]Aubel-Sadron, G., Londos-Gagliardi, D., *Biochimie*, **1984**, *66(5)*, 333-352.

[3]Preobrazhenskaya, M. N., Tevyashova, A. N., Olsufyeva, E. N., Huang Kuo-Feng, Huang Hsu-Shan, *J. Med. Sci.*, **2006**, *26(4)*, 119-128.

[4]Campanelli, A. R., D'Alagni, M., Marini-Bettolo, G. B., *FEBS Letters*, **1980**, *122*, 256-260.

[5]Koch, T., Ropp, J. D., Sligar, S. G., Schuster, G. B., *Photochem. Photobiol.*, **1993**, *58(4)*, 554-8.

[6]Ou, C. N., Tsai, C. H., Song, P.-S., In: *Research in Photobiology*, ed. A. Castellani. New York Plenum, **1977**, 257.

[7]Sage, E., Le Doan, T., Boyer, V., Helland, D. E., Kittler, L., Moustacchi, H. C., *J. Mol. Biol.*, **1989**, *209(2)*, 297-314.

[8]Kellogg, G. E., Scarsdale J. N., Fornari Jr, F.A., *Nucleic Acids Res.*, **1998**, *26(20)*, 4721-32.

[9]Nabiev, I., Chourpa, I., Manfait, M., *J. Phys. Chem*., **1994**, *98*, 1344-50.

[10]Thati, B., Noble, A., Creaven, B. S., Walsh, M., McCann, M., Kavanagh, K., Devereux, M., Egan, D. A., *Cancer Lett*., **2007**, *248(2)*, 321-331.

[11]Barcelo, F., Portugal, J., *FEBS Letters*, **2004**, *576*, 68-72.

[12]Al-Sehemi, A. G., El-Gogary, S. R., *Chin. J. Chem.*, **2012**, *30(2)*, 316-20.

[13]Demaret, J. P., Brunie, S., Ballini, J. P., Vigny, P., *Photochem. Photobiol*., **1989**, *50(1)*, 7-21.

[14]Rocha, M. S., Lúcio, A. D., Alexandre, S. S., Nunes, R. W., Mesquita, O. N., *Appl. Phys. Lett*., **2009**, *95*, 253703.

[15]Muniandy, P. A., Thapa, D., Thazhathveetil A. K., Liu, S-T., *J. Biol. Chem*., **2009**, *284(41)*, 27908-17.

[16]Csík, G., Rontó, G., Nocentini, S., Averbeck, S., Averbeck, D., Besson, T., Coudert, G., Guillaumet, G., *J. Photochem. Photobiol. B*., **1994**, *24(2)*, 129-39.

[17]Lee, H. H., Palmer, B. D., Boyd, M., Baguley, B. C., Denny, W. A., *J. Med. Chem.*, **1992**, *35(2)*, 258-66.

[18]Liebermann, C., *Chem. Ber*., **1899**, *32*, 916-25.

[19]Liebermann, C., *Chem. Ber*., **1900**, *33*, 566-78.

[20]Satori, M. F., *Chem. Rev*., **1963**, *63*, 279-296.

[21]Pechmann, H., *Chem. Ber*., **1884**, *17(1)*, 929-36.

[22]Cheng, C. C., Dong, Q., Liu, D. F., Luo, Y. L., Liu, L.F., Chen, A. Y., Yu, C., Savaraj, N., Chou, T. C., *J. Med. Chem*., **1993**, *36*, 4108-12.

[23]Kostanecki, S., von Lampe, V., *Chem. Ber*., **1908**, *41*, 2373.

[24]Chang, H. X., Chou, T. C., Savaraj, N., Liu L. F., Yu C., Cheng, C.C., *J. Med. Chem*., **1999**, *42*, 405-08.

[25]Tandon, V. K., Maurya, H. K., *Heterocycles*, **2009**, *77*, 611-615.

[26]Mosmann T., *J. Immunol. Methods*, **1983**, *65*, 55-63.

Received: 12.10.2014.
Accepted: 16.11.2014.

DENSITY OF SUSPENSION CULTURE OF SOMATIC EMBRYOGENIC CELLS OF *LARIX LEPTOLEPIS* DETERMINES THE FATE OF DEVELOPMENT: INVOLVEMENT OF PHOSPHATE UPTAKE AND METABOLISM

Hiroshi Ashihara[a]*, Hamako Sasamoto[b] and Shinjiro Ogita[c]

Keywords: *Larix leptolepis;* Pinaceae; Japanese larch; cell culture; somatic embryogenesis; cell density; phosphate; nucleic acid; phospholipid.

Cell density of suspension culture of *Larix leptolepis* embryogenic cells determined the fate of the development. In a low-density cell culture, somatic embryo development was promoted, but the cells continued to proliferate and formed small spherical cell aggregates in a high-density cell culture. In the present study, we compared the uptake and metabolism of ^{32}P-labelled inorganic phosphate (P_i) by the cells of low- (1 %) and high (10 %)-density cultures during first 30 h. Little difference was found in the uptake of ^{32} P_i by the cells in both the low- and high density-cultures up to 6 h, but Pi uptake in high-density culture almost ceased at 6 hr after inoculation. In contrast, P_i uptake continued linearly in the low-density culture. ^{32}P was distributed in small molecular organic compounds (mainly nucleotides and sugar phosphates), nucleic acids, phospholipids, and phosphoproteins along with unmetabolized Pi. The incorporation of ^{32}P into nucleotide and phospholipid fractions was significantly higher in the cells of low-density culture at 30 h after inoculation. No marked difference on the endogenous levels of purine and pyrimidine nucleotides was observed in both density cultures. From these results it is speculated that the *de novo* nucleic acids and phospholipids synthesis required in the conversion of embryonic cells into somatic embryos may be caused by sufficient amounts of P_i from the medium occurring only in cells of the low-density culture. The nucleotide levels in both cultures were similar at least up to 72 h. Therefore, sufficient levels of nucleotides for proliferation may be supplied even in cells of the high-density culture. The involvement of P_i uptake in the phenomena observed in the low- and high-density cultures is discussed.

* Corresponding Author
Fax: +81-3-5700-4225
E-Mail: ashihara.hiroshi@ocha.ac.jp
[a] Department of Biology, Ochanomizu University, Tokyo, 112-8610, Japan
[b] Research Institute for Integrated Science, Kanagawa University, Hiratsuka, Kanagawa, 259-1293, Japan
[c] Biotechnology Research Center, Toyama Prefectural University, Imizu, Toyama,939-0398, Japan

Introduction

Japanese larch (*Larix leptolepis*) is an important tree in forestry plantations in Japan. The optimization of tissue culture methods has allowed the generation and propagation of viable plants from somatic cells in culture through somatic embryogenesis. Somatic embryogenesis results in the generation of bipolar structures with a well defined root-shoot axis. The techniques have been successfully employed in *L. leptolepis*, an economically important species in Japan, where it is utilized by the forestry industry for wood and lumber production.[1] However, in contrast to other woody plant species such as *Picea glauca*,[2] *L. leptolepis* culture has not been used for physiological and biochemical studies to reveal the mechanism on embryogenesis.

The morphogenetic changes of embryogenic cells which are caused by different cell densities in suspension culture of some Japanese conifers have been reported by Ogita et al.[1,3] They found that in a low cell density culture of *L. leptolepis*, development of embryogenic tissue into somatic embryos was promoted, while in a high cell density culture, the embryogenic tissue continued to proliferate as small spherical cell aggregates and no further development occurred (Fig. 1). The aim of this study is to elucidate the causes of the changing mechanism from embryonic cells to somatic embryos biochemically.

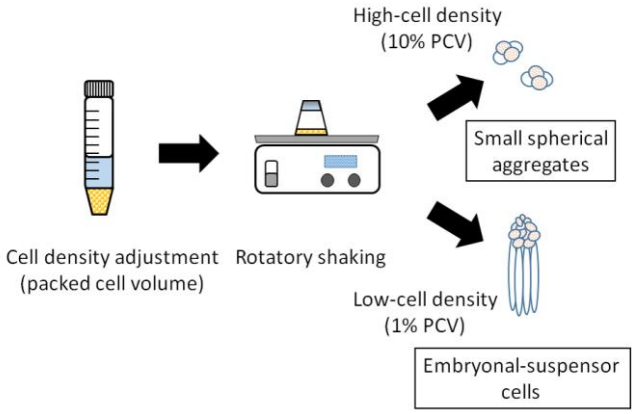

Figure 1. Outline of the high- and low-density cell suspension culture of *Larix leptolepis*. The somatic embryos are produced only in low-density culture.

The growth and development of cultured plant cells were largely influenced by the utilization of nutrients of culture medium. Among the many inorganic nutrients, inorganic phosphate (P_i) has been shown to participate in many metabolic processes affecting the growth and development.[4,5]

Overall changes in cellular metabolism by different concentration of P_i have been observed. In the cells grown in low availability of P_i, several metabolic changes were observed, including reduced rates of respiration,[6,7] decreased protein and nucleic acid synthesis,[8,9] development of P_i - deficient inducible bypasses of respiration,[7,10,11] as well as changes in nucleotide pool size and composition.[6,12-15] The growth of culture is strictly dependent upon P_i availability in the medium. Complete uptake of P_i by cultured plant cells is generally achieved during the first few days after inoculation into fresh medium.[16,17]

In the present studies, we tested the hypothesis that the supply of P_i to individual cells of *L. leptolepis* is satisfactory in a low-density culture, but not in a high-density culture where supply of P_i is limited. As a result of these differences, the embryogenic cells continue to proliferate as small spherical cell aggregates and no further development occurred. In order to elucidate the involvement of P_i uptake in the different developing pattern in the low- and high-density cultures, uptake and metabolism of $[^{32}P]P_i$ were compared. Furthermore, the cellular level of nucleotides was also determined.

Materials and Methods

Plant materials

Embryogenic tissues of *L. leptolepis* (=*L. kaempferi*) were maintained on the modified Campbell and Durzan (mCD, 1975) medium[18] which contained 7 µM 2,4-dichlorophenoxyacetic acid, 3 µM 6-benzylaminopurine, half a concentration of NH_4NO_3 (400 mg L^{-1}) and an additional 600 mg L^{-1} of L-glutamine. Liquid suspensions of the embryogenic tissues were generated as shown in the previous paper.[1] In order to investigate the effects of different cell densities on the proliferation and development of embryogenic cells, different volumes of cells (1 and 10 % as packed cell volume) were added to a 10 ml liquid mCD medium. The flasks were then placed on a rotary shaker with a speed of 100 rpm. The packed cell volume was determined by placing embryogenic cells in conical tubes and centrifuged using a centrifuge (Model 5400, Kubota Corporation, Tokyo, Japan) at 500 rpm for 3 min.

^{32}P-tracer experiments

The tracer experiments performed in this study are essentially the same as described in our earlier paper.[19] Sodium dihydrogen $[^{32}P]$orthophosphate (specific activity 7.4 GBq $mmol^{-1}$) were obtained from Amersham International plc, Amersham, UK. Experimental cultures were initiated from 10-day-old stock cultures at low- and high- inoculum density; 1 % and 10 % cultures were obtained by the transfer of 100 mg FW cells into 10 ml and 1 ml culture media in 50 ml- and 10 mL-conical flask flasks, respectively. The culture medium contained 1.25 mM $[^{32}P]KH_2PO_4$ (specific activity, 3.7 MBq mL^{-1}). The cultures were grown in the dark at 27 °C on a horizontal rotary shaker. The amount of P_i added as $[^{32}P]P_i$ is negligible in comparison to the original concentration in the medium.

The total cells of each flask were harvested by vacuum filtration through a layer of Miracloth (Calbiochem-Behring, La Jolla, U.S.A.) and washed with 100 ml distilled water. The fresh weight of the cells was determined after the washed cells had been left between four layers of filter paper to absorb water. The cells were dried overnight at 80 ºC. Total radioactivity was then measured using a Geiger-Muller counter connected to a digital recorder. Correction for radioactive decay was made by direct comparison of sample count rates with a standard containing $[^{32}P]P_i$.

The analysis of ^{32}P-metabolites was carried out by the modified Ashihara and Tokoro method.[19] A flow sheet of the separation of the labelled metabolites is shown in Fig. 2. The cells (~100 mg) harvested and washed as described above were homogenized in 4 ml of 6 % perchloric acid (PCA) for 2 min in an ice bath using a Potter-Elvehjem homogenizer. The homogenate was extracted successively with (i) 6 % PCA at 2 °C for 20 min (twice), (ii) an ethanol-ether (1: 1 v/v) mixture at 50 °C for 15 min (twice), (iii) 6 % PCA at 100 °C for 15 min and at 2 °C for 15 min, (iv) 3 N NaOH at 100 °C for 20 min. The first PCA-soluble fraction was neutralized with KOH, and after removal of the precipitated potassium perchlorate, a portion (4 ml) was concentrated *in vacuo*, and was analysed by thin-layer chromatography (TLC) using microcrystalline cellulose plates. The solvent system used was *n*-butanol-acetic acid-water (4:1:2 v/v).[20] Most of the radioactivity in the PCA soluble fraction was recovered as Pi, nucleotides and sugar phosphates (data not shown). In this paper, distribution of ^{32}P in P_i and organic phosphates (the sum of the various nucleotides and sugars) is shown. In preliminary studies, the ethanol-ether soluble fraction was also analysed by TLC as shown in our previous paper[19] and confirmed that most radioactivity in this fraction was distributed in phospholipids including phosphatidylcholine (data not shown).

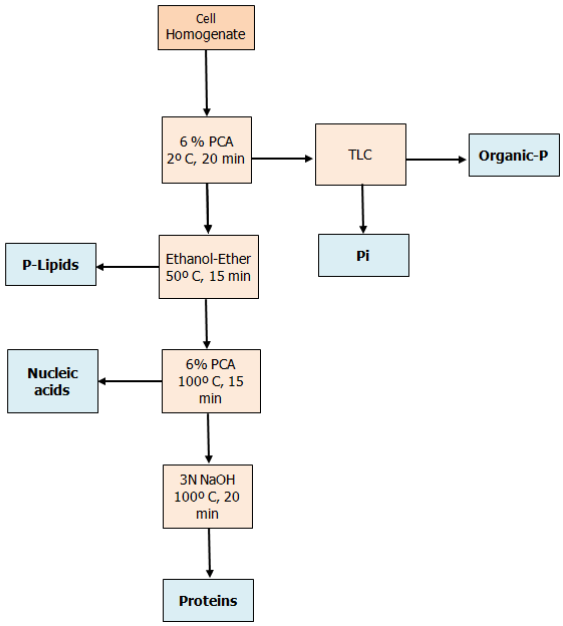

Figure 2. Flow sheet of the separation of ^{32}P-labelled metabolites.

The radioactivity in liquid fractions was determined using and scintillation fluid ACS-II (Amersham International plc, Amersham, UK) and a multi-purpose scintillation counter (type LS 6500, Beckman Instruments, Fullerton, CA, USA). Radioactivity on the TLC sheet was determined using a Bio-Imaging Analyser (Types FLA-2000, Fuji Photo Film Co., Ltd. Tokyo, Japan).

Determination of nucleotide level

Nucleotides were extracted from fresh cells (500 mg fresh weight) and were analysed using a HPLC system, as detailed in Ashihara et al.[21] with slight modifications. Nucleotide contents were determined using an anion exchange column, Shim-pack WAX-1 (Shimadzu Corporation, Kyoto, Japan). Freshly harvested cells were homogenized in chilled 6 % PCA with a glass homogeniser. The homogenates were centrifuged at 30,000 g for 15 min at 2 ºC, and the supernatant was collected and neutralized with 20 % KOH. After brief centrifuging to remove potassium perchlorate, the samples were lyophilised. The dried samples were dissolved in the solvent for HPLC and were filtered using disposable syringe filter units. Aliquots of 10–50 µl were used for determination by HPLC with a Shimadzu LC 10A HPLC system. The absorbance at 260 nm was monitored using a Shimadzu type SPD-10A, UV–Vis detector. Experiments to assess recovery were performed in parallel with all assays. Known amounts of standard were added to the extraction medium for one member of each pair of duplicate samples prior to homogenisation, and recovery was examined. Recoveries of standards were usually more than 90 %. Since some loss of nucleoside tri- and diphosphates was observed when the cells were frozen with liquid nitrogen and stored in a deep-freezer at -80 ºC, all assays were therefore performed using freshly harvested cells and were completed on the same day.

Results and Discussion

Cell density is an important factor that decides the fate of cultured cells.[1] In *L. leptolepis* cultures, low cell densities favour further development of the embryogenic tissue into embryonal-suspensor cell masses, while high densities result in the formation of small spherical cell aggregates. Morphology of embryogenic tissue after 4 weeks of culture in *L leptolepis* indicated that small spherical aggregates proliferated in a high-density culture (Fig. 3A). In contrast, an embryogenic tissue having a well organized embryonal head region and an elongated suspensor region formed in a low-density culture (Fig. 3B). In high-density cultures, rapid utilization of medium components might have resulted in some components becoming limiting factors for further growth and development. Since it has been reported that P_i is one of the important components that regulate the growth of plant cultures, we considered that P_i concentration might be closely related to the embryogenic tissue morphogenesis.

The total uptake of [^{32}P]P_i from the medium by the cells is shown in Fig. 4. P_i taken up by the cells was very rapid during first 3 hr in both high- and low-density cultures. The rate reached a plateau at 6 hr and then increased again. This rapid uptake was also found in suspension culture of *Catharanthus roseus*.[19] The large difference in the total uptake by the cells was observed in the high- and the low-density cultures at 30 hr after inoculation. The amounts of P_i uptake expressed per 100 mg fresh weight are 438 and 285 nmol in the low- and high-density cultures, respectively.

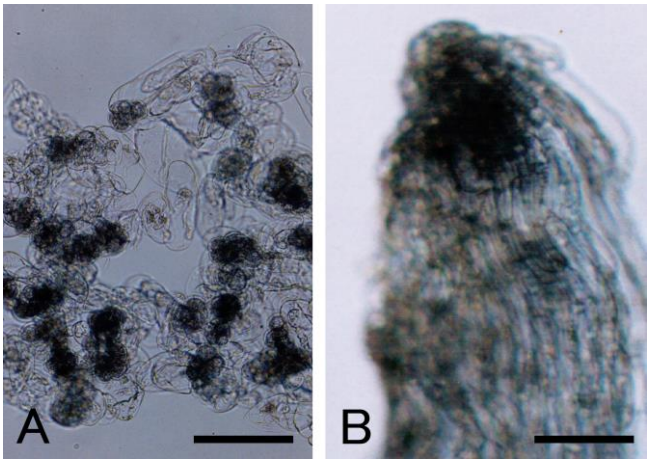

Figure 3. Morphology of embryogenic tissue after 4 weeks of culture in *L. leptolepis*. (A) Small spherical aggregates proliferated in the high-density culture. (B) An embryo having a well organized embryonal head region and an elongated suspensor region formed in a low-density culture. Scale bars represent 100 µm.

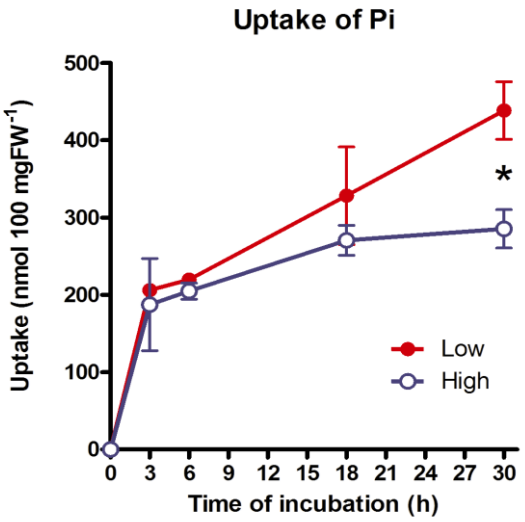

Figure 4. Uptake of [^{32}P]P_i by *L. leptolepis* cells cultured in the low- and high-density culture. The values are expressed as nmol 100 mg FW^{-1}. Values for high-density culture marked with asterisks differ significantly from the value for low-density culture according to the t-test ($P < 0.05$).

The incorporation of ^{32}P into individual cellular components is shown in Fig. 5. At 3 hr, nearly 70 % of the ^{32}P taken up by the cells was incorporated into organic components; the fractions of the PCA-soluble organic compounds consisted of nucleotides and sugar phosphates (50–52 %), nucleic acids (~9 %) and phospholipids (~6 %) and proteins (~0.5 %) in both low- and high-density cultures. Unmetabolized P_i was 32–35 % of total ^{32}P taken up by the cells. At 6 hr, distribution of radioactivity in nucleic acids (11–12 %) and phospholipid (10–12 %) was slightly increased. Nevertheless, small differences in the ^{32}P distribution into individual metabolites between two different density cultures were found up to 6 hr after inoculation.

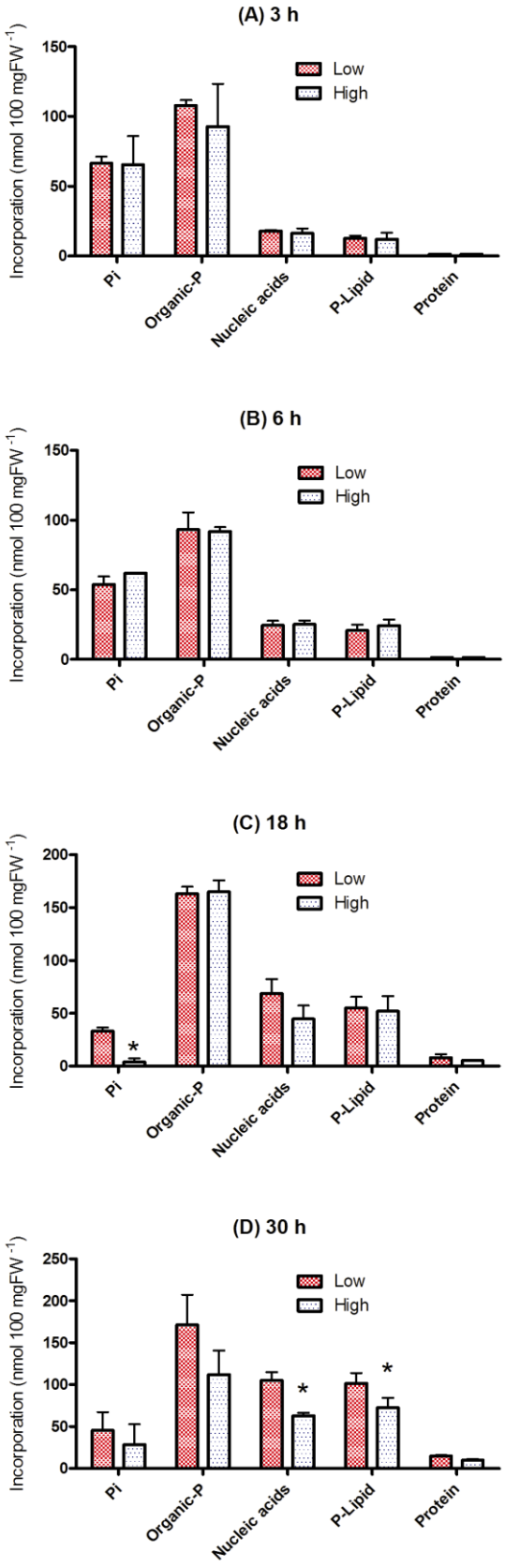

Figure 5. Distribution of ^{32}P taken up by *L. leptolepis* cells cultured in the low- and high-density culture. The samples are obtained at 3, 6, 18 and 30 h after inoculation. The values are expressed as nmol 100 mg FW^{-1}. Values for high-density culture marked with asterisks differ significantly from the value for low-density culture according to the *t*-test ($P < 0.05$). **P_i**, inorganic phosphate; **Organic-P**, cold PCA-soluble ^{32}P metabolites consists of nucleotide and sugar phosphates; **Nucleic acids**, RNA and DNA; **P-Lipid**, phospholipids; **Protein**, phosphoproteins.

The cellular [^{32}P]P_i level, especially in the high density-cultures, decreased 18 hr after inoculation (1–10 % of total ^{32}P taken up by the cells), and more than 90 % of ^{32}P was incorporated into the organic components. Although little difference in incorporation into nucleotides, sugar phosphates, phospholipids and phosphoproteins was found between the low- and high-density cultures, amounts of incorporation into nucleic acid in the low density culture (68.8 nmol) was higher in the high- density cultures (44.7 nmol). The trend was marked at 30 hr after culture where incorporation of ^{32}P into nucleic acid (105.2 nmol) and phospholipid (101.5 nmol) in the low density-cultures was higher than into those components (respectively, 62.8 and 72.3 nmol) in the high density-cultures.

In relation of phosphate and cell proliferation, Amino et al.[22] shows a linear relationship between initial P_i concentration in the medium (0–2.5 mM) and the stationary phase cell number, 10 days after inoculation. No cell number increase was observed in phosphate-free medium. These results indicate that P_i was limiting division of *Catharanthus roseus* cells. Ashihara et al.[23] determined the levels of purine and pyrimidine nucleotides in suspension cultures of *Catharanthus roseus* 24 h after stationary phase cells were transferred to fresh complete or phosphate-deficient medium containing 1.25 mM P_i. The levels of ATP, GTP, UTP and CTP were from approx. 3 to 5-fold greater in the cells grown in complete (with optimal level of P_i) medium than in the cells grown in the P_i -deficient medium. The levels of almost all other nucleotides were slightly higher in the cells in the complete medium. The authors suggested that increments in the levels of nucleotides, especially nucleoside triphosphates caused by P_i may induce a variety of biosynthetic reactions, such as nucleic acids, proteins, lipids and polysaccharides, and the proliferation of cells is believed to be triggered by such biochemical reactions.

To examine if increased level of nucleotides occurred in cells of the low-density culture, we extracted cellular nucleotides and analysed by HPLC. Table 1 shows the nucleotide levels in the cells grown in low density- and high-density cultures. All purine and pyrimidine nucleoside mono-, di- and triphosphates, except CMP were determined. The peak of CMP was sometimes contaminated by small amounts of impurities. No marked differences were found in nucleotide profiles in cells of the low- and high-density cultures. ATP levels in both cultures (~100 nmol gFW^{-1}) is similar to the value obtained from *C. roseus* cells in complete medium.[23] Compared to several cultured plant cells,[4] AMP level was high in *L. leptolepis* cells, as a result, the energy charge in the cells in the low- and high-density cultures varied 0.38–0.68 and 0.38–0.63, respectively. These values were much lower than those of plant cells reported,[4,24] although similar lower value was also found in *Datura innoxia* cells.[25] The results obtained here suggest that *L. leptolepis* cells even cultured in high-density culture possessed the sufficient amounts of nucleotides to continue proliferation at least up to 72 h.

For the formation of somatic embryos, induction of new RNA expression and rapid DNA replication seems to be required.[26] Therefore, sufficient P_i supply seems to be essential for the somatic embryogenesis of *L. leptolepis*. In general, embryogenic cells tissue is maintained in the presence of plant growth regulators, auxin and cytokinin.

Table 1. The effect of embryonic cell density on the concentration of nucleotides in *Larix leptolepis* cultures

	0 h	6 h		24 h		48 h		72 h	
		Low	High	Low	High	Low	High	Low	High
UMP	8±5	13±5	31±10	7±8	21±4	30±13	18±8	21±18	31±8
CMP	*	*	19±16	27±18	*	*	*	*	*
AMP	61±35	98±29	180±27	54±47	134±29	190±53	87±8	146±44	194±47
GMP	11±2	15±5	27±5	13±3	19±5	28±8	14±6	19±7	28±6
UDP	43±22	63±17	70±2	63±10	69±11	73±12	46±25	71±10	79±8
CDP	6±2	6±3	3±2	2±2	3±1	5±1	2±1	4±1	5±2
ADP	47±22	68±11	103±8	66±7	92±21	103±17	55±27	86±6	120±12
GDP	11±3	13±3	20±2	12±5	16±2	21±5	14±4	16±2	22±1
UTP	72±5	76±22	82±9	74±1	98±22	86±16	78±13	90±29	74±16
CTP	47±11	33±8	27±3	47±13	32±3	27±5	44±12	24±4	17±3
ATP	96±7	81±11	91±10	107±7	102±4	100±14	116±6	105±8	95±13
GTP	37±7	25±6	29±2	42±10	32±1	31±7	43±6	35±6	30±4

Nucleotide concentration is expressed as nmol gFW^{-1}. * not determined due to difficulty of the removal of contaminants.

Initiation of embryo development in suspension culture is induced by removal of plant growth regulators.[27] However, the present culture contained phytohormons throughout its entire culture period including induction of embryogenesis. Therefore, the effect of different amounts of plant growth regulators remained in the inoculated cultures as contaminants on the embryogenesis in low- and high-density cultures can be excluded.

In conclusion, the development of embryogenic cells into somatic embryos in the low-density culture seems to be complete supply of P_i, which is required for the synthesis of nucleic acid and phospholipid. In contrast, inhibition of the formation of somatic embryos in high-density culture is due to the limitation of P_i supply. Although other factors may be participated, difference in the phosphate availability for growth appeared to be one of the most important factors to determine the fate of development of cells of different density cultures.

Acknowledgements

The authors thank Professor Claudio Stasolla, University of Manitoba, and Professor Tatsuhito Fujimura, University of Tsukuba, for their valuable comments.

References

[1]Ogita, S., Sasamoto, H. and Kubo, T., *Transplant Production in the 21st Century*, Kluwer Academic Publishers, **2000,** 209-214.

[2]Stasolla, C. and Yeung, E. C., *Plant Cell Tiss. Org. Cult.*, **2003,** *74*, 15-35.

[3]Ogita, S., Kubo, T. and Fushitani, M., *Forest Resour. Environ.*, **1997**, *35*, 45-51.

[4]Wagner, K. G. and Backer, A. I., *Int. Rev. Cytol.*, **1992,** *134*, 1-84.

[5]Ukaji, T. and Ashihara, H., *Z. Naturforsch.*, **1986**, *41c*, 1045-1051.

[6]Li, X.N. and Ashihara, H., *Phytochemistry*, **1990**, *29*, 497-500.

[7]Nagano, M. and Ashihara, H., *Plant Cell Physiol.*, **1993**, *34*, 1219-1228.

[8]Ukaji, T. and Ashihara, H., *Ann. Bot.*, **1987**, *60*, 109-114.

[9]Li, X. N. and Ashihara, H., *Ann. Bot.*, **1989**, *64*, 33-36.

[10]Duff, S. M. G., Moorhead, G. B. G., Lefebvre, D. D. and Plaxton, W. C., *Plant Physiol.*, **1989**, *90*, 1275-1278.

[11]Nagano, M., Hachiya, A. and Ashihara, H., *Z. Naturforsch.*, **1994**, *49c*, 742-750.

[12]Ukaji, T. and Ashihara, H., *Int. J. Biochem.*, **1987**, *19*, 1127-1131.

[13]Dancer. J., Veith, R., Feil, R., Komor, E. and Stitt, M., *Plant Sci.*, **1990**, *66*, 59-63.

[14]Shimano, F. and Ashihara, H., *Phytochemistry*, **2006**, *67*, 132-141.

[15]Yin, Y., Shimano, F. and Ashihara, H., *J. Exp. Bot.*, **2007**, *58*, 1025-1033.

[16]Wylegalla, C., Meyer, R. and Wagner, K. G., *Planta*, **1985**, *166*, 446-451.

[17]Ashihara, H. and Ukaji, T., *J. Plant Physiol.*, **1986**, *124*, 77-85.

[18]Campbell, R. A. and Durzan, D. J., *Can. J. Bot.*, **1975**, *53*, 1652-1657.

[19]Ashihara, H. and Tokoro, T., *J. Plant Physiol.*, **1985**, *118*, 227-235.

[20]Ashihara, H. and Nobusawa, E., *Z. Pflanzenphysiol.*, **1981**, *104*, 443-458.

[21]Ashihara, H., Mitsui, K. and Ukaji, T., *Z. Naturforsch.*, **1987**, *42c*, 297-290.

[22]Amino, S., Fujimura, T. and Komamine, A., *Physiol. Plant.*, **1983**, *59*, 393-396.

[23]Ashihara, H., Li, X. N. and Ukaji, T., *Ann. Bot.*, **1988**, *61*, 225-232.

[24]Stasolla, C., Katahira, R., Thorpe, T. A. and Ashihara, H., *J. Plant Physiol.*, **2003**, *160*, 1271-1295.

[25]Mitsui, K. and Ashihara, H., *Plant Cell Physiol.*, **1988**, *29*, 1171-1183.

[26]Fujimura, T., *Plant Biotech. Rep.*, **2014,** *8*, 23-28.

[27]Stasolla, C., *Method. Mol. Biol.*, **2006**, *318*, 87-99.

Received: 13.10.2014.
Accepted: 05.11.2014.

BIOSORPTIVE-FLOTATION OF Pb^{2+} AND Cd^{2+} FROM WATER USING EGGSHELLS AS SORBENT AND OLEIC ACID AS SURFACTANT

S. E. Samra,[a] A. M. El-Nokrashy,[b] and A. A. El-Asmy[a,c]*

Keywords: Ionic flotation, Eggshells, Cadmium, Lead, Surfactant

The removal and recovery of Pb^{2+} and Cd^{2+} is important for environmental protection and economic reasons. A new method, sorptive flotation, for the removal of Pb^{2+} and Cd^{2+} from aqueous solutions and water samples using eggshells as sorbent and oleic acid (HOL) as surfactant has been investigated. The process parameters (solution pH, initial concentration of metal ions, sorbent dose, shaking time, oleic acid (HOL) concentration, and temperature) on the flotation of Pb^{2+} and Cd^{2+} were studied in batch system. Under the optimum experimental conditions suggested, the removal of ~ 100 % of Pb^{2+} and Cd^{2+} was attained. The procedure was successfully applied for the removal of Pb^{2+} and Cd^{2+} from different natural water samples.

* Corresponding Authors
Tel.: +96566734989:
E-Mail: aelasmy@yahoo.com
[a] Chemistry Department, Faculty of Science, Mansoura University, Mansoura, Egypt.
[b] Central Laboratory of drinking water, Dakahliya Company for Water & Wastewater, Mansoura, Egypt.
[c] Chemistry Department, Faculty of Science, Kuwait University, Kuwait.

Introduction

Toxic heavy metals such as cadmium and lead are released into the environment. They are environmental pollutants due to strong tendency to concentrate in environment and in food chains.[1-5]

Heavy metal contamination exists in aqueous waste streams of metal plating facilities, mining operations and tanning, metal finishing industries, chemical and battery manufacturing, paints and metal extraction.[5-7] Wastewaters from chemical industry polluted by heavy metal ions represent a hazard for all living organisms especially for human.[8,9] These metals can cause danger for ecosystems and human health if they are discharged into natural water resources and may pose finally a serious health hazard.[10-12] As these toxic metals accumulate by living organisms, they produced diseases and disorders.[13]

Lead is one of the major pollutants because of its presence in automobile fuel and subsequent emission into the atmosphere in the exhaust gases.[14,15] Pb(II) is very toxic, causing many health problems to human such as: nausea, renal disturbances ending with renal failure hepatitis, encephalopathy, anemia, lung inefficiency, bone lesions, hypertension, cancer, nervous disorder, coma, convulsions and subtle effects on metabolism, intelligence and sickness even death.[14 17] Due to toxic effects of lead ions, its removal from waters and wastewaters is important in terms of protection of public health and environment.[18,19]

Also, cadmium is one of the heavy metals with a greatest potential hazard to humans and environment. It makes a way to water bodies through wastewater from metal plating industries, industries of Cd–Ni batteries, phosphate fertilizer, lead–zinc mining, pigments, stabilizers, ceramics, photograph development, textile printing industries and alloys.[20,21] The poisoning of cadmium in human causes high blood pressure, kidney damage, destruction of testicular tissue and red blood cells. In small amounts, cadmium is associated with hypertensive diseases and considered as carcinogenic to men.[20]

One of the cheap and easily available materials having great sorption for heavy metals is eggshells. Due to its high calcium content, eggshells usually have no commercial importance. Disposal of eggshells is also a serious problem for egg processing industries due to stricter environmental regulations and high landfill costs.[22] It is proposed to apply hen eggshells as low-cost biological sorbent of metal ions. In USA annually 120,000 tons of waste eggshells is generated and disposed in landfills.[23,24] The hen eggshells consists of mammillary matrix (i.e., eggshell membrane) consisting of interwoven protein fibers and spherical masses, and spongy matrix (i.e., calcified eggshell) made of calcium carbonate.[25,26]

The by-product eggshell weighs approximately 10 % of the total mass (~ 60 g) of hen egg,[27] representing a significant waste from the egg-derived products processor because it was traditionally useless and commonly disposed of in landfills without any pretreatment.[26] The chemical composition (by weight) of byproduct eggshell is calcium carbonate (94 %), magnesium carbonate (1 %), calcium phosphate (1 %) and organic matter (4 %).[27,28]

The sorptive-flotation process is variant for the adsorbing colloid flotation process and employs particles as sorbing material for the pollutants. Sorptive-flotation resembles oxide flotation activation by metal ions, sulfides depression by anions and coal flotation with oil. The sorbent may be minerals, polymeric resins, activated carbon, powdered marble wastes, by-products, biomass or microorganisms and

must have a high surface area, high reactivity with the pollutants to be removed and good characteristics of coagulation/flocculation and flotation.[29-31]

Experimental

Chemicals and solutions

Unless otherwise stated, all chemical reagents used in this study were of analytical grade.

Surfactant preparation

Oleic acid (HOL) stock solution (6.36×10^2 mol L^{-1}) was prepared from the food grade with sp.gr, 0.895 (provided from J.T. Baker chemical Co.) by dispersing 20 ml of oleic acid in one liter of kerosene. Further dilution was prepared as required for another concentration.

Pb^{2+} and Cd^{2+} stock solutions

Stock solution (1000±2 mg L^{-1}) was prepared from Merck CRM (Germany) $Pb(NO_3)_2$ or $Cd(NO_3)_2$, respectively, in HNO_3. The working solutions were made by diluting with deionized water. Standard aqueous solutions of HNO_3 and/or NaOH were used for controlling the pH.

Eggshells (ES)

The eggshells were obtained from eggshells processing markets. The sample was washed, dried for 2 h in an oven maintained at 125 °C allowed to cool to room temperature and crushed. The sample sieved with size (25-63 µm) and stored in a desiccator. The functional groups of ES were characterized through IR spectra. The observable bands at 710, 875, 1420, 1797 and 2516 cm^{-1} coincide with pure $CaCO_3$.[25] The chemical analysis of the sample was found to be $CaCO_3$ (94 %), $MgCO_3$ (1 %), $Ca_3(PO_4)_2$ (1 %) and organic matter (4 %) as previously mentioned.[27,28]

Apparatus

Atomic Absorption Spectrometer (AAS)-Varian AA240FS, Australian, was used for the determination of lead and cadmium concentrations at 217 and 228 nm respectively, provided with micro burette 5 and 10 ml. The infrared analysis was undertaken via a Mattson 5000 FT-IR Spectrophotometer and using KBr disc. The X-ray diffraction was recorded *via* a XRD Bruker, Germany. The scan electron microscope analysis was undertaken *via* SEM-JEO/JSMS 410, Japan with energy dispersive X-ray EDX Unit, Oxford, England. The pH was measured using a Symphony pH meter, USA, provided with a glass electrode. Also, Milli-Q A10/ Elix Millipore-deionizer, France was used for deionized water, Binder FD240-drying oven, Germany. The flotation cell was a cylindrical tube of 1.5 cm inner diameter and 29 cm length with a stopcock at the bottom and a quick-fit stopper at the top.

Procedures

To study the different parameters affecting the sorptive-flotation process, 10 ml aliquot of suspension containing defined amounts of metal ions, sorbent sample, HCl or HNO_3 and/or NaOH (for controlling pH) was introduced into a flotation cell. The flotation cell was shaken for the optimized time, to ensure complete flotation of metal ions with sorbent. To this suspension inside the cell, 2 ml of HOL was added. Again, the cell was inverted upside down many times by hand and kept standing for 5 min to complete flotation.

The flotation efficiency (R_e %) of metal ion was calculated from the following relation:

$$R_e = 100\frac{(C_i - C_f)}{C_i}$$

where

C_i and C_f denote the initial and final concentrations, respectively.

Results and Discussion

Effect of pH

As a function of solution pH, Pb and Cd species may exist as soluble Pb^{2+}, hydroxo-species $[Pb(OH)^+$, $Pb(OH)^{3-}$ or $[Pb(OH)_4]^{2-}$ in addition to insoluble lead hydroxide, $Pb(OH)_2$, and hydrolytic species, $Cd(OH)^+$.[32,33]

The tendency of hydroxyl species in the float is sensitive to the solution pH. In order to find the optimal pH value for the sorptive-flotation process, the removal efficiency of Pb^{2+} and Cd^{2+} at pH 3, 6, 7 and 9 was studied. Figure 1 shows the effect of pH on the sorption-flotation for the removal 10 mg L^{-1} M^{2+} using 0.3 g ES and 5 x 10^{-2} mol L^{-1} HOL.

It should be noted that the removal of Pb^{2+} and Cd^{2+} increases with pH reaching ~ 100 % at pH 6- 9 due to the adsorption of hydrolytic species in the same manner as that reported[34] and/or surface precipitation of the metal as insoluble carbonate, forming successive layers on the sorbent surface,[35] the predominant species at this pH range and the negatively charged surface of eggshells and precipitation of metal carbonate on ES surface. The aggregates of ES-M^{2+} precipitate, being made hydrophobic by combination with undissociated oleic acid through hydrogen bonding and/or chemically with oleate anions. These hydrophobic aggregates are floated to the solution surface. Therefore, pH 6 was recommended throughout all other experiments. At pH < 6, the hydrolytic species of M^{2+} may adsorb or ion exchange with calcium sites of the ES sorbent. The adsorbent-adsorbate system is hydrophobic by combining with undissociated oleic acid molecules. Such combination may occur through hydrogen bonding of the hydroxide group of HOL.

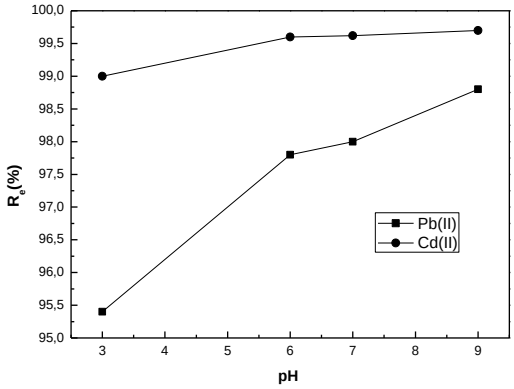

Figure 1. Removal of 10 mg L^{-1} metal ions on 0.3 g ES at different pH and 5 min shaking time.

Effect of ES and M^{2+} concentrations

Series of experiments were performed to study the influence of the eggshell dose (Figure 2) and changing the M^{2+} concentrations (Figure 3) on the removal percentage of Pb^{2+} and Cd^{2+} from aqueous solutions at pH 6 using 5 x 10^{-2} mol L^{-1} HOL. As the concentration of M^{2+} increases, the removal % of the M^{2+} ions on ES increases.

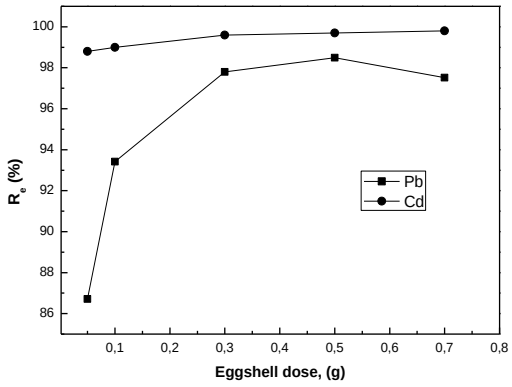

Figure 2. Removal % of 10 mg L^{-1} M^{2+} using different concentrations of ES and 5 × 10^{-2} mol L^{-1} HOL at pH 6 and 4 min shaking time

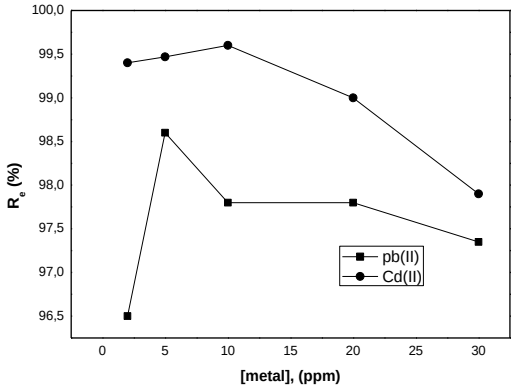

Figure 3. Removal % of different concentrations of M^{2+} using 0.3 g ES and 5 × 10^{-2} mol L^{-1} HOL at pH 6

Effect of HOL concentration

Series of experiments was undertaken to float 10 mg L^{-1} M^{2+} from aqueous solution at pH 6 in presence of 0.3 g of ES using different concentrations of HOL. The obtained results (Figure 4) showed that a maximum removal of M^{2+} (~100 %) was attained over HOL concentration of 5 x 10^{-2} mol L^{-1}. Consequently, the concentration of HOL employed was fixed at 5 x 10^{-2} mol L^{-1} throughout the study.

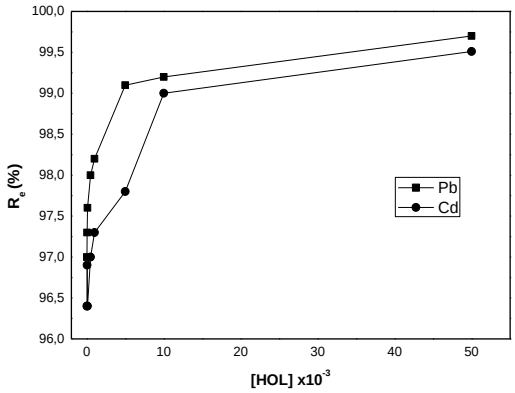

Figure 4. Removal % of 10 mg L^{-1} M^{2+} using 0.3 g ES and different concentrations of HOL at pH 6

Effect of shaking time

The % removal of M^{2+} with shaking time was studied using 10 mg L^{-1} M^{2+}, 0.3 g ES and 5 × 10^{-2} mol L^{-1} of HOL at pH 6. The shaking time was varied from 0.5 to 5 min. The obtained results (Figure 5) showed that the % removal increases to ~100 % after 4 min for 10 mg L^{-1} M^{2+}. Therefore, 4 min shaking was considered sufficient for the adsorption and flotation of M^{2+} having a concentration of 10 mg L^{-1} at pH 6.

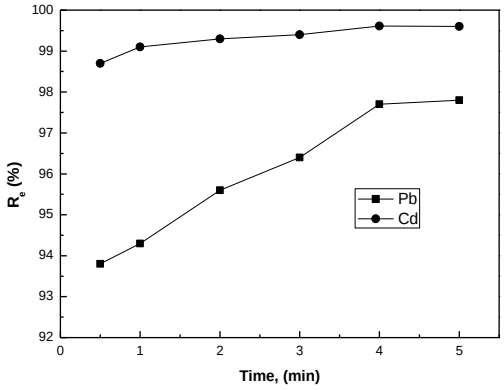

Figure 5. Removal % of 10 mg L^{-1} M^{2+} using 0.3 g ES and 5 × 10^{-2} mol L^{-1} HOL at different shaking time

Effect of temperature

Solutions of definite pH containing 10 mg L^{-1} M^{2+} and 0.3 g of ES and another solution containing 5 × 10^{-2} mol L^{-1} HOL were either heated or cooled. The surfactant solution was quickly poured onto the M^{2+} solution in the flotation cell. The mixture was then floated using the previous procedure. The obtained results (Figure 6) indicate that the % removal of M^{2+} increases as the temperature increases. Such data proposed that the adsorption of Pb^{2+} and Cd^{2+} may proceed through chemical-bond formation and ion exchange. Moreover, the increase of temperature to 60°C resulted in an increase in the rate of M^{2+} removing for the same dose of ES sorbent, 0.3 g. Such results suggest the creation of new active sites on ES surface available for adsorption of M^{2+}.

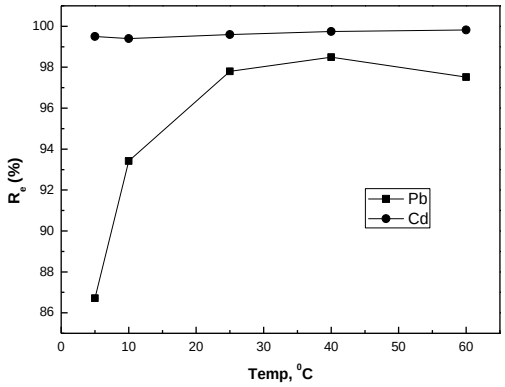

Figure 6. The removal of 10 mg L^{-1} metal ions using 0.3 g of ES and 5 × 10^{-2} mol L^{-1} HOL at different Temperature.

Application

The recommended procedure was performed to recover 10 mg L^{-1} M^{2+} added to aqueous and some natural water samples. The sorptive-flotation experiments were carried out using 10 ml of sample solutions with its initial pH. The obtained results (Table 1) show that the recovery is satisfactory.

Table 1. Recovery of 10 mg l^{-1} metal ions added to some water samples using 0.3 g of ES sorbent and 5 x 10^{-2} mol L^{-1}.

Sample (location)	Found (mg L^{-1})		R_e %	
	Pb(II)	Cd(II)	Pb(II)	Cd(II)
Distilled water	9.95	9.961	99.50	99.61
Tap water (our laboratory)	9.87	9.846	98.70	98.46
Nile water (Mansoura City)	9.92	9.910	99.20	99.10
Underground water (Mansoura City)	9.89	9.786	98.90	97.86
Sea water (Sharm El-Sheikh)	9.78	9.698	97.80	96.98

Instrumental studies

The Pb^{2+} and Cd^{2+} sorption by ES is interpreted by XRD, EDX and SEM analyses. Powered XRD studies help in understanding the changes occurred on the structure of ES sorption. XRD data (Figures 7a-7c) provided clear evidence of modification in the surface morphologies in form of cleavage.

In the EDX graph (Figures 8a-8c), the presence of Pb^{2+} and Cd^{2+} after treatment is observed. The SEM image of ES before and after metal ions adsorption (Figures 9a-9c) is corresponding to the morphological changes in the surface of the adsorbents in the coverage of pores of the ES due to the adsorption of Pb^{2+} and Cd^{2+}.

(a)

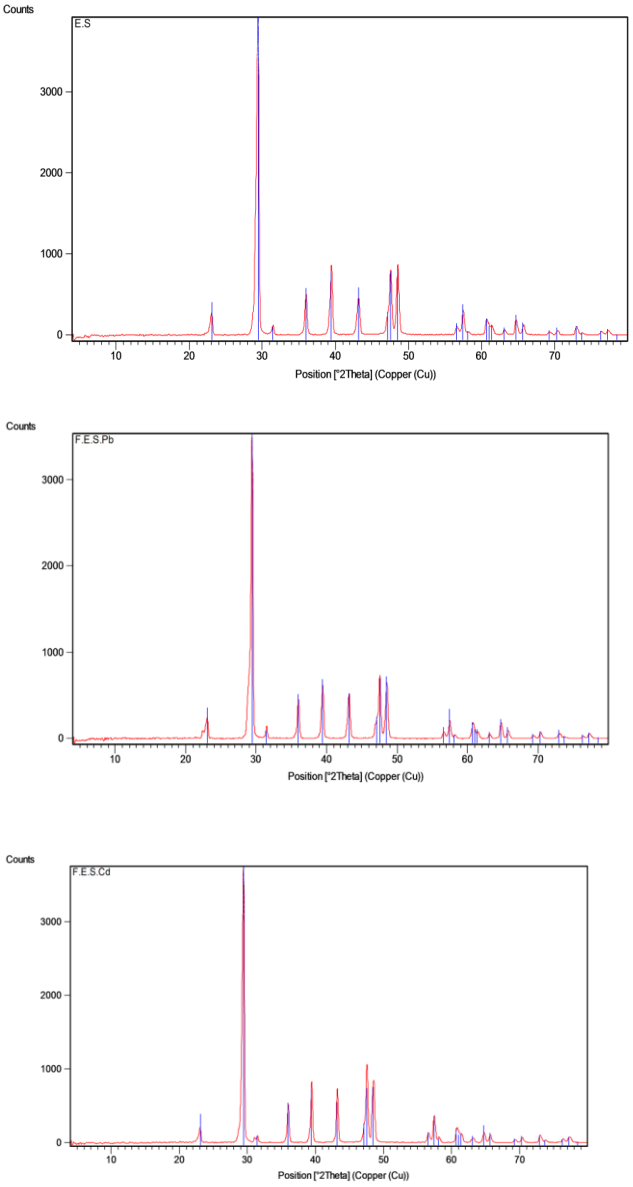

Figure 7. XRD of ES (a) before flotation; (b) after flotation with Pb^{2+} (c) after flotation with Cd^{2+}.

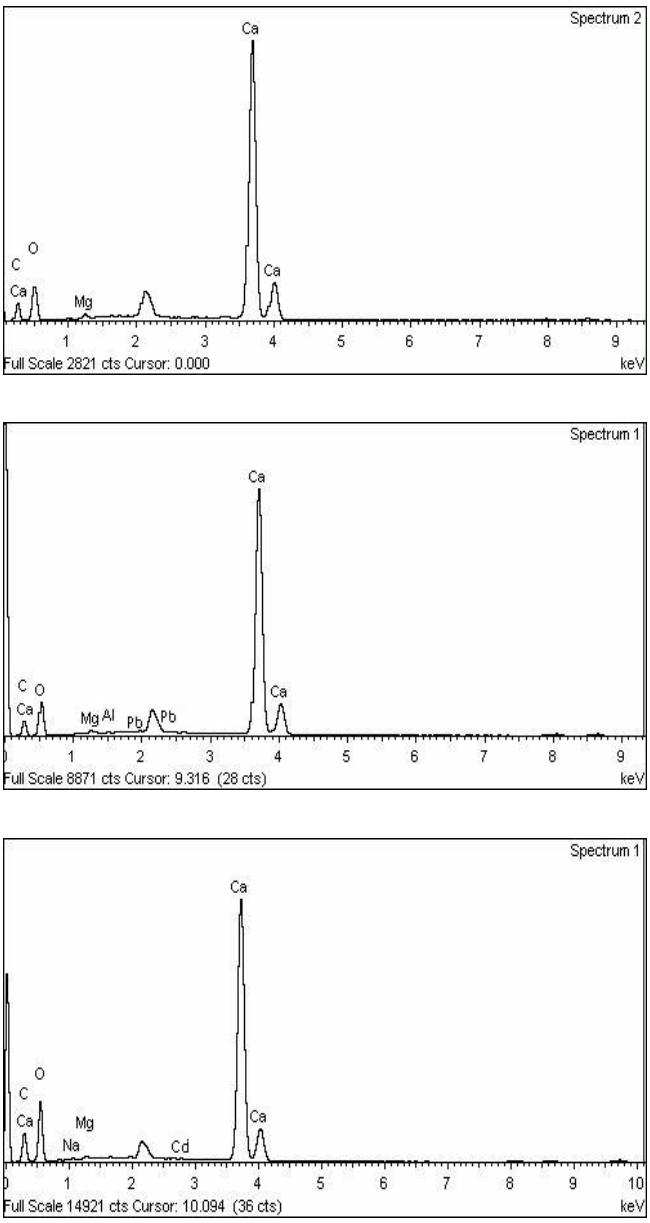

Figure 8. EDX of ES (a) before flotation; (b); after flotation with Pb^{2+} (c) after flotation with Cd^{2+}.

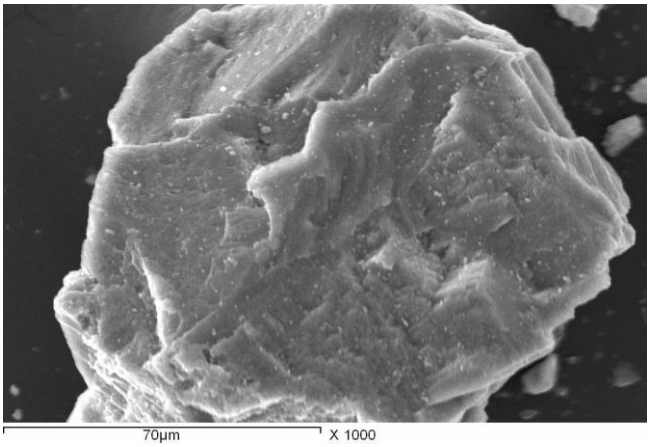

(a)

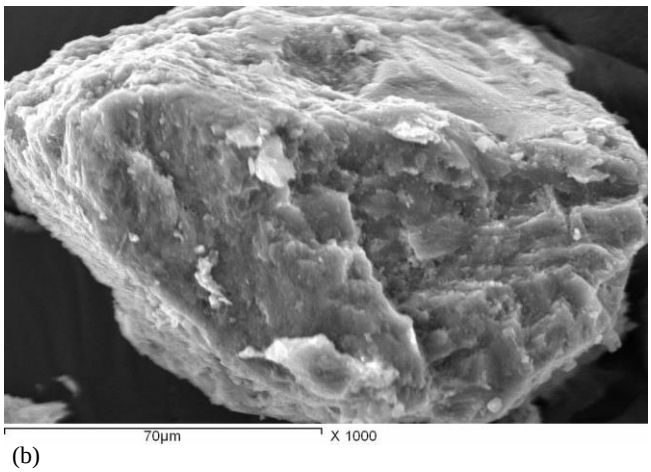

(b)

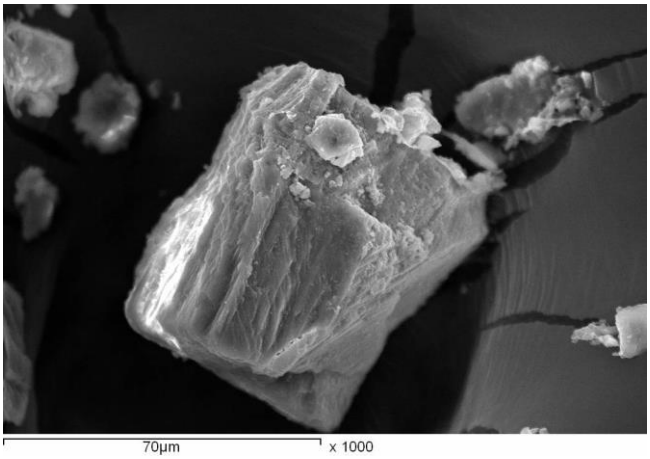

(c)

Figure 9. SEM of ES (a) before flotation; (b); after flotation with Pb^{2+} (c) after flotation with Cd^{2+}.

References

[1]Conti, M. E. and Botre, F., *Environ. Monit. Assess.*, **2001**, *69*, 282-267.

[2]Nyangababo, J. T., Henry L. and Omutange, E., *Bull. Environ. Contam. Toxicol.*, **2005,** *750*, 196-189.

[3]Hora, S., Simu, G., Rad, R., Papa, A. and Milos, M., *Rev. Chem.*, **2004**, *55*, 948-951.

[4]Yao, J., Jankowiski , K., Tuo, Y., Yao, Z. F., Xiao, Y., Xiao, S. H. and Tan, Z. Z., *J. Wuhan Univ. Tech. Mater. Sci. Edit.*, **2004,** *19*, 17-20.

[5]Bulut, Y. and Baysal, Z., *J. Enviton. Manag.*, **2006**, 78, 107-110.

[6]Carrillo-Morales, G., Davila-Jimenez, M. M., Elizalde-Gonzalez, M. P. and Pelaez-Cid, *J. Chromy. A*, **2001,** *938*, 237-242.

[7]Matheickal, J. T. and Yu, Q., *Miner. Eng.*, **1997,** *10*, 947-957.

[8]Rao, M. M., Ramesh, A., Rao, G. P. C. and Seshaiah, K., *J. Hazard. Mater. B,* **2006**, *129*, 123-129.

[9]Bayrak, Y., Yesiloglu, Y. and Gecgel, U., *Microporous Mesoporous Mater.*, **2006**, *91*, 107-110.

[10]Kadirvelu, K., Thamordiselvi, K. and Navasivayam, C., *Sep. Purif. Technol.*, **2001**, *24*, 479-505.

[11]Hasar, H., *J. Hazards Mater. B*, **2003,** *97*, 49-54.

[12]Al-Asheh S. and Duvnjok, Z., *J. Hazards Mater.*, **1997**, *56*, 35-51.

[13]Palma, G., Freer, J. and Baeza, J., *Water Res.*, **2003**, *37*, 4974-4980.

[14]Li, X., Zheng, W., Wang, D., Yang, Q., Cao, J., Yue, X., Shen, T. and Zeng, G., *Desalination*, **2010**, *258*, 148-153.

[15]Santos, A. C. V. and Masini, J. C., *Anal. Bioanal. Chem.*, **2006**, *385*, 1538-1544.

[16] Prado, A. G. S., Moura, A. Q., Holand M. S., Carvalho, T. O., Andrade, R. D. A., Pescara, I. C., Oliveira A. H. A., Okino, E.Y. A., Pastore, T. C. M., Silvea, D. J. and Zara, L. F., *Chem. Eng. J.*, **2010**, *160*, 549-555.

[17]Kul, A. R. and Koyuncu, H., *J. Hazard. Mater.*, **2010**, *179*, 332-339.

[18]Unlu, N. and Ersoz, M., *J. Hazard. Mater.*, **2006,** *136*, 272-280.

[19]Karatas, M., *J. Hazard. Mater.*, **2012,** *200*, 383-389.

[20]Krika, F., Azzouz, N. and Ncibi, M. C., *Arabian J. Chem.*, **2014**, in press.

[21]Tang, Q., Tang, X., Hu, M.,. Li, Z., Chen, Y. and Lou, P., *J. Hazard. Mater.*, **2010,** *179*, 95-103.

[22]Ozcan A. S., Erdem, B. and Ozcan A., *Colloids Surf. A,* **2005**, *266*, 73-81.

[23]Chojnacka, K., *J. Hazard. Mater.*, **2005,** *121*, 167-173.

[24]Anonymous, *Food Eng. Int..*, **2000**, *25*, 45-48.

[25]Ghazy, S. E., El-Asmy, A. A. and El-Nokrashy, A. M., *Int. J. Ind. Chem.*, **2011**, *2*, 242-252.

[26]Tsai, W. T., Hsein, K. J., Lin, C. M., Lin, K. Y. and Chiu, C. H., *Bioresource Tech.*, **2008**, *99*, 1623-1629.

[27]Stadelman, W. J. "*Eggs and Egg Products*", John Wiley & Sons, New York, **2000**.

[28]Poland, A. L. and Sheldon, B. W., *J. Food Prot.*, **2001**, *54*, 486-492.

[29]Mizuike, A. and Hiraide M., *Appl. Chem.*, **1982**, 54, 1555-1563.

[30]Rubio, J. and Tessele, F., *Miner. Eng.*, **1997**, *10*, 671-679.

[31]Zouboulis, A. I. and Matis, K. A., "*The 4th International conference, Flotation in Water and Waste Water Treatment*" Helsinki, **2000**.

[32]Bradi, H. B., A Hubbard (Ed.), "*Encyclopedia of surface and colloid science*", *Dekker, New York,* **2002.**

[33]Ghazy, S. E., Kabil, M.A, Shallaby, A. M. and Ammar, N. S., *Ind. J. Chem. Technol.*, **2001**, *8*, 211-218.

[34]Ghazy, S. E., Samra, S. E., Mahdy, A. M. and El-Morsy, S. M., *Sep. Sci. Tech.*, 2005, *40*, 1797-1815.

Received: 03.09.2014.
Accepted: 06.11.2014.

CYCLOKETONES AS PRECURSOR FOR CONVENIENT SYNTHESIS OF AZOLOPYRIMIDINES AND 5-ARYLAZOTHIAZOLES

Sayed A. Ahmed[a], Nadia A. Abdelriheem [b] and Abdou O. Abdelhamid[b*]

Keywords: hydrazonoyl halides; aminopyrazoles; pyrazolo[1,5-*a*]pyrimidines; pyrazolo[1,5-*a*]quinazolines; imidazo[1,2-*a*]cycloal-ka[*e*]pyrimidine; hydrazine-carbothioamide; arylazothiazoles

Condensation of sodium (3-oxocycloalkylidene)methenolate with several heterocyclic amines afforded pyrazolo[1,5-*a*]pyrimidine and pyrazolo[1,5-*a*]quinazoline derivatives. Also, 2-(2-cycloalkylidenehydrazinyl)-4-substituted-5-(phenyldiazenyl)-thiazole derivatives were synthesized via reaction of hydrazonoyl halides with 2-cycloalkylidene-hydrazinecarbothioamide. Structures of the newly synthesized compounds were elucidated by elemental analysis, spectral data, alternative synthethic routes and chemical transformation whenver possible.

* Corresponding Authors
E-Mail: Abdelhamid45@gmail.com
[a] Department of Chemistry, Faculty of Science, Beni-Suef University, Beni-Suef 62514 Egypt.
[b] Department of Chemistry, Faculty of Science, Cairo University, Giza 12613, Egypt

Introduction

Compounds containing the pyrimidine nucleus are of significant biological importance and are used as antibacterial,[1-5] antifungal,[6,7] antitumour [8,9], antiviral [9-13], anti-inflammatory [14,15] and antihypertensive [16-18] agents. Also, thiazole derivatives have been reported to posse's broad spectrum of pharmacological activities like anticancer [19], antidiabetic [20], CNS depressant [21], analgesic [22], antifilarial [23], antifungal and antibacterial [24], anthelmintic and antitumoral [25] activities. Mostly thiazole derivatives are known to posse's interesting biological properties that show anticancer [26] and antimicrobial activities. In this work, we synthesized some new pyrazolo[1,5-*a*]pyrimidine and 5-arylazothiazole derivatives.

Results and discussion

Treatment of 3-amino-5-phenyl-1*H*-pyrazole (**3a**) with sodium (2-oxocyclopentylidine)methenolate [27] (**2a**) in acetic acid containing piperidinum acetate afforded a product that may be 2-phenyl-7,8-dihydro-6*H*-cyclopenta[*e*]pyrazolo[1,5-*a*]pyrimidine (**6a**) or isomeric 2-phenyl-6,7-dihydro-5*H*-cyclopenta[*d*]pyrazolo[1,5-*a*]pyrimidine (**10a**) (Scheme 1). The structure **6a** was confirmed by elemental analysis, spectral data. IR (cm^{-1}) spectrum of the product revealed bands at 3085 (CH, aromatic), 2986 (CH, aliphatic), 1615 (C=N), 1597 (C=C). Its ^1H NMR spectrum showed signals at δ = 2.57 (m, 2H, CH_2), 2.87-2.92 (m, 4H, $2CH_2$), 6.51 (s, 1H, pyrazole H-4), 7.34-7.89 (m, 5H, ArH's), 8.23 (s, 1H, pyrimidine H-4). The reaction seems to occur *via* the initial formation of the intermediate **5** followed by dehydration cyclization to give of the **6a** as end product (Scheme 1).

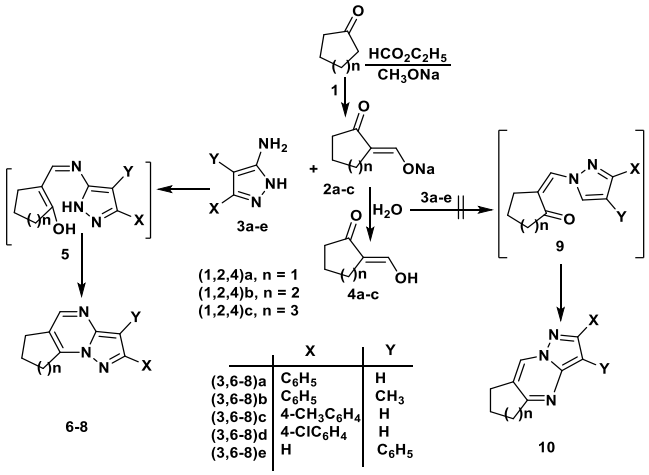

Scheme 1: Synthesis of pyrazol[1,5-a]pyrimidines (6-8)a-e

The suggestion of the formation of the alternative isomeric product **9** is based on the initial attack of the pyrazole NH group at the formyl group **4a.** This suggestion is excluded due to the higher nucleophilicity of the exocyclic primary amino group than the endocyclic NH group. Similarly, treatment of the appropriate **3b-e** were reacted with each of **2a-c** to give the tetrahydrocyclopenta- **5b-e**, tetrahydrocyclohexa- **6a-e**, and tetrahydrocycloheptapyrazolo[1,5-*a*]pyrimidine derivatives **7a-e**, respectively.

Analogously, the reaction of 2-aminobenzimidazole with each of **2a-c** in piperidinum acetate gave 2,3-dihydro-1*H*-benzo[4,5]imidazo[1,2-*a*]cyclopenta[*e*]pyrimidine (**11a**),

1,2,3,4-tetrahydrobenzo[4,5]imidazo[1,2-*a*]quinazoline (**11b**) and 2,3,4,5-tetrahydro-*1*H-benzo[4,5]imidazo[1,2-*a*]cyclohepta[*e*]pyrimidine (**11c**), respectively (Scheme 2).

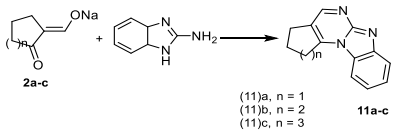

Scheme 2. Imidazo[1,2-a]cyclopenta[*e*]pyrimidine **11a**, imidazo[1,2-a]quinazoline **11b** and imidazo[1,2-*a*]cyclohepta[*e*]pyrimidine **11c**.

Next, we studied the reactions of hydrazonoyl halides with 2-cycloalkylidene-hydrazinecarbothioamide [28] **13a-c**. Thus, reaction of compound **13a** reacted with 2-oxo-*N'*, 2-diphenylacetohydrazonoyl bromide (**14a**) in ethanol in presence of catalytically amount of triethylamine gave one isolable product evidenced by *tlc* that proved to be 2-(2-cyclopentylidenehydrazinyl)-4-phenyl-5-(phenyldiazenyl)-thiazole (**20a**) (Scheme 3). Structure of **20a** was confirmed by elemental analysis, spectral data and alternative synthesis. For example, IR spectrum its exhibit revealed band at 3320 (NH), it show no of any CO group. ^{1}H NMR showed signals at δ 1.56-1.60 (m, 4H, $2CH_2$), 2.13-2.25 (m, 4H, $2CH_2$), 7.33-7.98 (m, 10H, ArH's) and 9.08 (s, br., 1H, NH). Moreover, **24a** [29], which was prepared via reaction of ω-bromoacetophenone (**23**) with **13a** in ethanol, was reacted with benzendiazonium chloride in ethanolic sodium acetate at 0 °C afforded product identical in all aspect (mp., mixed mp. and spectra) with **20a** (Scheme 3).

Two possible pathways can account for the formation **20a** via 1,3-addition of the thiol tautomer of **13** to the nitriliimine **15**, (generated in situ from hydrazonoyl halide **14a** and triethylamine), to form the thiohydrazonate ester **19a**, which undergoes dehydrative cyclization to yield **20a**. The formations of **19** and **20** are similar to the reaction of hydrazonoyl chloride with 1-phenyl-1,4-dihydrotetrazole-5-thione [30] and 5-phenyl-1,3,4-thiadiazole-2(3*H*)-thione [31] or 1,3-cycloaddition of nitrilimine **15** to C=S double bond of **13a** can give directly **16**. The latter intermediate **16** was converted to **17a,** by loss one molecule of ammonia (Scheme 3). The latter pathway was ruled out on the base of IR, ^{1}H NMR and alternative synthetic route.[32]

Similarly, the appropriate **13a-c** reacted with each of hydrazonoyl halides **14a,b** and ω-bromoacetophenone in ethanol gave **(20-22)a-d** and **24a-c** (Scheme 3).

Finally, reaction of sodium 3-oxo-3-phenylprop-1-en-1-olate was reacted with thiosemicarbazide (**12**) in acetic acid containing piperidinum acetate afforded 2,2'-(1-phenylpropane-1,3-diylidene)bis(hydrazinecarbothioamide) (**25**) and not 3-phenyl-1*H*-pyrazole-1-carbothioamide (**26**) according to mp. and reaction of benzoylacetaldehyde with thiosemicarbazide [33]. Treatment of compound **25** was reacted with the appropriate hydrazonoyl halides afforded 4-phenyl-2-(2-(1-phenyl-3-(4-phenyl-5-(phenyldiazenyl)thiazol-2-yl)diazenyl)allylidene)-hydrazinyl)-5-(phenyldiazenyl)-thiazole (**30a**) (Scheme 4).

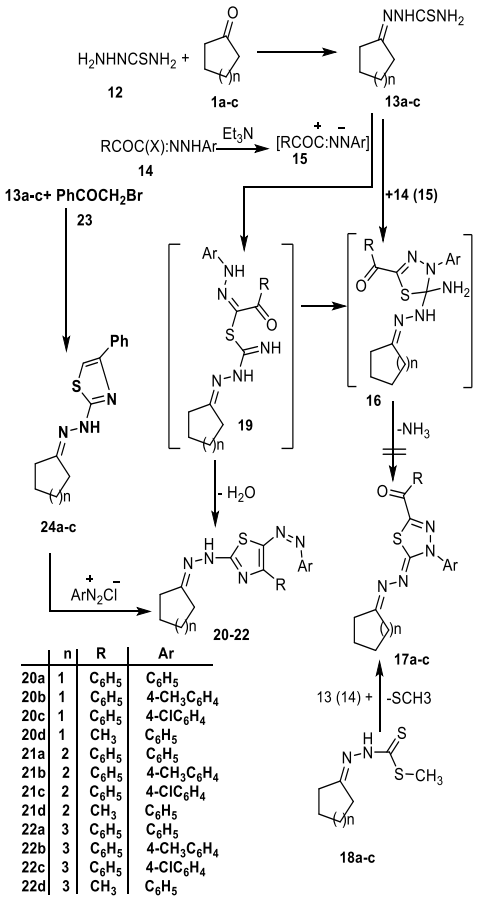

Scheme 3: 2-(2-Cycloalkylidenehydrazinyl)-4,5-disubstituted thiazoles (20-22)a-d

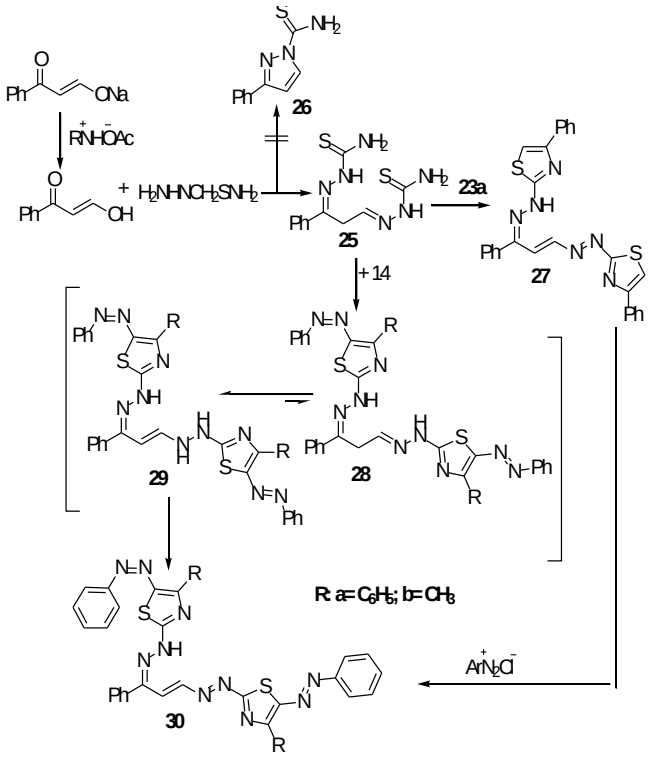

Scheme 4: Synthesis of thiazoles **30a** and **30b**

Structure of **30a** was confirmed by elemental analysis, spectral data and alternative synthetic route. Thus, treatment of 4-phenyl-2-(2-(-1-phenyl-3-(4-phenyl-5-phenylthiazol-2-yl)diazenyl)allylidene)hydrazin-yl)thiazole (**27a**), which obtained by reaction of **25** with ω-bromoacetophenone, with benzenediazonium chloride ethanolic sodium acetate solution at 0-5 ºC afforded product identical in all aspect (mp., mixed mp. and spectra) with **30a**.

Experimental

All melting points were determined on an electrothermal apparatus and are uncorrected. IR spectra were recorded (KBr discs) on a Shimadzu FT-IR 8201 PC spectrophotometer. NMR spectra were recorded in $CDCl_3$ and $(CD_3)_2SO$ solutions on a JNM-LA 400 FT-NMR system and a Varian Gemini 300 MHz spectrometer and chemical shifts are expressed in δ ppm units using TMS as an internal reference. Mass spectra were recorded on a GC-MS QP1000 EX Shimadzu. Elemental analyses were carried out at the Microanalytical Center of Cairo University. Sodium (2-oxocycloalkylidine)methenolate [27] (**2a-c**), 2-cycloalklidenehydrazinecarbothioamide [28] **13a-c**, and hydrazonoyl halides [34,35] **14,** methyl 2-cyclopentylidenehydrazine-1-carbodithioate **(18)** [36] were synthesized as previously reported.

Synthesis of pyrazolo[1,5-*a*]pyrimidines (6-8)a-e, benzo[4,5]imidazo[1,2-*a*]cyclopenta[*e*]pyrimidine 11a, benzo[4,5]imidazo-[1,2-*a*]quinazoline 11b and benzo[4,5]imidazo[1,2-*a*]cyclohepta[*e*]pyrimidine 11c.

A solution of sodium salt of (2-oxocycloalkylidine)-methanolates **2a-c (**0.01 mol), aminopyrazoles, 2-aminobenzimidazole (0.01 mol) and piperidine acetate (1 ml) in H_2O (3 ml) was refluxed for 15 minutes. Acetic acid (1.5 ml) was added to the hot solution. The solid product was filtered off and recrystallized from ethanol to give **(5-7)a-e, 11a, 11b and 11c.**

2-Phenyl-7,8-dihydro-6*H*-cyclopenta[*e*]pyrazolo[1,5-*a*]pyrimidine (6a)

This compound was obtained as yellow solid (78 %). m.p. 185-86 °C. IR (KBr): 3085 (CH, aromatic), 2986 (CH, aliphatic), 1615 (C=N), 1597 (C=C) cm^{-1}. MS (EI, 70 eV) *m/z*: 235 (M+). ^{1}H NMR (400 MHz, $CDCl_3$) δ = 2.57 (m, 2H, CH_2), 2.87-2.92 (m, 4H, $2CH_2$), 6.51 (s, 1H, pyrazole H-4), 7.34-7.89 (m, 5H, ArH's), 8.23 (s, 1H, pyrimidine H-4). ^{13}C NMR δ = 21.87, 28.74, 30.62, 100.45, 118.77, 127.62, 128.23, 130.19, 133.18, 143.57, 144.47, 150.75, 154.66. Anal. Calcd for $C_{15}H_{13}N_3$: C, 76.57; H, 5.57; N, 17.86 Found: C, 76.47; H, 5.53; N, 17.93

3-Methyl-2-phenyl-7,8-dihydro-6*H*-cyclopenta[*e*]pyrazolo[1,5-*a*]pyrimidine (6b)

This compound was obtained as yellow solid (72 %). m.p. 165-66 °C. IR (KBr): 3080 (CH, aromatic), 2987 (CH, aliphatic), 1620 (C=N), 1595 (C=C) cm^{-1}. MS (EI, 70 eV) *m/z*: 249 (M+). ^{1}H NMR (400 MHz, $CDCl_3$) δ = 2.20 (s, 3H, CH_3), 2.57 (m, 2H, CH_2), 2.87-2.92 (m, 4H, $2CH_2$), 7.34-7.89 (m, 5H, ArH's), 8.23 (s, 1H, pyrimidine H-4). ^{13}C NMR δ = 8.12, 21.43, 28.74, 30.62, 106.27, 118.86, 128.67, 128.75, 128.99, 132.12, 135.23, 143.90, 148.57, 152.34. Anal. Calcd for $C_{16}H_{15}N_3$: C, 77.08; H, 6.06; N, 16.85. Found: $C_{16}H_{15}N_3$ (249.31); C, 77.15; H, 6.20; N, 16.97

2-(p-Tolyl)-7,8-dihydro-6*H*-cyclopenta[*e*]pyrazolo[1,5-*a*]pyrimidine (6c)

This compound was obtained as yellow solid (77 %). m.p. 190-92 °C. IR (KBr): 3057 (CH, aromatic), 2984 (CH, aliphatic), 1618 (C=N), 1595 (C=C) cm^{-1}. MS (EI, 70 eV) *m/z*: 249 (M+). ^{1}H NMR (400 MHz, $CDCl_3$) δ = 2.30 (s, 3H, CH_3), 2.64-2.69 (m, 2H, CH_2), 3.16-3.18 (t, 2H, *J* = 4 Hz, CH_2), 3.62-3.68 (m, 2H, CH_2), 6.47 (s, 1H, pyrazole H-4), 7.34-7.36 (d, 2H, *J* = 4 Hz, ArH's), 7.81-7.83 (d, 2H, *J* = 4 Hz, ArH's), 8.34 (s, 1H, pyrimidine H-4); ^{13}C NMR δ = 21.43, 21.77, 28.74, 30.48, 100.42, 118.44, 128.27, 130.56, 132.27, 136.20, 142.27, 143.45, 149.99, 152.14. Anal. Calcd for $C_{16}H_{15}N_3$; C, 77.08; H, 6.06; N, 16.85. Found: C, 77.11; H, 6.17; N, 17.00.

2-(p-Chlorophenyl)-7,8-dihydro-6*H*-cyclopenta[*e*]pyrazolo[1,5-*a*]pyrimidine (6d)

This compound was obtained as yellow solid (72 %). m.p. 175-77 °C. IR (KBr): 3069 (CH, aromatic), 2985 (CH, aliphatic), 1620 (C=N), 1600 (C=C) cm^{-1}. MS (EI, 70 eV) *m/z*: 269 (M+), 271 (M+2). ^{1}H NMR (400 MHz, $CDCl_3$) δ = 2.64-2.69 (m, 2H, CH_2), 3.16-3.18 (t, 2H, *J* = 4 Hz, CH_2), 3.62-3.68 (m, 2H, CH_2), 6.47 (s, 1H, pyrazole H-4), 7.54-7.56 (d, 2H, *J* = 4 Hz, ArH's), 7.80-7.82 (d, 2H, *J* = 4 Hz, ArH's), 8.30 (s, 1H, pyrimidine H-4); ^{13}C NMR δ = 21.43, 28.57, 30.42, 100.32, 118.48, 128.75, 130.95, 132.11, 133.89, 142.45, 143.49, 150.12, 152.24. Anal. Calcd for $C_{15}H_{12}ClN_3$: C, 66.79; H, 4.48; N, 15.58. Found: C, 66.67; H, 4.39; N, 15.48.

3-Phenyl-7,8-dihydro-6*H*-cyclopenta[*e*]pyrazolo[1,5-*a*]pyrimidine (6e)

This compound was obtained as yellow solid (82 %). m.p. 170-72 °C. IR (KBr): 3072 (CH, aromatic), 2983 (CH, aliphatic), 1615 (C=N), 1598 (C=C) cm^{-1}. MS (EI, 70 eV) *m/z*: 235 (M+). ^{1}H NMR (400 MHz, $CDCl_3$) δ = 2.64-2.69 (m, 2H, CH_2), 3.16-3.18 (t, 2H, *J* = 4 Hz, CH_2), 3.62-3.68 (m, 2H, CH_2), 6.93-6.95 (d, 2H, J = 4 Hz, ArH's), 7.54-7.62 (m, 3H, ArH's), 8.22 (s, 1H, pyrimidine H-4), 8.34 (s, 1H, pyrazole H-3); ^{13}C NMR δ = 21.42, 28.48, 30.67, 113.45, 118.62, 126.65, 128.22, 128.74, 130.76, 143.28, 144.18, 144.78, 149.52. Anal. Calcd for $C_{15}H_{13}N_3$: C, 76.57; H, 5.57; N, 17.86. Found: C, 76.67; H, 5.49; N, 17.78.

2-Phenyl-6,7,8,9-tetrahydropyrazolo[1,5-*a*]quinazoline (7a)

This compound was obtained as yellow solid (76 %). m.p. 190-92 °C. IR (KBr): 3072 (CH, aromatic), 2980 (CH, aliphatic), 1612 (C=N), 1600 (C=C) cm^{-1}. MS (EI, 70 eV) *m/z*: 249 (M+). ^{1}H NMR (400 MHz, $CDCl_3$) δ = 1.58-1.66 (m, 2H, CH_2), 1.80-190 (m, 2H, CH_2), 2.62-2.68 (m, 2H, CH_2), 3.15-3.17 (t, 2H, J = 4 Hz, CH_2), 6.50 (s, 1H, pyrazole

H-4), 7.45-7.82 (m, 5H, ArH's), 8.32 (s, 1H, pyrimidine H-4), ^{13}C NMR δ = 21.67, 23.20, 24.56, 38.63, 100.12, 115.23, 127.40, 128.15, 130.21, 132.98, 142.52, 150.97, 153.27. Anal. Calcd for $C_{16}H_{15}N_3$: C, 77.08; H, 6.06; N, 16.85. Found: C, 76.87; H, 5.96; N, 16.78.

3-Methyl-2-phenyl-6,7,8,9-tetrahydropyrazolo[1,5-*a*]quinazoline

This compound was obtained as yellow solid (76 %). m.p. 160-61 °C. IR (KBr): 3057 (CH, aromatic), 2982 (CH, aliphatic), 1615 (C=N), 1594 (C=C) cm^{-1}. MS (EI, 70 eV) *m/z*: 263 (M+). ^{1}H NMR (400 MHz, $CDCl_3$) δ = 1.58-1.66 (m, 2H, CH_2), 1.80-190 (m, 2H, CH_2), 2.47 (s, 3H, CH_3), 2.62-2.68 (m, 2H, CH_2), 3.15-3.17 (t, 2H, J = 4 Hz, CH_2), 7.24-7.36 (m, 3H, ArH's), 7.81-7.83 (d, 2H, J= 4 Hz, ArH's), 8.25 (s, 1H, Pyrimidine H-4), ^{13}C NMR δ = 8.12, 21.67, 23.21, 24.56, 38.63, 105.18, 115.23, 128.75, 128.89, 131.79, 135.23, 146.12, 149.31, 153.45. Anal. Calcd for $C_{17}H_{17}N_3$ (263.31): C, 77.54; H, 6.51; N, 15.96. Found: C, 77.67; H, 6.45; N, 15.78.

2-(p-Tolyl)-6,7,8,9-tetrahydropyrazolo[1,5-*a*]quinazoline (7c)

This compound was obtained as yellow solid (76 %). m.p. 170-72 °C. IR (KBr): 3057 (CH, aromatic), 2982 (CH, aliphatic), 1615 (C=N), 1594 (C=C) cm^{-1}. MS (EI, 70 eV) *m/z*: 263 (M+). ^{1}H NMR (400 MHz, $CDCl_3$) δ = 1.58-1.66 (m, 2H, CH_2), 1.80-190 (m, 2H, CH_2), 2.28 (s, 3H, CH_3), 2.62-2.68 (m, 2H, CH_2), 3.15-3.17 (t, 2H, J = 4 Hz, CH_2), 6.48 (s, 1H, pyrazole H-4), 7.34-7.36 (d, 2H, ArH's), 7.81-7.83 (d, 2H, J= 4 Hz, ArH's), 8.35 (s, 1H, pyrimidine H-4), ^{13}C NMR δ = 21.67, 21.88, 23.32, 24.67, 38.63, 100.20, 115.32, 128.26, 130.65, 132.24, 135.19, 124.52, 145.37, 150.97, 153.18. Anal. Calcd for $C_{17}H_{17}N_3$ (263.31): C, 77.54; H, 6.51; N, 15.96. Found: C, 77.59; H, 6.57; N, 15.89.

2-(4-Chlorophenyl)-6,7,8,9-tetrahydropyrazolo[1,5-*a*]quinazoline (7d)

This compound was obtained as yellow solid (76 %). m.p. 180-82 °C. IR (KBr): 3057 (CH, aromatic), 2982 (CH, aliphatic), 1615 (C=N), 1594 (C=C) cm^{-1}. MS (EI, 70 eV) *m/z*: 283 (M+). ^{1}H NMR (400 MHz, $CDCl_3$) δ = 1.58-1.66 (m, 2H, CH_2), 1.80-190 (m, 2H, CH_2), 2.62-2.68 (m, 2H, CH_2), 3.15-3.17 (t, 2H, J = 4 Hz, CH_2), 6.48 (s, 1H, pyrazole H-4), 7.64-7.66 (d, 2H, ArH's), 7.80-7.82 (d, 2H, J= 4 Hz, ArH's), 8.32 (s, 1H, Pyrimidine H-4), ^{13}C NMR δ = 21.67, 23.30, 24.56, 38.63, 100.20, 115.32, 128.57, 130.64, 131.98, 133.76, 142.28, 145.13, 150.78, 153.27. Anal. Calcd for $C_{16}H_{14}ClN_3$: 283.76: C, 67.72; H, 4.97; N, 14.81. Found: C, 67.65; H, 5.00; N, 14.76.

3-Phenyl-6,7,8,9-tetrahydropyrazolo[1,5-*a*]quinazoline (7e)

This compound was obtained as yellow solid (76 %). m.p. 170-72 °C. IR (KBr): 3057 (CH, aromatic), 2982 (CH, aliphatic), 1615 (C=N), 1594 (C=C) cm^{-1}. MS (EI, 70 eV) *m/z*: 249 (M+). ^{1}H NMR (400 MHz, $CDCl_3$) δ = 1.58-1.66 (m, 2H, CH_2), 1.80-190 (m, 2H, CH_2), 2.62-2.68 (m, 2H, CH_2), 3.15-3.17 (t, 2H, J = 4 Hz, CH_2), 7.64-7.82 (m, 5H, ArH's), 8.32 (s, 1H, pyrimidine H-4), 8.34 (s, 1H, pyrazole H-3), ^{13}C NMR δ = 21.67, 23.45, 24.56, 38.63, 100.20, 115.32, 123.25, 127.42, 128.78, 131.26, 131.75, 133.27, 137.27, 149.68, 143.38, 145.13, 150.87, 152.35. Anal. Calcd for $C_{16}H_{15}N_3$: 249.14: C, 77.08; H, 6.06; N, 16.85. Found: C, 77.15; H, 5.89; N, 16.76.

2-Phenyl-7,8,9,10-tetrahydro-6*H*-cyclohepta[*e*]pyrazolo[1,5-*a*]-pyrimidine (8a)

This compound was obtained as yellow solid (76 %). m.p. 155-56 °C. IR (KBr): 3057 (CH, aromatic), 2982 (CH, aliphatic), 1615 (C=N), 1594 (C=C) cm^{-1}. MS (EI, 70 eV) *m/z*: 263 (M+). ^{1}H NMR (400 MHz, $CDCl_3$) δ = 1.60-1.90 (m, 4H, CH_2), 2.70-2.80 (d, 1H, *J* = 6 Hz, CH_2), 2.85 (t, 2H, *J* = 6 Hz, CH_2), 3.15 (d, 1H, CH), 3.5 (t, 2H, *J* = 6 Hz, CH_2), 6.50 (s, 1H, pyrazole H-4), 7.45-7.82 (m, 5H, ArH's), 8.30 (d, 1H, *J* = 6Hz, pyrimidine H-4). ^{13}C NMRδ = 23.12, 26.58, 28.13, 28.42, 29.15, 100.20, 115.12, 127.38, 128.27, 130.19, 133.25, 142.52, 145.35, 145.65, 151.78, 154.56. Anal. Calcd for $C_{17}H_{17}N_3$: 263.34: C, 77.54; H, 6.51; N, 15.96. Found: C, 77.45; H, 6.38; N, 16.10.

3-Methyl-2-phenyl-7,8,9,10-tetrahydro-6*H*-cyclohepta[*e*]pyrazolo[1,5-*a*]pyrimidine (8b)

This compound was obtained as yellow solid (76 %). m.p. 149-150 °C. IR (KBr): 3057 (CH, aromatic), 2982 (CH, aliphatic), 1615 (C=N), 1594 (C=C) cm^{-1}. MS (EI, 70 eV) *m/z*: 277 (M+). ^{1}H NMR (400 MHz, $CDCl_3$) δ = 1.60-1.90 (m, 4H, CH_2), 2.20 (s, 3H, CH_3), 2.70-2.80 (d, 1H, *J* = 6 Hz, CH_2), 2.85 (t, 2H, *J* = 6 Hz, CH_2), 3.15 (d, 1H, CH), 3.5 (t, 2H, *J* = 6 Hz, CH_2), 7.45-7.82 (m, 5H, ArH's), 8.30 (s, 1H, pyrimidine H-4). ^{13}C NMR δ = 8.24, 23.11, 26.59, 28.23, 29.18, 105.27, 115.23, 126.76, 128.79, 129.Anal. Calcd for $C_{18}H_{19}N_3$: 277.16: C, 77.95; H, 6.90; N, 15.15. Found: C, 78.10; H, 6.78; N, 15.29.

2-(p-Tolyl)-7,8,9,10-tetrahydro-6*H*-cyclohepta[*e*]pyrazolo[1,5-*a*]pyrimidine (8c)

This compound was obtained as yellow solid (76 %). m.p. 160-61 °C. IR (KBr): 3057 (CH, aromatic), 2982 (CH, aliphatic), 1615 (C=N), 1594 (C=C) cm^{-1}. MS (EI, 70 eV) *m/z*: 277 (M^+). ^{1}H NMR (400 MHz, $CDCl_3$) δ = 1.60-1.90 (m, 4H, CH_2), 2.20 (s, 3H, CH_3), 2.70-2.80 (d, 1H, *J* = 6 Hz, CH_2), 2.85 (t, 2H, *J* = 6 Hz, CH_2), 3.15 (d, 1H, CH), 3.5 (t, 2H, *J* = 6 Hz, CH_2), 6.48 (s, 1H, pyrazole H-4), 7.34-7.36 (d, 2H, ArH's), 7.81-7.83 (d, 2H, J= 4 Hz, ArH's), 8.35 (s, 1H, pyrimidine H-4), ^{13}C NMR δ = 21.77, 23.11, 26.57, 28.23, 29.18, 100.24, 115.31, 128.27, 130.65, 132.23, 138.30, 242.34, 145.30, 151.13, 154.65. Anal. Calcd for $C_{18}H_{19}N_3$ (277.36): C, 77.95; H, 6.90; N, 15.15. Found: C, 77.84; H, 7.10; N, 14.98.

2-(4-Chlorophenyl)-7,8,9,10-tetrahydro-6*H*-cyclohepta[*e*]pyrazolo[1,5-*a*]pyrimidine (8d)

This compound was obtained as yellow solid (76 %). m.p. 160-61 °C. IR (KBr): 3057 (CH, aromatic), 2982 (CH, aliphatic), 1615 (C=N), 1594 (C=C) cm^{-1}. MS (EI, 70 eV) *m/z*: 297 (M^+), 299 (M+2). ^{1}H NMR (400 MHz, $CDCl_3$) δ 1.60-1.90 (m, 4H, CH_2), 2.70-2.80 (d, 1H, *J* = 6 Hz, CH_2),

2.85 (t, 2H, *J* = 6 Hz, CH_2), 3.15 (d, 1H, CH), 3.5 (t, 2H, *J* = 6 Hz, CH_2), 6.48 (s, 1H, pyrazole H-4), 7.64-7.66 (d, 2H, ArH's), 7.80-7.82 (d, 2H, J= 4 Hz, ArH's), 8.32 (s, 1H, pyrimidine H-4), ^{13}C NMR δ = 23.11, 26.63, 28.12, 28.48, 29.13, 100.32, 115.23, 128.84, 136.57, 131.92, 133.80, 142.35, 145.30, 151.52, 154.75. Anal. Calcd for $C_{17}H_{16}ClN_3$ (297.78): C, 68.57; H, 5.42; N, 14.11. Found: C, 68.75; H, 5.35; N, 14.24

2-Phenyl-6,7,8,9-tetrahydro-5*H*-cyclohepta[*d*]pyrazolo[1,5-*a*]-pyrimidine (8e)

This compound was obtained as yellow solid (76 %). m.p. 170-72 °C. IR (KBr): 3057 (CH, aromatic), 2982 (CH, aliphatic), 1615 (C=N), 1594 (C=C) cm^{-1}. MS (EI, 70 eV) *m/z*: 263 (M+). ^{1}H NMR (400 MHz, $CDCl_3$) δ 1.60-1.90 (m, 4H, CH_2), 2.70-2.80 (d, 1H, *J* = 6 Hz, CH_2), 2.85 (t, 2H, *J* = 6 Hz, CH_2), 3.15 (d, 1H, CH), 3.5 (t, 2H, *J* = 6 Hz, CH_2), 7.64-7.82 (m, 5H, ArH's), 8.32 (s, 1H, pyrimidine H-4), 8.34 (s, 1H, pyrazole H-3), ^{13}C NMR δ = 23.12, 26.62, 28.13, 28.42, 29.13, 100.20, 111.23, 126.68, 126.14, 128.74, 130.81, 144.72, 145.29, 147.29, 150.90. Anal. Calcd for $C_{17}H_{17}N_3$: 263.34: C, 77.54; H, 6.51; N, 15.96. Found: C, 77.45; H, 6.37; N, 16.12

2,3-Dihydro-1*H*-benzo[4,5]imidazo[1,2-*a*]cyclopenta[*e*]pyri-midine (11a)

This compound was obtained as yellow solid (78 %). m.p. 185-87 °C. IR (KBr): 3085 (CH, aromatic), 2986 (CH, aliphatic), 1615 (C=N), 1597 (C=C) cm^{-1}. MS (EI, 70 eV) *m/z*: 209 (M+). ^{1}H NMR (400 MHz, $CDCl_3$) δ = 2.57 (m, 2H, CH_2), 2.87-2.92 (m, 4H, $2CH_2$), 7.21-7.54 (m, 4H, ArH's), 8.33 (s, 1H, pyrimidine H-4). ^{13}C NMR δ = 21.65, 30.98, 32.16, 113.46, 117.87, 118.42, 121.49, 123.79, 129.28, 145.62, 156.72, 158.44, 166.27. Anal. Calcd for $C_{13}H_{11}N_3$: C, 74.62; H, 5.30; N, 20.08. Found: C, 74.62; H, 5.29; N, 20.18

1,2,3,4-tetrahydrobenzo[4,5]imidazo[1,2-*a*]quinazoline (11b)

This compound was obtained as yellow solid (75 %). m.p. 202-204 °C. IR (KBr): 3085 (CH, aromatic), 2986 (CH, aliphatic), 1615 (C=N), 1597 (C=C) cm^{-1}. MS (EI, 70 eV) *m/z*: 223 (M+). ^{1}H NMR (400 MHz, $CDCl_3$) δ = 1.85-2.22 (m, 4H, $2CH_2$), 2.85-2.95 (m, 2H, CH_2), 3.15-3.24 (m, 2H, CH_2), 7.21-7.54 (m, 4H, ArH's), 8.21 (s, 1H, pyrimidine H-4). ^{13}C NMR δ = 22.76, 23.40, 24.90, 38.65, 113.43, 114.65, 118.33, 121.49, 123.79, 128.94, 145.61, 147.51, 159.24, 160.27. Anal. Calcd for $C_{14}H_{13}N_3$: C, 75.31; H, 5.87; N, 18.82. Found: C, 75.28; H, 5.78; N, 18.68.

2,3,4,5-tetrahydro-1*H*-benzo[4,5]imidazo[1,2-*a*]cyclohepta[*e*]-pyrimidine (11c)

This compound was obtained as yellow solid (75 %). m.p 220-22 °C. IR (KBr): 3085 (CH, aromatic), 2986 (CH, aliphatic), 1615 (C=N), 1597 (C=C) cm^{-1}. MS (EI, 70 eV) *m/z*: 237 (M+). ^{1}H NMR (400 MHz, $CDCl_3$) δ = 1.60-1.90 (m, 4H, CH_2), 2.70-2.80 (d, 1H, *J* = 6 Hz, CH_2), 2.85 (t, 2H, *J* = 6 Hz, CH_2), 3.15 (d, 1H, CH), 3.5 (t, 2H, *J* = 6 Hz, CH_2), 7.21-7.54 (m, 4H, ArH's), 8.28 (s, 1H, pyrimidine H-4). ^{13}C NMR δ = 22.99, 26.52, 28.62, 28.58, 36.03, 113.42, 114.56, 121.49, 123.79, 128.58, 145.59, 145.59, 147.40, 160.11, 160.47. Anal. Calcd for $C_{15}H_{15}N_3$: C, 75.92; H, 6.37; N, 17.71. Found: C, 76.12; H, 6.29; N, 17.82.

Synthesis of 5-arylthiazole derivatives (20-22)a-d

Method A: A mixture of thiosemicarbazide **13a-c** (5 mmol) and the appropriate hydrazonoyl halides **14a-c** (5 mmol) in ethanol (20 mL) containing triethylamine (5 mmol, 0.75 mL) was refluxed for 4h, allowed to cool and the solid formed was filtered off, dried and recrystallized from acetic acid to give **(20-22)a-d**.

Method B: To a appropriate of **24a-c** (5 mmol) in ethanol (30 mL) was added sodium acetate trihydrate (1.3 g, 5 mmol), and the mixture was cooled to 0-5 C in an ice bath. To the resulting cold solution was added portionwise a cold solution of arenediazonium chloride [prepared by diazotizing the appropriate of aniline, 4-methylaniline, 4-chloroaniline (5 mmol) dissolved in hydrochloric acid (6 M, 3 mL) with a solution of sodium nitrite (0.35 g, 5 mmol) in water (3 mL)]. After complete addition of the diazonium chloride, the reaction mixture was stirred for a further 30 min in an ice bath. The solid that separated was filtered off, washed with water and finally recrystallized from ethanol to give proved to be identical in all aspects (mp, mixed mp and spectra) with compound **(20-22)a-d** which obtained from method A.

2-(2-Cyclopentylidenehydrazinyl)-4-phenyl-5-(phenyldiaze-nyl)thiazole (20a)

This compound was obtained as brown solid (75 %). m.p. 190-93 °C. IR (KBr): 3320 (NH), 3085 (CH, aromatic), 2986 (CH, aliphatic), 1615 (C=N), 1597 (C=C) cm^{-1}. MS (EI, 70 eV) *m/z*: 361 (M+). ^{1}H NMR (400 MHz, $CDCl_3$) δ = 1.83-1.97 (m, 4H, $2CH_2$), 2.53 (t, 2H, *J* = 4 Hz, CH_2), 2.66 (t, 2H, CH_2), 7.21-8.12 (m, 10H, ArH's), 12.21 (s, br., 1H, NH). ^{13}C NMR δ = 24.90, 24.92, 30.10, 32.26, 107.70, 121.47, 126.89, 128.83, 129.14, 129.15, 130.41, 133.95, 136.75, 155.37, 173.78, 174.12, Anal. Calcd for $C_{20}H_{19}N_5S$: C, 66.46; H, 5.30; N, 19.37; S, 8.87. Found: C, 66.54; H, 5.18; N, 19.29; S, 8.78

2-(2-Cyclopentylidenehydrazinyl)-5-(phenyldiazenyl)-4-(p-to-lyl)thiazole (20b)

This compound was obtained as brown solid (82 %). m.p. 176-78 °C. IR (KBr): 3085 (CH, aromatic), 2986 (CH, aliphatic), 1615 (C=N), 1597 (C=C) cm^{-1}. MS (EI, 70 eV) *m/z*: 375 (M+). ^{1}H NMR (400 MHz, $CDCl_3$) δ = 1.83-1.97 (m, 4H, $2CH_2$), 2.34 (s, 3H, CH_3), 2.53 (t, 2H, *J* = 4 Hz, CH_2), 2.66 (t, 2H, CH_2), 7.38-8.15 (m, 9H, ArH's), 12.21 (s, br., 1H, NH). ^{13}C NMR δ = 21.41, 24.90, 24.92, 30.11, 32.26, 107.70, 121.67, 126.97, 128.88, 129.14, 129.18, 133.94, 136.76, 137.11, 152.46, 173.82, 174.12, Anal. Calcd for $C_{21}H_{21}N_5S$: C, 67.17; H, 5.64; N, 18.65; S, 8.54. Found: C, 67.17; H, 5.49; N, 18.56; S, 8.45

4-(4-Chlorophenyl)-2-(2-cyclopentylidenehydrazinyl)-5-(phenyldiazenyl)thiazole (20c)

This compound was obtained as brown solid (77 %). m.p. 180-81 °C. IR (KBr): 3085 (CH, aromatic), 2986 (CH, aliphatic), 1615 (C=N), 1597 (C=C) cm^{-1}. MS (EI, 70 eV) *m/z*: 395 (M+), 397 (M+2). ^{1}H NMR (400 MHz, $CDCl_3$) δ 1.83-1.97 (m, 4H, $2CH_2$), 2.53 (t, 2H, *J* = 4 Hz, CH_2), 2.66 (t, 2H, CH_2), 7.38-8.15 (m, 9H, ArH's), 12.21 (s, br., 1H, NH). Anal. Calcd for $C_{20}H_{18}ClN_5S$ (395.91); C, 60.67; H, 4.58; N, 17.69; S, 8.10. Found: C, 60.72; H, 4.49; N, 17.75; S, 8.22

2-(2-Cyclopentylidenehydrazinyl)-4-methyl-5-(phenyldiazenyl)-thiazole (20d)

This compound was obtained as brown solid (72 %). m.p. 205-207 °C. IR (KBr): 3085 (CH, aromatic), 2986 (CH, aliphatic), 1615 (C=N), 1597 (C=C) cm^{-1}. MS (EI, 70 eV) *m/z*: 299 (M+). ^{1}H NMR (400 MHz, $CDCl_3$) δ = 1.83-1.97 (m, 4H, $2CH_2$), 2.50 (s, 3H, CH_3), 2.53 (t, 2H, *J* = 4 Hz, CH_2), 2.66 (t, 2H, CH_2), 7.38-8.15 (m, 5H, ArH's), 12.21 (s, br., 1H, NH). ^{13}C NMR δ = 12.84, 24.90, 24.92, 30.11, 32.26, 114.40, 121.72, 129.15, 129.65, 130.23, 154.90, 166.98, 173.85, Anal. Calcd for $C_{15}H_{17}N_5S$: C, 60.18; H, 5.72; N, 23.39; S, 10.71. Found: C, 60.18; H, 5.72; N, 23.39; S, 10.71

2-(2-Cyclohexylidenehydrazinyl)-4-phenyl-5-(phenyldiazenyl)-thiazole (21a)

This compound was obtained as orange solid (76 %). m.p. 178-80 °C. IR (KBr): 3085 (CH, aromatic), 2986 (CH, aliphatic), 1615 (C=N), 1597 (C=C) cm^{-1}. MS (EI, 70 eV) *m/z*: 375 (M+). ^{1}H NMR (400 MHz, $CDCl_3$) δ 1.69-1.80 (m, 6H, $3CH_2$), 2.41 (t, 2H, *J* = 4 Hz, CH_2), 2.65 (t, 2H, CH_2), 7.12-8.15 (m, 10H, ArH's), 12.21 (s, br., 1H, NH). ^{13}C NMR δ = 26.99, 27.15, 27.95, 31.11, 31.76, 107.70, 121.47, 126.89, 128.83, 129.14, 129.15, 130.41, 133.94, 136.78, 155.37, 173.97, 196.65, Anal. Calcd for $C_{21}H_{21}N_5S$: C, 67.17; H, 5.64; N, 18.65; S, 8.54. Found: C, 67.04; H, 5.52; N, 18.57; S, 8.47

2-(2-Cyclohexylidenehydrazinyl)-5-(phenyldiazenyl)-4-(p-tolyl)thiazole (21b)

This compound was obtained as brown solid (79 %). m.p. 165-67 °C. IR (KBr): 3085 (CH, aromatic), 2986 (CH, aliphatic), 1615 (C=N), 1597 (C=C) cm^{-1}. MS (EI, 70 eV) *m/z*: 389 (M+). ^{1}H NMR (400 MHz, $CDCl_3$) δ = 1.69-1.80 (m, 6H, $3CH_2$), 2.45 (s, 3H, CH_3), 2.41 (t, 2H, *J* = 4 Hz, CH_2), 2.65 (t, 2H, CH_2), 7.12-8.15 (m, 9H, ArH's), 12.10 (s, br., 1H, NH). ^{13}C NMR δ = 21.41, 25.99, 27.15, 27.98, 31.11, 31.76, 107.70, 121.87, 126.97, 128.83, 129.14, 129.17, 133.98, 136.76, 137.12, 152.46, 174.12, 196.65, Anal. Calcd for $C_{22}H_{23}N_5S$: C, 67.84; H, 5.95; N, 17.98; S, 8.23. Found: C, 67.76; H, 6.10; N, 18.08; S, 8.32

4-(4-Chlorophenyl)-2-(2-cyclohexylidenehydrazinyl)-5-(phenyldiazenyl)thiazole (21c)

This compound was obtained as brown solid (79 %). m.p. 171-74 °C. IR (KBr): 3085 (CH, aromatic), 2986 (CH, aliphatic), 1615 (C=N), 1597 (C=C) cm^{-1}. MS (EI, 70 eV) *m/z*: 409 (M+), 411 (M+2). ^{1}H NMR (400 MHz, $CDCl_3$) δ = 1.69-1.80 (m, 6H, $3CH_2$), 2.41 (t, 2H, *J* = 4 Hz, CH_2), 2.65 (t, 2H, CH_2), 7.12-8.15 (m, 9H, ArH's), 12.10 (s, br., 1H, NH). ^{13}C NMR δ = 26.12, 27.15, 27.98, 31.11, 31.75, 107.70, 125.99, 126.97, 127.12, 128.79, 129.15, 133.94, 136.76, 138.99, 155.14, 174.12, 196.65, Anal. Calcd for $C_{21}H_{20}ClN_5S$ (409.93); C, 61.53; H, 4.92; N, 17.08; S, 7.82. Found: 409.93: C, 61.46; H, 4.86; N, 17.12; S, 7.78

2-(2-Cyclohexylidenehydrazinyl)-4-methyl-5-(phenyldiazenyl)thiazole (21d)

This compound was obtained as orange solid (79 %). m.p. 185-88 °C. IR (KBr): 3085 (CH, aromatic), 2986 (CH, aliphatic), 1615 (C=N), 1597 (C=C) cm^{-1}. MS (EI, 70 eV) *m/z*: 313 (M+). ^{1}H NMR (400 MHz, $CDCl_3$) δ = 1.69-1.80 (m, 6H, $3CH_2$), 2.41 (t, 2H, *J* = 4 Hz, CH_2), 2.49 (s, 3H, CH_3), 2.65 (t, 2H, CH_2), 7.12-7.38 (m, 5H, ArH's), 12.00 (s, br., 1H, NH). ^{13}C NMR δ = 12.94, 26.14, 27.15, 27.98, 31.11, 31.76, 114.40, 121.71, 129.15, 129.56, 130.41, 154.90, 167.12, 196.65, Anal. Calcd for $C_{16}H_{19}N_5S$ (313.42): C, 61.31; H, 6.11; N, 22.34; S, 10.23. Found: C, 61.21; H, 6.00; N, 22.45; S, 10.19

2-(2-Cycloheptylidenehydrazinyl)-4-phenyl-5-(phenyldiazenyl)thiazole (22a)

This compound was obtained as orange solid (82 %). m.p. 178-80 °C. IR (KBr): 3085 (CH, aromatic), 2986 (CH, aliphatic), 1615 (C=N), 1597 (C=C) cm^{-1}. MS (EI, 70 eV) *m/z*: 389 (M+). ^{1}H NMR (400 MHz, $CDCl_3$) δ = 1.50-1.54 (m, 4H, $2CH_2$), 1.68-1.69 (m, 2H, CH_2), 2.17-2.18 (m, 2H, CH_2), 2.24-2.26 (m, 2H, CH_2), 2.45-2.48 (m, 2H, CH_2), 7.12-8.22 (m, 10H, ArH's), 12.00 (s, br., 1H, NH). ^{13}C NMR δ = 22.25, 28.99, 29.80, 37.30, 107.40, 121.41, 126.87, 128.82, 129.14, 129.15, 130.41, 133.94, 136.76, 155.38, 173.99, 186.89, Anal. Calcd for $C_{22}H_{23}N_5S$ (389.52): C, 67.84; H, 5.95; N, 17.98; S, 8.23. Found: C, 67.78; H, 6.05; N, 18.10; S, 8.32

2-(2-Cycloheptylidenehydrazinyl)-5-(phenyldiazenyl)-4-(*p*-tolyl)thiazole (22b)

This compound was obtained as orange solid (82 %). m.p. 176-78 °C. IR (KBr): 3085 (CH, aromatic), 2986 (CH, aliphatic), 1615 (C=N), 1597 (C=C) cm^{-1}. MS (EI, 70 eV) *m/z*: 403 (M+). ^{1}H NMR (400 MHz, $CDCl_3$) δ = 1.50-1.54 (m, 4H, $2CH_2$), 1.68-1.69 (m, 2H, CH_2), 2.17-2.18 (m, 2H, CH_2), 2.24-2.26 (m, 2H, CH_2), 2.45-2.48 (m, 2H, CH_2), 7.12-8.23 (m, 9H, ArH's), 12.00 (s, br., 1H, NH). ^{13}C NMR δ = 21.23, 22.25, 28.99, 29.80, 37.30, 107.60, 121.67, 126.89, 129.83, 129.14, 129.17, 133.94, 136.76, 137.15, 152.46, 174.12, 186.97, Anal. Calcd for $C_{23}H_{25}N_5S$: 68.46; H, 6.24; N, 17.35; S, 7.95. Found: C, 68.38; H, 6.30; N, 17.51; S, 7.86

4-(4-Chlorophenyl)-2-(2-cycloheptylidenehydrazinyl)-5-(phenyldiazenyl)thiazole (22c)

This compound was obtained as orange solid (82 %). m.p. 185-88 °C. IR (KBr): 3085 (CH, aromatic), 2986 (CH, aliphatic), 1615 (C=N), 1597 (C=C) cm^{-1}. MS (EI, 70 eV) *m/z*: 423 (M+), 425 (M+2). ^{1}H NMR (400 MHz, $CDCl_3$) δ = 1.50-1.54 (m, 4H, $2CH_2$), 1.68-1.69 (m, 2H, CH_2), 2.17-2.18 (m, 2H, CH_2), 2.24-2.26 (m, 2H, CH_2), 2.45-2.48 (m, 2H, CH_2), 7.12-8.23 (m, 9H, ArH's), 12.00 (s, br., 1H, NH). ^{13}C NMR δ = 22.25, 29.11, 29.80, 37.30, 107.70, 125.99, 126.89, 127.11, 128.83, 129.14, 133.93, 136.67, 138.98, 155.14, 173.99, 186.89, Anal. Calcd. for $C_{22}H_{22}ClN_5S$: C, 62.33; H, 5.23; 16.52; S, 7.56. Found: C, 62.41; H, 5.32; 16.48; S, 7.65

2-(2-Cycloheptylidenehydrazinyl)-4-methyl-5-(phenyldiazenyl)thiazole (22d)

This compound was obtained as orange solid (82 %). m.p. 142-44 °C. IR (KBr): 3085 (CH, aromatic), 2986 (CH, aliphatic), 1615 (C=N), 1597 (C=C) cm^{-1}. MS (EI, 70 eV) *m/z*: 427 (M+). ^{1}H NMR (400 MHz, $CDCl_3$) δ = 1.50-1.54 (m, 4H, $2CH_2$), 1.68-1.69 (m, 2H, CH_2), 2.17-2.18 (m, 2H, CH_2), 2.24-2.26 (m, 2H, CH_2), 2.34 (s, 3H, CH3), 2.44-2.47 (m, 2H, CH_2), 7.12-8.23 (m, 5H, ArH's), 12.00 (s, br., 1H, NH). ^{13}C NMR δ = 12.92, 22.25, 29.12, 29.81, 37.30, 114.48, 121.72, 129.15, 129.65, 130.39, 154.88, 186.97, Anal. Calcd. for $C_{17}H_{21}N_5S$ (327.45): C, 62.36; H, 6.46; N, 21.39; S, 9.79. Found: C, 62.28; H, 6.37; N, 21.52; S, 9.68

2,2'-(1-phenylpropane-1,3-diylidene)bis(hydrazine-1-carbothioamide) (25).

A mixture of sodium 3-oxo-3-phenylprop-1-en-1-olate (1.7 g, 10 mmol) thiosemicarbazide (0.91 g, 10 mmol) and piperidine acetate (1 ml) in H_2O (3 ml) was refluxed for 15 minutes. Acetic acid (1.5 ml) was added to the hot solution. The solid product was filtered off and recrystallized from ethanol to give product identical in all aspect (mp., mixed mp., and spectra) with 2,2'-(1-phenylpropane-1,3-diylidene)bis(hydrazine-1-carbothioamide) (**25**) which prepared via reaction of thiosemicarbazide with 3-oxo-3-phenylpropanal.[33]

4-Phenyl-2-(2-(1-phenyl-3-((4-phenylthiazol-2-yl)diazenyl)allylidene)hydrazinyl)-thiazole (27), 4-phenyl-2-(2-(1-phenyl-3-(4-phenyl-5-(phenyldiazenyl)thiazol-2-yl)diazenyl)allylidene)hydrazinyl)-5-(phenyldiazenyl)thiazole (30a) and 4-methyl-2-(2-(3-((4-methyl-5-(phenyldiazenyl)thiazol-2-yl)diazenyl)-1-phenyl-allylidene)-hydrazinyl)-5-(phenyldiazenyl)thiazole (30b).

A mixture of 2,2'-(1-phenylpropane-1,3-diylidene)bis(hydrazine-1-carbothioamide) (**25**) (1.47 g, 5 mmol), the appropriate of ω-bromoacetophenone, 2-oxo-N,2-diphenylacetohydrazonoyl bromide or 2-oxo-N-phenylpropanehydrazonoyl chloride and triethylamine (5 mmol) in ethanol (15 mL) was refluxed for 2 h. The solid which precipitated after cooling was collected and recrystallized from proper solvent afforded **27**, **30a** and **30b**, respectively.

4-Phenyl-2-(2-(1-phenyl-3-((4-phenylthiazol-2-yl)diazenyl)-allylidene)hydrazinyl)-thiazole (27)

This compound was obtained as pale brown solid (77 %). m.p. 175-787 °C (from ethanol). IR (KBr): 3085 (CH, aromatic), 2986 (CH, aliphatic), 1615 (C=N), 1597 (C=C) cm^{-1}. MS (EI, 70 eV) *m/z*: 492 (M+). ^{1}H NMR (400 MHz, $CDCl_3$) δ = 5.31 (d, 1H, CH=CH), 5.85 (d, 1H, CH=CH), 7.27-7.98 (m, 17H, (3x 5) ArH's and 2 thiazole H-5) and 12.15 (s, br, 1H, NH). ^{13}C NMR δ = 105.34, 110.12, 116.71, 126.48, 127.45, 127.60, 127.91, 128.20, 128.30, 128.87, 135.45, 135.68, 136.47, 152.67, 155.28, 156.75, 167.53, 170.24, 171.32, Anal. Calcd. for $C_{27}H_{20}N_6S_2$: C, 65.83; H, 4.09; N, 17.06; S, 13.02. Found: C, 65.72; H, 4.17; N, 16.89; S, 13.00

4-Phenyl-2-(2-(1-phenyl-3-(4-phenyl-5-(phenyldiazenyl)thiazol-2-yl)diazenyl)-allylidene)hydrazinyl)-5-(phenyldiazenyl)-thiazole (30a)

This compound was obtained as orange solid (69 %). m.p. 208-209 °C (from acetic acid). IR (KBr): 3085 (CH, aromatic), 2986 (CH, aliphatic), 1615 (C=N), 1597 (C=C) cm^{-1}. MS (EI, 70 eV) *m/z*: 700 (M+). ^{1}H NMR (400 MHz, $CDCl_3$) δ = 5.31 (d, 1H, CH=CH), 5.85 (d, 1H, CH=CH), 7.17-7.88 (m, 25H, (5x 5) ArH's and 12.10 (s, br, 1H, NH). ^{13}C NMR δ = 106.54, 110.42, 112.76, 116.71, 119.98, 121.46, 126.88, 127.45, 127.86, 128.30, 128.83, 129.89, 130.41, 133.18, 134.43, 136.77, 137.00, 138.54, 155.20, 155.28, 158.37, 167.53, 171.33, 172.39, Anal. Calcd for $C_{39}H_{28}N_{10}S_2$: C, 66.84; H, 4.03; N, 19.99; S, 9.15. Found: C, 66.68; H, 4.12; N, 20.14; S, 9.28

4-Methyl-2-(2-(3-((4-methyl-5-(phenyldiazenyl)thiazol-2-yl)-diazenyl)-1-phenyl-allylidene)-hydrazinyl)-5-(phenyldiazenyl)-thiazole (30b)

This compound was obtained as orange solid (70 %). m.p. 220-22 °C (from acetic acid). IR (KBr): 3085 (CH, aromatic), 2986 (CH, aliphatic), 1615 (C=N), 1597 (C=C) cm^{-1}. MS (EI, 70 eV) *m/z*: 576 (M+). ^{1}H NMR (400 MHz, $CDCl_3$) δ = 2.45 (s, 6H, $2CH_3$), 5.31 (d, 1H, CH=CH), 5.85 (d, 1H, CH=CH), 7.17-7.88 (m, 15H, (3x 5) ArH's and 12.10 (s, br, 1H, NH). ^{13}C NMR δ = 12.94, 113.23, 112.99, 116.71, 119.79, 121.72, 127.91, 127.45, 128.30, 128.43, 129.15, 130.41, 138.44, 154.73, 154.90, 155.28, 164.34, 165.40, 167.53, Anal. Calcd for $C_{29}H_{24}N_{10}S_2$: C, 60.40; H, 4.19; N, 24.29; S, 11.12. Found: C, 60.40; H, 4.19; N, 24.29; S, 11.12

Conclusion

In conclusion, compounds of type 2 proved to be useful precursors for synthesis of various fused pyrimidines via their reactions with heterocyclic amines. Also, 2 reacted with thiosemicarbazones then with hydrazonoyl halides gave thiazole derivatives in good yields. The structures of the newly synthesized compounds were confirmed by spectral data and elemental analyses.

References

[1]Sharma, P., Rane, N., Gurram, V. K., *Bioorg. Med. Chem. Lett.* **2004**, *14*, 4185-4190.

[2]Prakash, O., Bhardwaj, V., Kuma, R., Tyagi, P., Areja, K. R., *Eur. J. Med. Chem.*, **2004**, *39*, 1073-1077.

[3]Botta, M.; Artico, M.; Massa, S.; Gambacorta, A., Maronigu, M. E., Pani, A., Lacolla P. *Eur. J. Med. Chem.*, **1992**, *27*, 251-257.

[4]Agarwal, N., Srivastava, P., Raghuwanshi, S. K, Upadhyay, D. N, Shukla, P. K., Ram, V., *J. Bioorg. Med. Chem.*, **2002**, *10*, 869-874.

[5]Agarwal, N., Srivastava, P., Raghuwanshi, S. K., Upadhyay, D. N., Shukla, P. K., Ram, V. J. *Bioorg. Med. Chem.*, **2002**, *10*, 869-874.

[4]Forsch, R. A., Queener, S. F., Rosowsky, A. *Bioorg. Med. Chem, Lett*, **2004**, *14*, 1811-1815.

[5]Agarwal. N., Raghuwanshi, S. K., Upadhyay, D. N., Shukla, P. K., Ram, V. *J. Bioorg. Med. Chem. Lett* , **2000**, *10*, 703-706.

[6]Agarwal, N., Srivastava, K., Puvi, S. K., Sinha, S., Chauhan, P. M. S., *Bioorg. Med. Chem. Lett*, **2005**, *15*, 5218-5221.

[6]Delia, T. J., Baumann, M., Bunker, A., *Heterocycles*, **1993**, *35*, 1397-1410.

[7]Cocco, M. T., Congin, C., Lilliu, V., Onnis, V., *Bioorg. Med. Chem. Lett.*, **2006**, *14*, 366-372.

[8]Malik, V., Singh, P., Kumar, S. *Tetrahedron*, **2006**, *62*, 5944-5951.

[9]Fan, X.; Zhang, X., Zhou, L., Keith, K. A., Kern, E. R., Torrence, P. F. *Bioorg. Med. Chem. Lett*, **2006**, *16*, 3224-3228.

[10]Botta, M., Occhionero, F., Nicoletti, R., Mastromarino, P., Conti, C., Magrini, M., Saladino, R. *Bioorg. Med. Chem.*, **1999**, *7*, 1925-1931.

[11]Srivastava, R., Mishra, A., Ratap, R., Bhakuni, D. S., Srimal, R. C. *Thromb Res*, **1989**, *54*, 741-749.

[12]Skulnick, H. I., Ludens, J. H., Wendling, M. G., Glenn, E. M., Rohloff, N. A., Smith, R. J., Wierenga, W. *J. Med. Chem.*, **1986**, *29*, 1499-1504.

[13]Atwal, K. S., Swanson, B. N., Unger, S. E., Floyed, D. M., Moreland, S., Hedberg, A., O'Reilly, B. C. *J. Med. Chem.*, **1991**, *34*, 806-811.

[14]Rovnyak, G. C., Atwal, K. S., Hedberg A., Kimball, S. D., Moreland, S., Gougoutas, J. Z., O'Reilly, B. C., Schwartz, J., Marllery, M. F. *J. Med. Chem.*, **1992**, *35*, 3254-3263.

[15]Grover, G. J., Dzwonczyk, S., McMullen, D. M., Norandin, D E., Parham, C. S., Sleph, P. G., Moreland, S. *J. Cardiovasc. Pharm.*, **1995**, *26*, 289-294.

[16]Wells, G., Bradshaw, T. D., Diana, P., Seaton, A., Shi, D.-F., Westwell, A. D., Stevens, M. F.G. *Bioorg. Med. Chem. Lett*, **2000**, *10*, 513-5.

[17]Pattan, S. R., Suresh, C. H., Pujar, V. D., Reddy, V. V. K., Rasal, V. P., Koti, B. C. *Indian J. Chem., Sect B.*, **2005**; *44*, 2404-8.

[18]Pingle, M. S. *Indian J. Heterocycl. Chem*., **2003**, *12*, 343-46.

[19]Kumar, Y., Green, R., Wise, D.S., Wotring, L.L.,Townsend, L. B. *J. Med. Chem.*, **1993**, *36*, 3849-52.

[20]Rollas, S., Kucukguzel, S. G. *Molecules.* **2007**, *12*, 1910-39.

[21]Chavan, A. A., Pai, N. R. *Arkivoc* **2007**, *14*, 148-55.

[22]Vijaya, J., Jayachandrane, R. S., Kalpesh, P., Sreenivasa G. M. *International journal of pharma and bio sciences* **2010**; *1*(3).

[23]Kaur, H., Kaur, H., Chawla, A., Baghel, U. S., Dhawan, R. K. A. *Journal of Global Trends in Pharmaceutical Sciences* **2014**, *5*(2), 1684 –1691.

[24]Ahmed, S. A., Hussein, A. M., Hozayen, W. G. M., El-Ghandour, A. H. H., Abdelhamid, A. O. *J. Heterocyclic Chem.*, **2007**, *44*, 803-810.

[25]Dimmock, J. R., McColl, J. M., Wonko, R. L., Thayer, R. S., Hancock, D. S. *Eur. J. Med. Chem*. **1991**, *26*, 529-534

[26]Cardia, M. C., Begala, M., DeLogu, A., Maccioni, A., Plumitallo, A. *IL Farmaco* **2000,** *55*, 93-95.

[27]Butler, R. N. **1996,** *Comprehensive Heterocyclic Chem*. II, Pergamon, Oxford; vol. *4*: pp. 621-678.

[28]Huisgen, R., Grashey, R., Seidel, M., Knupfer, H., Schmidt, R. *Lieb. Ann*.**1962**, 658, 169-180.

[29]Zohdi, H. F., Rateb, N. M., Sallam, M. M. M., Abdelhamid, A. O. *J. Chem. Res*.**1998**; (S), 742, (M) 4429.

[30]Losse, G., Hessler, W., Barth, A. *Chem. Ber.***1958**, *91*, 150-158.

[31]Shawali, A. S., Abdelhamid, A. O. *Bull. Soc. of Japn*., **1976**, *49*, 321-324.

[32]Eweiss, N. F, Osman, A. *J.. Heterocycl.. Chem.*, **1980**, *17*, 1713-1717.

[36]Zohdi, H. F., Emam, H. A., Abdelhamid, A. O. *Phosphorus, Sulfur, Silicon*, **1997**, *129*, 147-154

Received 04.09.2014.

Accepted: 07.11.2014.